Mechanical Properties and Microstructure Investigation Of Lead Free Solder

Qing Wang
William F. Gail
R. Wayne Johnson

Auburn University
162 Broun Hall/ECE Dept.
Auburn, AL 36849
334-844-1880
johnson@eng.auburn.edu

Mark Strickland
NASA/MSFC

Jim Blanche
NASA/MSFC/Allied Aerospace

June 24, 2005

Abstract

While the electronics industry appears to be focusing on Sn-Ag-Cu as the alloy of choice for lead free electronics assembly, the exact composition varies by geographic region, supplier and user. Add to that dissolved copper and silver from the printed circuit board traces and surface finish, and there can be significant variation in the final solder joint composition. A systematic study of the mechanical and microstructural properties of Sn-Ag-Cu alloys with Ag varying from 2wt% to 4wt% and Cu varying from 0.5wt% to 1.5wt%, was undertaken in this research study. Different sample preparation techniques (water quenched, oil quenched and water quenched followed by reflow) were explored and the resulting microstructure compared to that of a typical reflowed lead free chip scale package (CSP) solder joint.

Tensile properties (modulus, 0.2% yield strength and the ultimate tensile strength) and creep behavior of selected alloy compositions (Sn-4Ag-1.5Cu, Sn-4Ag-0.5Cu, Sn-2Ag-1.5Cu, Sn-2Ag-0.5Cu, Sn-3.5Ag-0.8Cu) were determined for three conditions: as-cast; aged for 100 hours at 125°C; and aged for 250 hours at 125°C. There was no significant difference in Young's Modulus as a function of alloy composition. After an initial decrease in modulus after 100 hours at 125°C, there was an insignificant change with further aging. The distribution of 0.2% strain yield stress and ultimate tensile strength as a function of alloy composition was more significant and decreased with aging time and temperature. The microstructures of these alloys were examined using light and scanning electron microscopy (LM and SEM) respectively and SEM based energy dispersive x-ray spectroscopy (EDS). Fracture surface and cross-section analysis were performed on the specimens after creep testing. The creep testing results and the effect of high temperature aging on mechanical properties is presented for the oil quenched samples. In general the microstructure of oil quenched specimen exhibited a eutectic region of Sn with moderately dispersed Ag_3Sn intermetallic, surrounded by a dendritic Sn-rich phase. The SEM images of the fracture surface indicated the presence of a tough shear surface at the initial cavity break area and a break line in the middle of specimen along the failure direction. A hyperbolic-sine creep model was adopted and used to fit the creep experiment data.

The effect on the mechanical properties of adding the quaternary element bismuth to the Sn-3.5Ag-0.8Cu alloy was measured and compared with the mechanical properties of the ternary alloys. The results of this research study provide necessary data for the modeling of solder joint reliability for a range of Sn-Ag-Cu compositions and a baseline for evaluating the effects of subsequent quaternary additions.

CHAPTER 1

Introduction

Lead free solders are increasingly used in interconnection systems for electronic packages as a result of pending legislation in the European Union, environmental and health concerns, and market competition. The European Commission's (EC) draft directives, Waste Electrical and Electronic Equipment (WEEE) and Restriction of Hazardous Substances (RoHS), have approved banning the use of lead in electronics in European Union countries effective July 2006. Furthermore, several Japanese electronics manufacturers have successfully created a market differentiation and increased market share based on "green" products that use Pb-free solders. The conversion to Pb-free solders in the global electronics assembly business appears imminent [1].

At present, the industry is in compliance with the existing international legislation (US, Japan, Europe, Australia, Denmark, Sweden), that addresses the environmental and health issues associated with lead. Since the WEEE Directive was issued in 1986, trade and research organizations within the industry have begun to create task forces to research the issues involved in the replacement of lead solder (IPC, EIA, NCMS, NEMI, NIST, PCIF, ITRI). However, so far no viable alternatives have been found that can be used to directly replace the lead bearing solders in all the applications where it is presently used [39].

A large number of lead free solder research studies [3-8] have been reported which have focused primarily on microstructural analysis and mechanical properties such as Young's modulus, Poisson's ratio, tensile strength, and creep properties for specified compositions of lead free solders. According to a research report issued by the National Center for Manufacturing Science (NCMS) and the National Electronics Manufacturing Initiative (NEMI), there is no "drop in" replacement for Sn-Pb eutectic solder at present [5]. Sn-Ag-Cu alloy is considered the preferred substitute for tin-lead solder in reflow applications due to its relatively low melting temperature, and superior mechanical properties and solderability compared with other lead free solders. In Japan, the Japan Electronic Industry Development Association (JEIDA) has recommended 96.5wt%Sn-3wt%Ag-0.5wt%Cu; in the EU, the European Consortium - the Industrial and Materials Technologies Program Brite-Euram, recommended 95.5wt%Sn-3.8wt%Ag-0.7wt%Cu; and in US, NEMI has recommended 95.5wt%Sn-3.9wt%Ag-0.6wt%Cu for reflow soldering and 99.3Sn-0.7Cu for wave soldering [9].

1.1 Research Objectives

The NEPP Lead Free Solder Program research was funded through NASA's Marshall Space Flight Center. The goals of the project were:

- Develop a new specimen preparation method that will make it possible to characterize Sn-Ag-Cu solder alloy system performance under realistic conditions in electronic packages.
- Develop a systematic comprehensive database on alloy composition-microstructure-mechanical property relationships for Sn-Ag-Cu alloy systems.
- Investigate the effect on the mechanical properties of Sn-Ag-Cu alloys of adding small quantities of quaternary element metals.

The work done for this study included process development for a new specimen fabrication technique, tensile and creep testing, an analysis of test data and extraction of the critical parameters from experimental data to fit the constitutive creep model and the prediction of BGA solder joint life by Finite Element Analysis (FEA) modeling based on the above parameters.

Chapter 1 reviews and summarizes the current research on the most popular lead free solder systems (Sn-Ag, Sn-Ag-Cu, Sn-Cu), including tensile properties and creep resistance measurement results, microstructure investigations under different cooling options, specimen geometries, aging conditions, and the relationship between microstructure and mechanical properties.

A systematic study of the tensile and microstructural properties of Sn-Ag-Cu alloys with Ag varying from 2wt% to 4wt% and Cu varying from 0.5wt% to 1.5wt% is discussed and presented in Chapter 2. A range of sample preparation techniques (water quenched, oil quenched and water quenched followed by reflow) were explored and the resulting microstructure compared to that of a typical reflowed lead free chip scale package (CSP) solder joint. The tensile strength, 0.2% yield strength and the ultimate tensile strength were measured for the range of alloys at conditions of as-cast, aged for 100h at 125°C and aged for 250h at 125 ^{o}C.

Chapter 3 presents an investigation of the creep behavior for selected alloy compositions (Sn-4Ag-1.5Cu, Sn-4Sg-0.5Cu, Sn-2Ag-1.5Cu, Sn-2Ag-0.5Cu, Sn-3.5Ag-0.8Cu) at three conditions: as-cast; aged for 100 hours at 125 ^{o}C; and aged for 250 hours at 125 ^{o}C. Tests were conducted at three different temperatures (22 ^{o}C, 100 ^{o}C and 150 ^{o}C) at different constant stress levels (5MPa - 35MPa). Critical parameters for the hyperbolic-sine power-law creep model were extracted from the creep experimental database and compared with published data. Creep fracture analysis was conducted for selected creep specimens under different condition.

The effect of adding a quaternary element, bismuth, to Sn-Ag-Cu alloys was investigated under different aging conditions and wt% of Bi, and reported in Chapter 4. Here the mechanical properties of the Sn-Ag-Cu-Bi alloys were compared with those of comparable Sn-Ag-Cu alloys.

Chapter 5 summarizes the study's results and discusses the research findings. These results will provide the baseline information for the future study in lead free solder materials. Several topics are proposed for future work.

1.2 Lead Free Solder Candidate

The currently available supplies of elements that are potential candidates as components in lead-free solders are listed in Table 1. Generally, the following criteria need to be considered when evaluating the lead free alloy candidates [10]:

> melting temperature similar to Sn-Pb solders, particularly 63Sn-37Pb solder
> adequate wetting properties for the metallization used in the electronics industry
> physical properties no poorer than those of Sn-Pb solder
> good fatigue resistance
> compatible with existing liquid flux systems
> adequate shelf life and performance as a solder paste
> low dross formation when used in a wave soldering operation
> low cost

Table 1. Supply status of potential candidate elements for lead-free solder applications [10]

Element	World production (10^3 kg)	World capacity (10^3 kg)	Spare capacity (10^3 kg)
Ag	12,200	13,600	1,360
Bi	3,630	7,260	3,630
Cu	7,256,000	9,251,000	1,995,000
Ga	27	72	45
In	109	218	109
Sb	70,920	110,920	40,000
Sn	145,000	233,800	78,600
Zn	6,258,000	6,893,000	679,000

L. Ning-Chen [10] pointed out that although Sn-In-containing systems are promising in terms of solder mechanical properties and soldering performance, the price of In is high. In other options, eutectic Sn-Ag solder doped with Zn, Cu, or Sb exhibits good mechanical strength and creep resistance, Bi-Sn systems doped with other elements may find a niche in the low temperature soldering field, and eutectic Sn-Cu shows potential due to its good fatigue resistance, while eutectic Sn-Zn system modified with In and/or Ag may be promising in terms of mechanical properties.

1.3 Tensile Property Measurement and Microstructure Analysis for Lead free Solder

1.3.1 Tensile Stress and Strain

Figure 1.1 shows the typical engineering stress - strain curve for a pure metal or alloy [15].

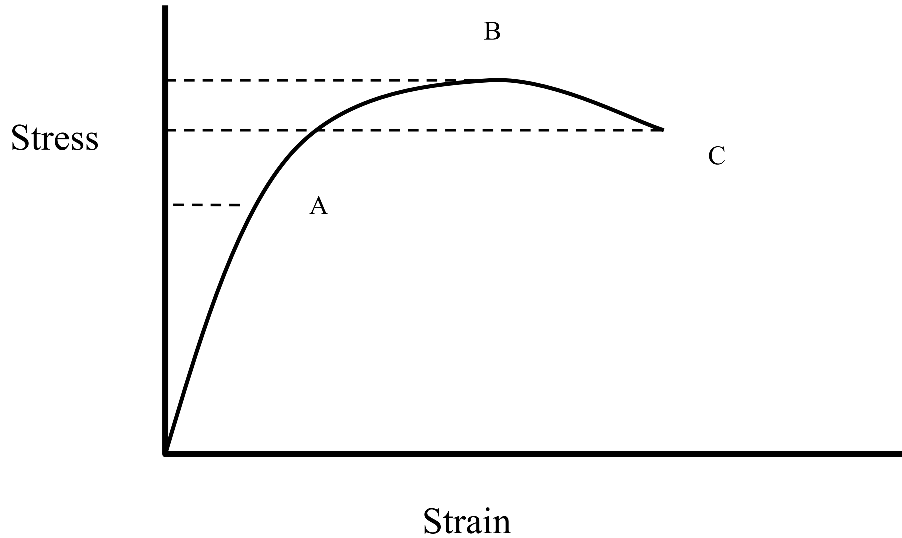

Figure 1.1 Typical Stress – Strain Curve

The engineering stress and strain can be defined as:

$$\text{Engineering Stress:} \quad \sigma = \frac{F}{A_0} \tag{1-1}$$

$$\text{Engineering Strain:} \quad \varepsilon = \frac{l - l_0}{l_o} \tag{1-2}$$

where A_0 is the original cross sectional area of the specimen before testing; l_0 is the original gage length and l is the gage length after the force has been applied.

The first part of the curve (0--A) which is linear, represents the elastic deformation up to the yield point A, when plastic deformation starts. The slope of the elastic section is defined as Young's modulus ($E = \frac{\sigma}{\varepsilon}$) of the alloy which is very important in determining the mechanical properties. Point A is the yield stress at which the alloy starts to deform plastically and is normally defined in terms of the stress that produces a 0.002 strain for engineering applications. From point A onwards, the alloy starts to experience strain-hardening, with an increased stress becoming necessary for additional plastic deformation. The maximum point B is the ultimate tensile strength that the alloy can endure [61].

The ductility of an alloy is defined as the amount of plastic deformation at the breaking point C (% Elongation $= \frac{l - l_0}{l_0} \times 100\%$) or the reduction in area at C. The Hall-

Petch equation gives the relationship between the grain size and the yield strength of the alloy [15]:

$$\sigma_y = \sigma_0 + Kd^{-1/2} \qquad (1\text{-}3)$$

where σ_y is the yield strength of the alloy, d is the average diameter of the grains, and σ_0 and K are constants for the alloy. A hypothetical curve is shown in figure.1.2 exhibiting the general relationship of yield stress and grain diameter. This clearly shows how the yield stress increases with decreasing grain diameter [61].

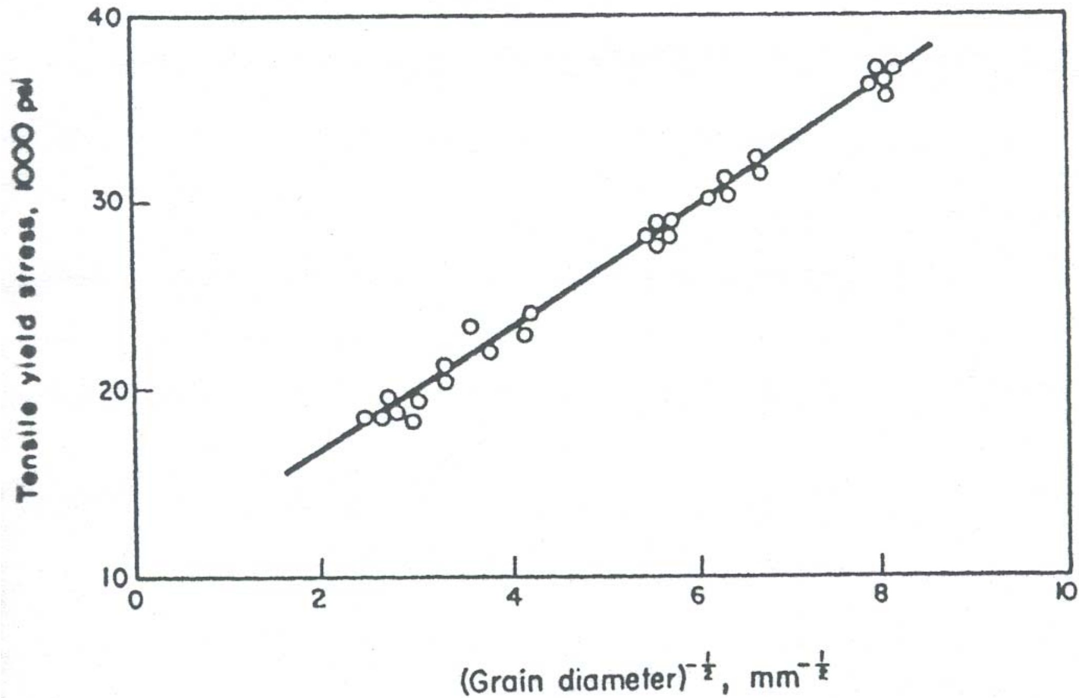

Figure 1.2 General relationship of yield stress and grain diameter [61]

1.3.2 Tensile Properties Measurement Review

The tensile properties of lead free solder, such as Young's modulus, yield strength and ultimate tensile strength are very important for characterizing the solder joint reliability of popular electronic packages (CSP, BGA, flip chip). Figure 1.3 shows the typical solder joint geometry of a flip chip chip-scale package (CSP) and a plastic BGA packages with a solder joint height of 0.25-0.5 mm. The tensile specimen geometry, strain rate, temperature, and cooling rate all have an effect on the measurement of tensile properties [18-27]. The cooling rate under different cooling options and testing temperatures is the most important factor in the study of tensile properties of lead free solders.

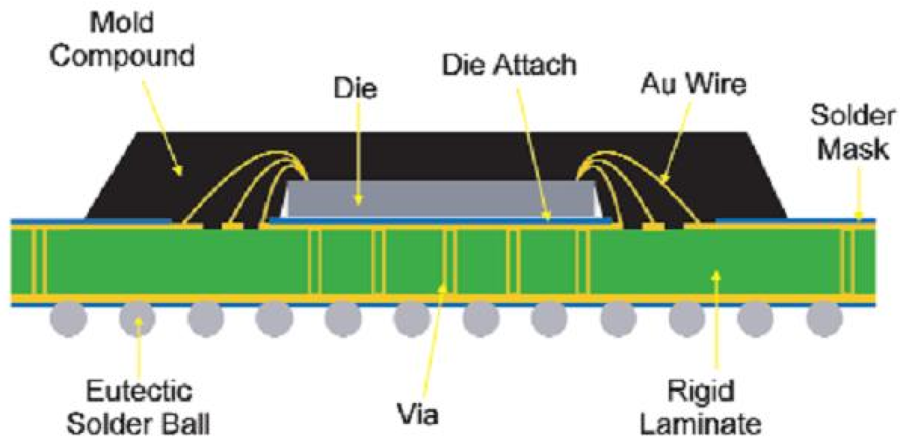

Figure1.3 (a) PBGA [16]

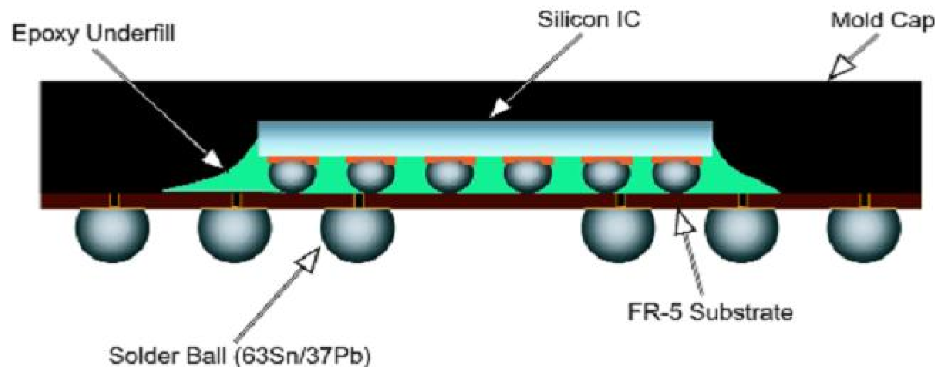

Figure1.3 (b) FC CSP [17]

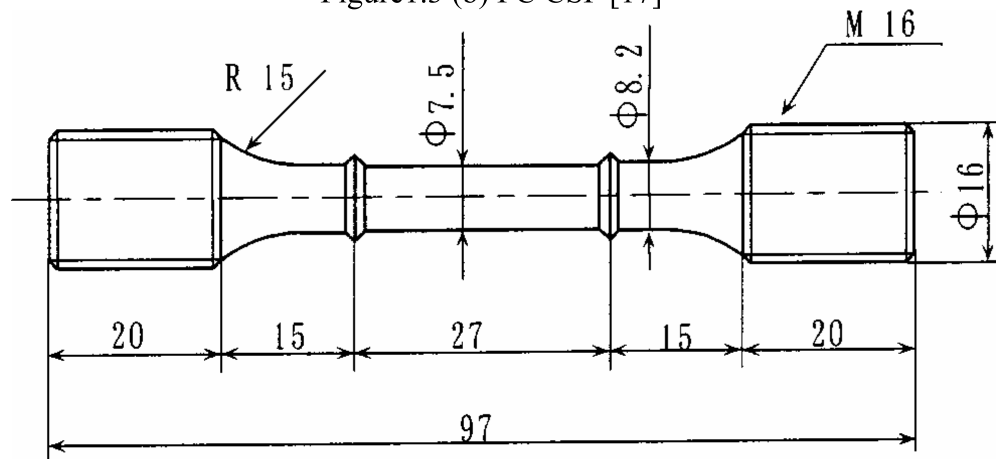

Figure 1.4 Shape and dimensions (mm) of a typical Dog-bone tensile specimen [18]

A very common tensile specimen is the "dog-bone" shaped bulk sample (Figure 1.4), which is used extensively for tensile testing. The specimen is annealed in an oven at a specified temperature for a specified time and then cooled in air to stabilize the microstructure. However, this type of specimen is bigger than the real solder joint dimensions typically found in electronic packages and its thermal history diverges

strongly from that of solder joints so it is a poor guide to actual solder performance in real applications [28]. To overcome this shortcoming, a new specimen that can be used to simulate the real solder joint dimensions was developed by Kariya, et al.[20], as shown in Figure 1.5. In this specimen, the solder balls (composed of the lead free solder under investigation) were used to attach a Si chip on a FR-4 substrate, forming the solder joint through a specific reflow process. This specimen has the advantage that it has been treated in a manner close to that found in real package situations, although it is still not possible to separate out the effects of different process variables (alloy thermal history, CTE mismatch, etc.). Development of a new specimen for tensile testing that is close to the real solder joint dimensions and microstructure is very important for the accurate measurement of mechanical properties and the characterization of new lead free solder alloys.

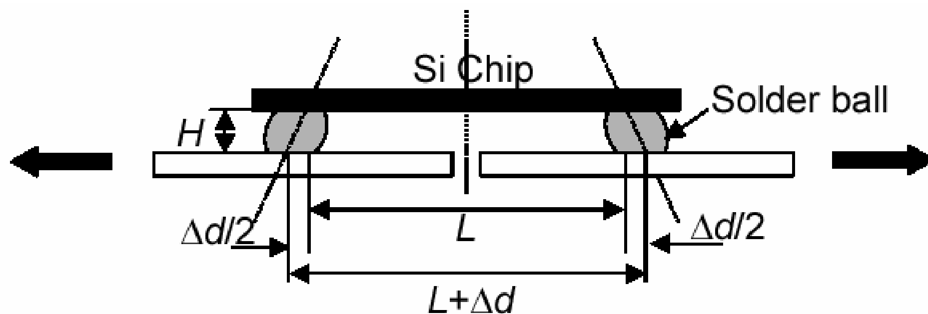

(a) Schematic illustration of the shear deformation of a split board specimen [20]

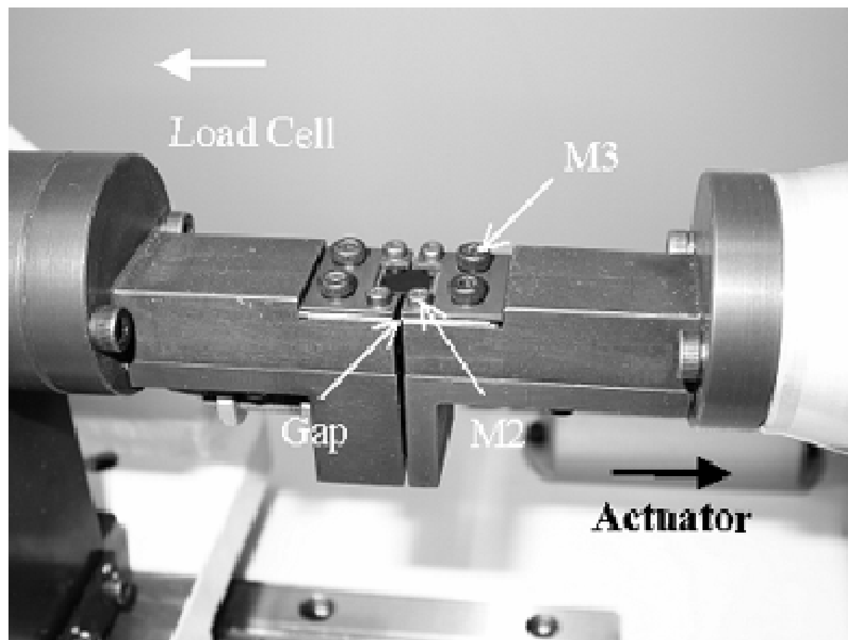

(b) Specimen held by jigs in a tensile machine [20]
Figure 1.5 Lap shear solder joint specimen

Nose, et al. [18] investigated the effect of temperature and strain rate on the tensile strength and inelastic constitutive relationship of Sn-Pb solders. The results indicated that strain rates faster than 2.0%/s are required in order to obtain the time independent tensile properties of solders. John, et al. [19] derived theoretical values for the mechanical properties for 95.5Sn-3.8Ag-0.7Cu solder alloy for bulk specimen and lap shear solder joint specimens at three temperatures (25°C, 75 °C and 125 °C) and three different strain rates ($5.6 \times 10^{-4}\ s^{-1}$, $5.6 \times 10^{-3}\ s^{-1}$, $5.6 \times 10^{-2}\ s^{-1}$) (Figure1.6). He reported that yield stress (YS) decreased with increasing temperature, and increased with decreasing strain rate. This trend also applied to Young's modulus (E) and ultimate tensile stress (UTS).

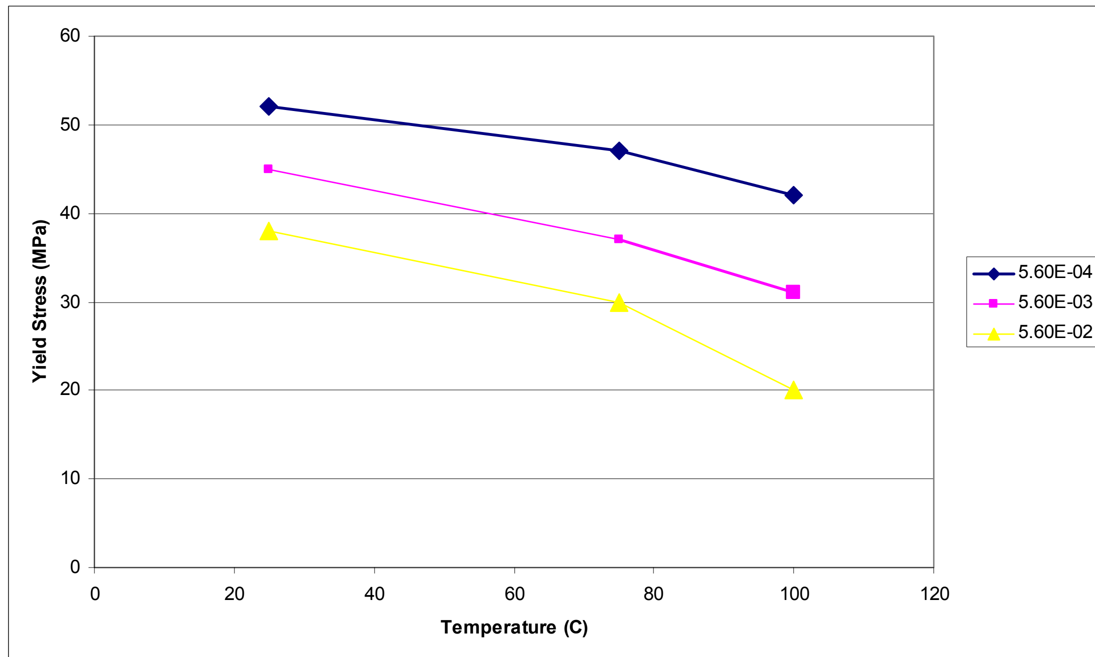

Figure 1.6 Effect of temperature and strain rates on tensile yield stress [19]

The yield stress of the bulk solder was compared to the equivalent yield stress calculated from the shear test result using the von Mises relationship for equivalent stress and strain: $\sigma = \sqrt{3}\tau$, $\varepsilon = \gamma / \sqrt{3}$. Figure 1.7 [19] shows the close match between the yield stress measurements for the bulk solder and a lap shear solder joint.

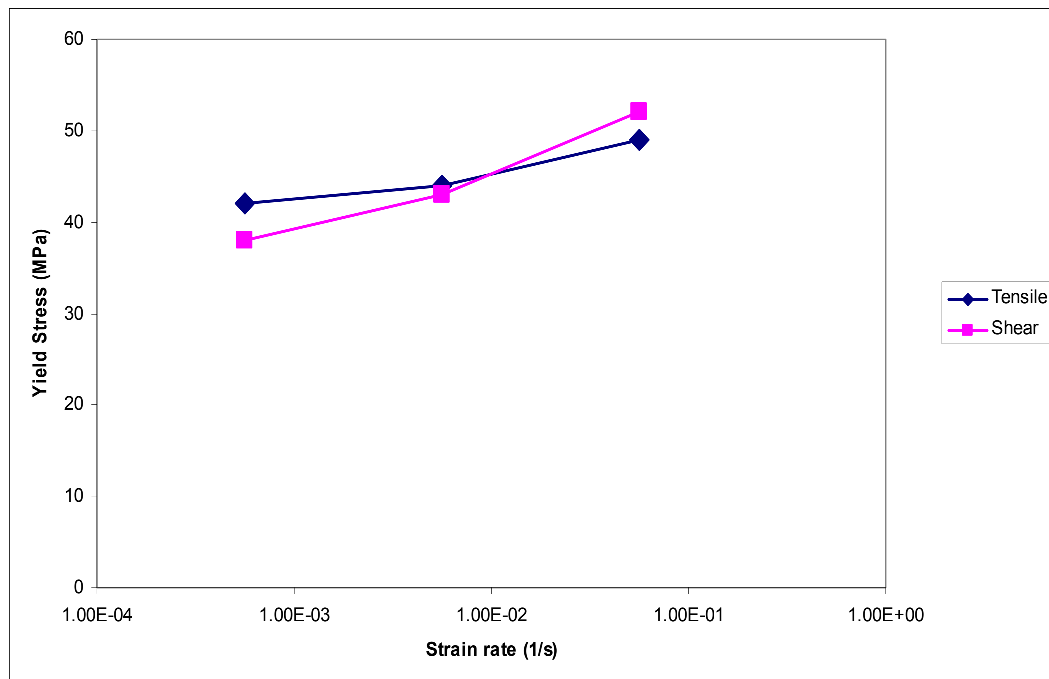

Figure 1.7 Comparison of yield stress for bulk specimens and lap shear solder joint specimens [19]

The effect of Ag content on the fatigue life of Sn-xAg-0.5Cu solder alloys was investigated by Kariya, et al. [20], who found that the strength of the solder alloy increased with increasing Ag content and resulted in shear plastic deformation of the solder bump. As a result, high Ag contents (here 4Ag and 3Ag) exhibited longer fatigue lives than alloys with 1Ag and 2Ag (Figure 1.8). Ma et al. [22] conducted tensile tests of 95.5Sn-4Ag-0.5Cu to determine the temperature dependent stress-strain curves and elastic Young's modulus change with temperature from -75°C to 175°C (Figure 1.9).

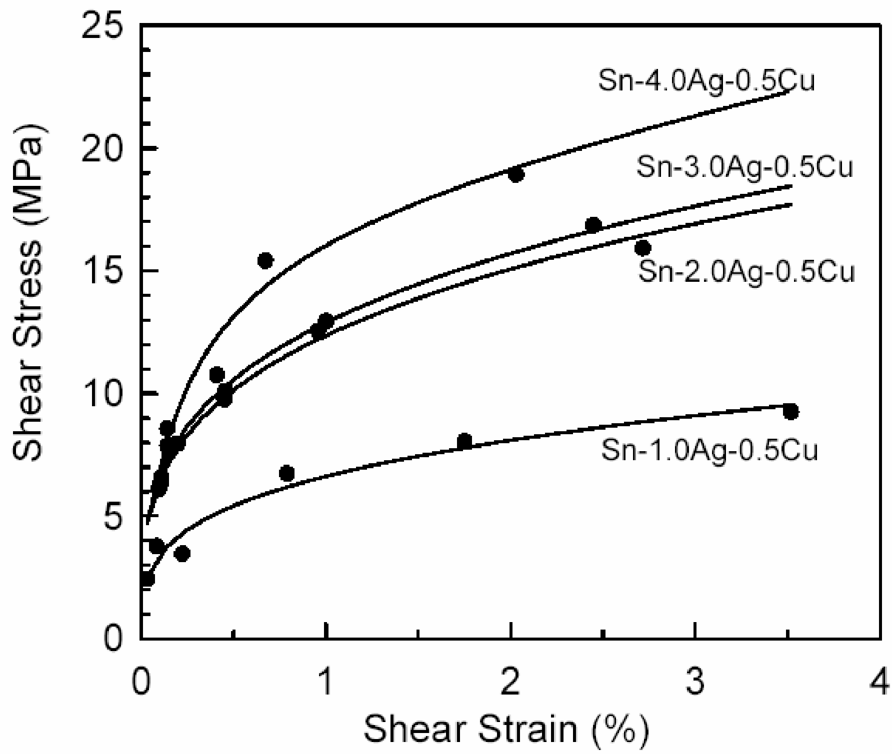

Figure 1.8 Effect of Ag content on stress-strain curves with flip chip solder joint [20]

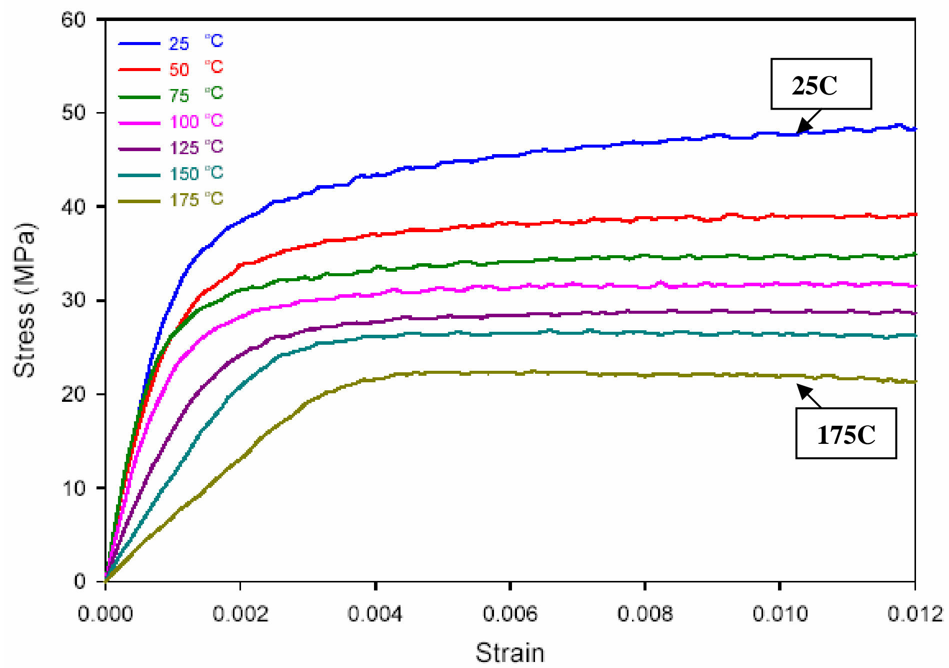

Figure 1.9 (a) Sn-4Ag-0.5Cu tensile stress-strain curves at different temperatures [22]

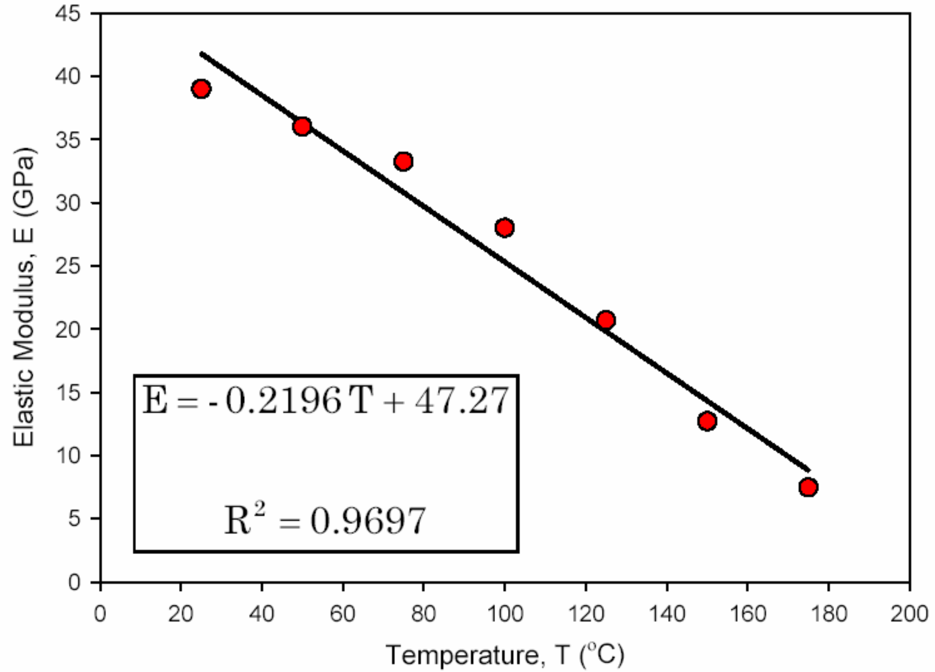

Figure 1.9 (b) Elastic Young's modulus vs. temperature [22]

1.3.3 Microstructure and Tensile Properties of Lead Free Solders

The correlation between the microstructure and mechanical properties of lead free solder is very important as the mechanical properties are dependent on the microstructure, which is in turn affected by different alloy compositions, aging conditions and cooling rates. The investigation of potential lead free solder candidates will provide the fundamental information for electronic package application and solder joint reliability life prediction.

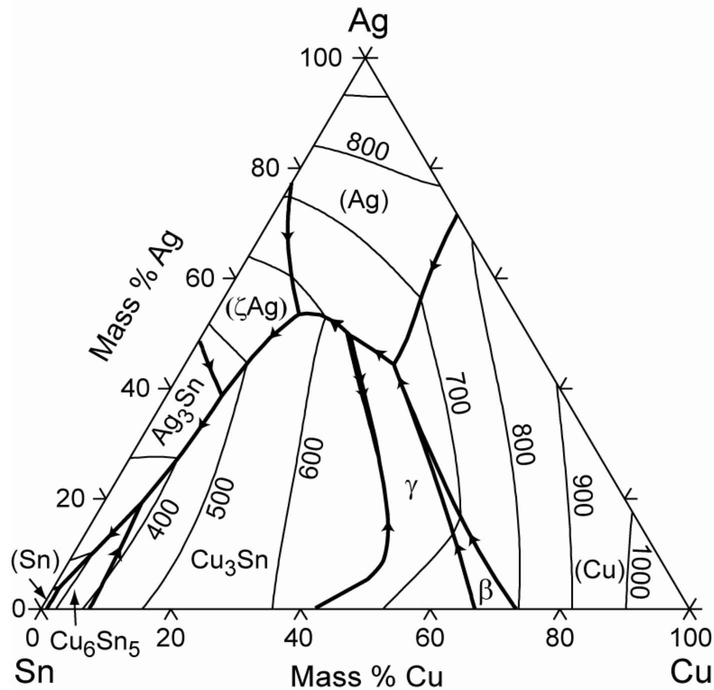

Figure 1.10 Sn-Ag-Cu [11]

Many different solder alloys have been proposed as potential Pb-free solder replacements and the most promising of these fall into the general alloy families of tin-silver (Sn–Ag) and tin–silver–copper (Sn–Ag–Cu). Figures 1.10 and 1.11 show the phase diagrams for Sn-Ag-Cu ternary alloy and Ag-Cu, Sn-Ag and Sn-Cu binary alloys.

Single element systems have a single melting point where the material changes from a single-phase solid material to a single-phase liquid material. This can take a considerable time, but the temperature will remain constant as heat is absorbed to dissociate the solid-state atoms into a liquid state. For example, pure Ag melts at 961°C, while pure Sn melts at 232°C. However when other elements are added to a pure metal, the melting point of the mixture (alloy) may be depressed and additional eutectic and peritectic reactions can occur due to thermodynamic considerations. When Ag and Sn are combined for example, there is a single composition 96.5%Sn–3.5%Ag (all alloy compositions in this study are by % weight) where the two-phase solid transforms to a single phase liquid at a single temperature (221°C), much like a pure element. This is called the eutectic temperature. Deviating from this composition causes the change from solid to liquid to occur over a range of temperatures, sometimes referred to as the "mushy zone". The temperature at the bottom of the mushy zone is called the solidus, or the point where the first liquid begins to form. The point at the top of the mushy zone is the liquidus, or the point where the last solid melts into liquid. Multiple component systems are more complicated and have more phases that can form, including even lower temperatures where eutectic liquids can exist [60].

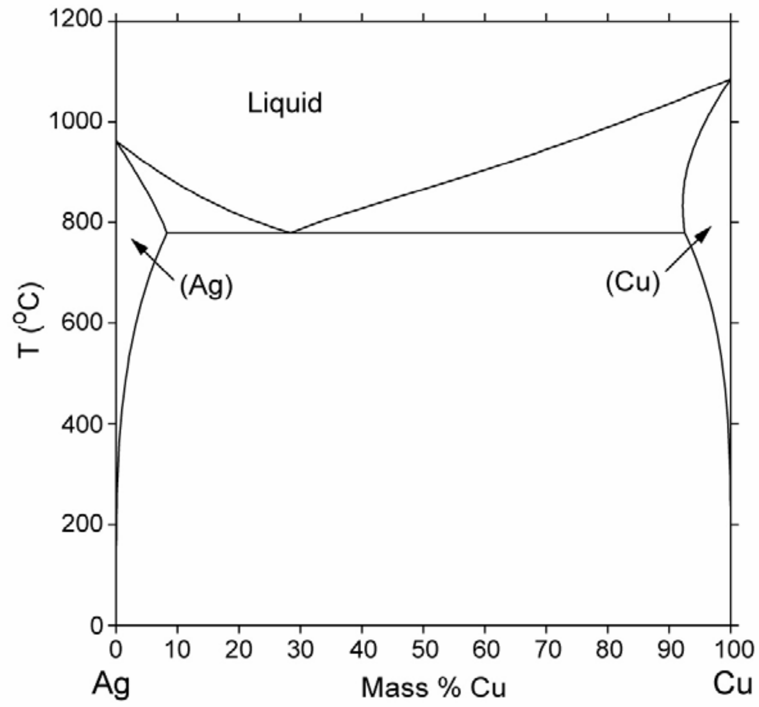

Figure 1.11 (a) Ag-Cu Phase diagram [12]

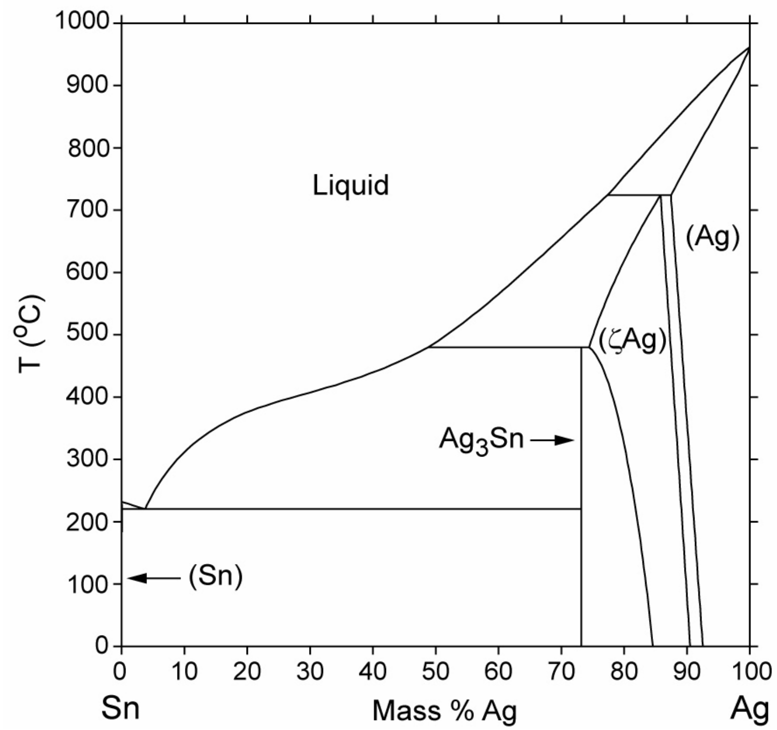

Figure 1.11 (b) Sn-Ag Phase Diagram [13]

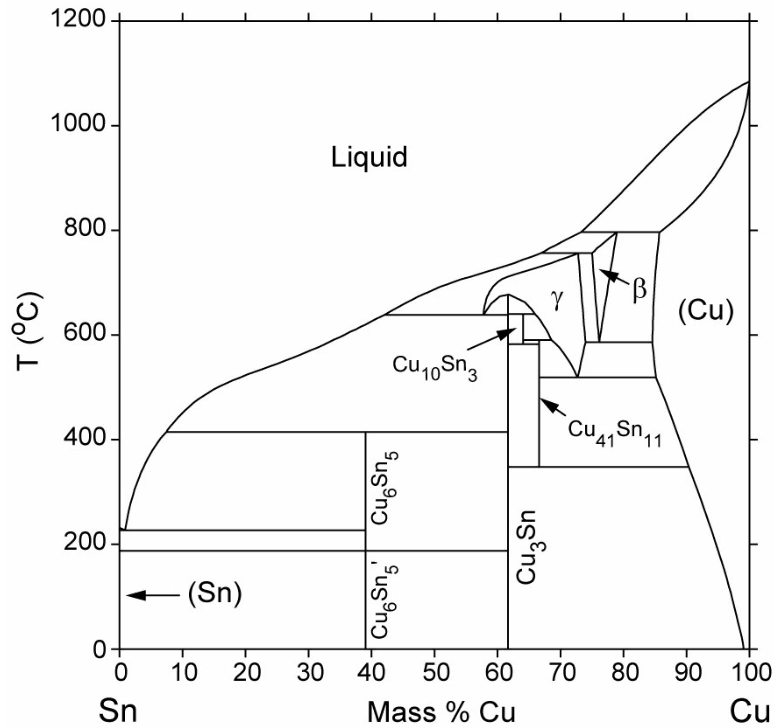

Figure 1.11 (c) Sn-Cu Phase Diagram [14]

Different cooling rates due to different cooling media (water, air or furnace) will produce different microstructures [23]. For example, the microstructure of a eutectic Sn-Ag solder consists of Ag_3Sn intermetallic in an Sn-rich matrix phase. The cooling rate will determine the morphology of the Ag_3Sn intermetallic and modify the extent of dendrite formation in the Sn matrix (Figure 1.12). Chawla, et al. [23] measured the Young's modulus of an Sn-3.5Ag wt% solder alloy by two techniques: loading-unloading measurements in tension, and non-destructive resonant ultrasound spectroscopy (RUS). Table 1.2 reveals that the Ag_3Sn morphology, as controlled by the cooling rate, had no significant effect on Young's modulus.

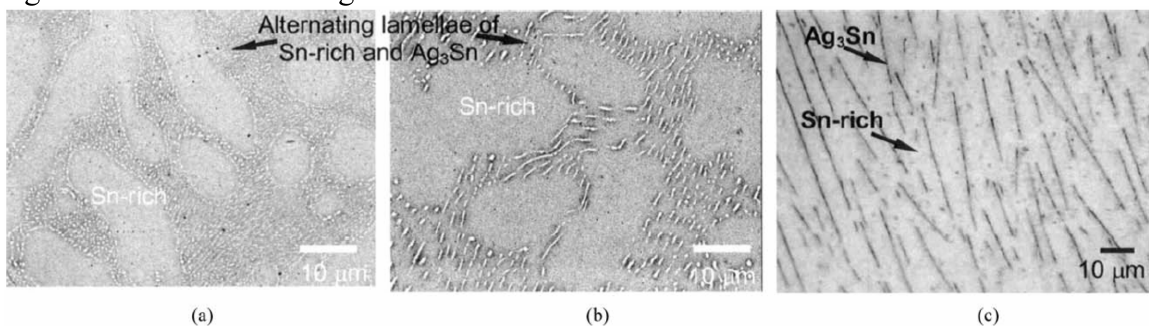

Figure 1.12 Microstructure of Sn-3.5Ag solder at different cooling rates (a) 24 ^{o}C/s spherical Ag_3Sn morphology, (b) 0.5 ^{o}C/s, lower aspect ratio needles, (c) 0.08 ^{o}C/s, high aspect ratio needles. [24]

Table1.2 Young's modulus of Sn-3.5Ag solder measured by tensile loading-unloading [24]

Cooling rate ($^{\circ}C\,s^{-1}$)	Porosity (%)	Young's modulus – tensile (GPa)
24 (water)	0.7 ± 0.2	48.1 ± 0.9
0.5 (air)	0.9 ± 0.1	47.3 ± 0.02
0.08 (furnace)	0.7 ± 0.1	48.7 ± 0.9

Research on the aging effects on microstructure has focused on the growth kinetics of the intermetallic layers that form between the different alloys and substrates. Phase coarsening was observed during thermo-mechanical cycling [29-31]. A planarization of scallop-type intermetallic compounds was observed in solid-state aging, and the growth of layer-type intermetallics was shown to follow diffusion-controlled kinetics [31]. The relationship between microstructural and mechanical aging effects in eutectic and Pb-free solder alloy Sn3.9Ag0.6Cu was reported by Xiao, et al. [21]. When aged at room temperature this alloy continually age-softened, which correlated with the growth of relatively large tin-rich crystals. When aged at 180 ^{o}C, the same alloy initially age softened, reaching the minimum flow strength after one day, which correlated with the growth of relatively large tin-rich crystals and with coarsening of the Ag_3Sn particles. However, after one day the alloy began to age-harden which correlated with the dispersion of Ag_3Sn into tin-rich crystals that had previously contained no intermetallic precipitates (Figure 1.13 and 1.14). These results indicated that the aging effects which directly influence new specimen microstructure and resulting tensile and creep properties change must be investigated for the Sn-Ag-Cu system.

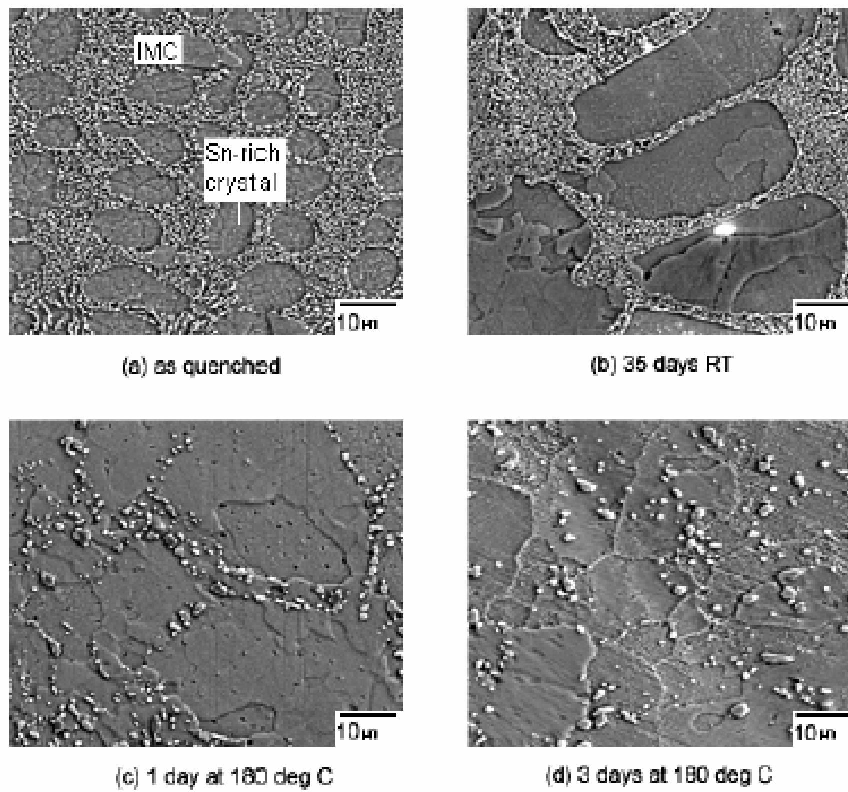

Figure 1.13 SEM-BSE (Backscattered Electron Mode) micrographs of as-aged Sn3.9Ag0.6Cu lead free solder [21]

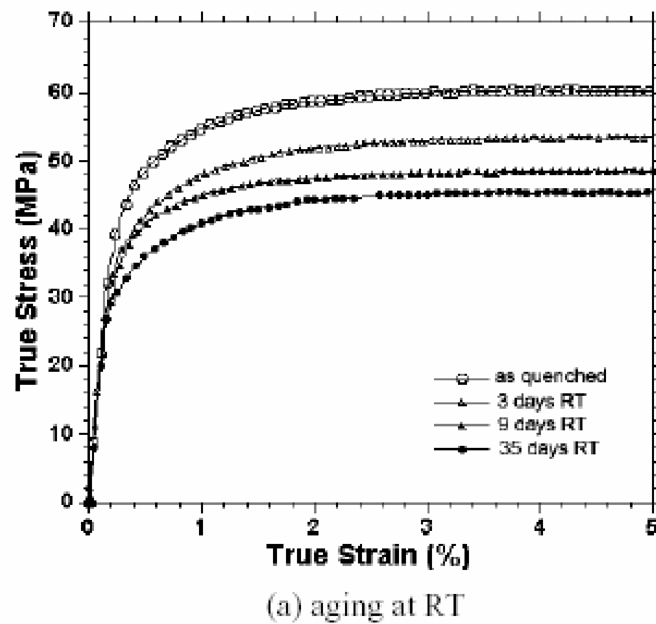

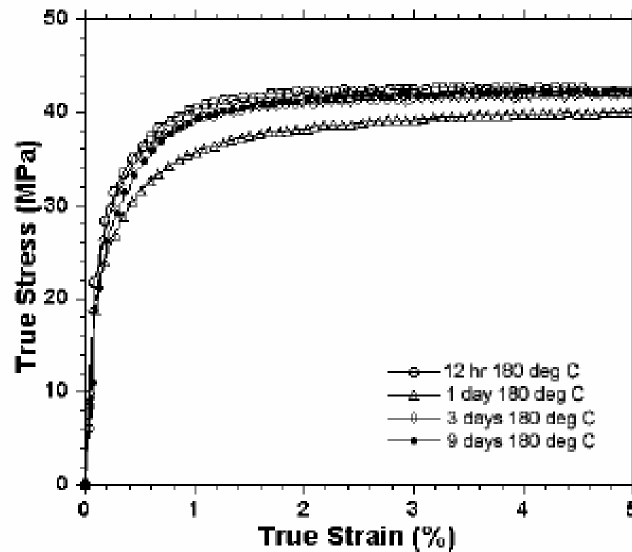

(b) aging at 180 deg C

Figure 1.14 True stress versus true strain data for as-aged Sn3.9Ag0.6Cu lead free solder [21]

1.4 Creep Behavior Investigation for Lead Free Solder

1.4.1 Creep Properties

Creep is the time-dependent deformation of a solid under a stress that below its yield strength. Generally, time-dependent creep deformation can occur at any temperature above absolute zero (0 K), In the low temperature region ($T< 0.5T_M$, where T_M is the absolute melting temperature), the creep strain is very limited and deformation normally does not lead to eventual fracture. The creep phenomenon is generally significant only at temperatures ($T> 0.5T_M$) [61]. The creep curves display typical primary creep, quasi-steady state (constant strain rate) and tertiary rupture stages (Figure 1.15). The quasi-steady state is often dominant in the creep process, which experiences a constant strain rate. The creep strain rate is determined by differentiating the creep strain with respect to time [5]. There is an instantaneous strain formed at the beginning of the process. In the primary stage, the transient strain rate decreases rapidly as strain hardening occurs. The quasi-steady state stage creep correlates with the self-diffusion process, which has a steady strain rate as a result of the balance between strain hardening and recovery [5].

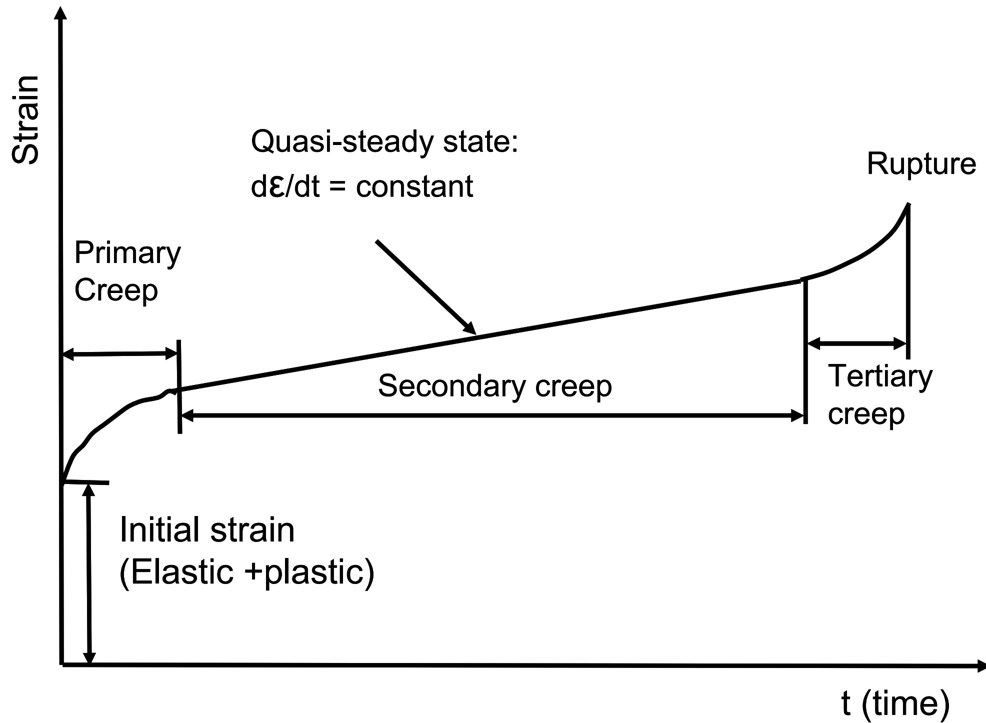

Figure 1.15 - Conventional Steady Strain Rate Creep Curve [5]

1.4.2 Investigation of Reviews of Creep Behavior for Lead Free Solders

Previous studies have shown that the test specimen geometry, cooling option, applied stress, aging time and temperature all affect the creep behavior of lead free alloys [1, 3, 4-6, 36-38]. A double lap joint specimen (Figure 1.16) can be used to provide deformation information for the solder following relative in-plane displacement comparable to that experienced by real surface mount solder joints. Nottay, et al. [3] conducted creep tests using this type of specimen for the alloy 95.8%Sn-3.5Ag-0.7Cu at temperatures of 22, 75 and 125°C and shear stresses of 2.48, 4.97, 6.21 and 7.45 MPa.

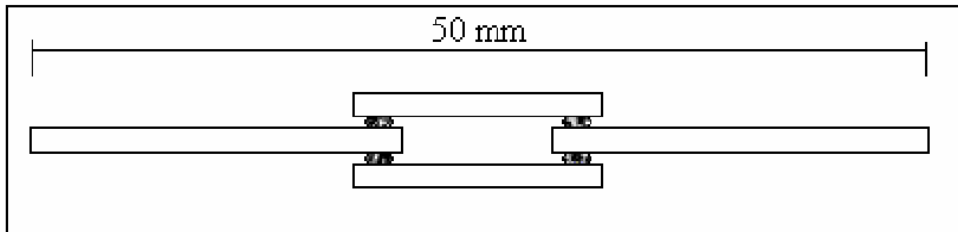

Figure 1.16 Double lap joint specimen [3]

The creep model can be expressed by the Darveaus Model :

$$\frac{d\varepsilon_{cr}}{dt} = A \times \sinh^{n}(\alpha\sigma_{e})\exp(\frac{-Q}{RT}) \qquad (1.3)$$

where $d\varepsilon_{cr}/dt$ is the scalar creep strain rate; T is the absolute temperature, R is the gas constant, σ_e is the Von Mises effective stress, Q is the activation energy, α and n are material dependent constants [3]. Figure 1.17 shows the creep curve, which indicates that the creep rate of SnAgCu is close to that of SnAg and SnPb in the lower stress range but is much higher at higher stresses. Nottary et al. suggested that this difference was caused by the joint area, geometry and test setup used in their experiments [3]. From formula (1.3) we can also concluded that as the temperature increases, the creep strain rate will increase.

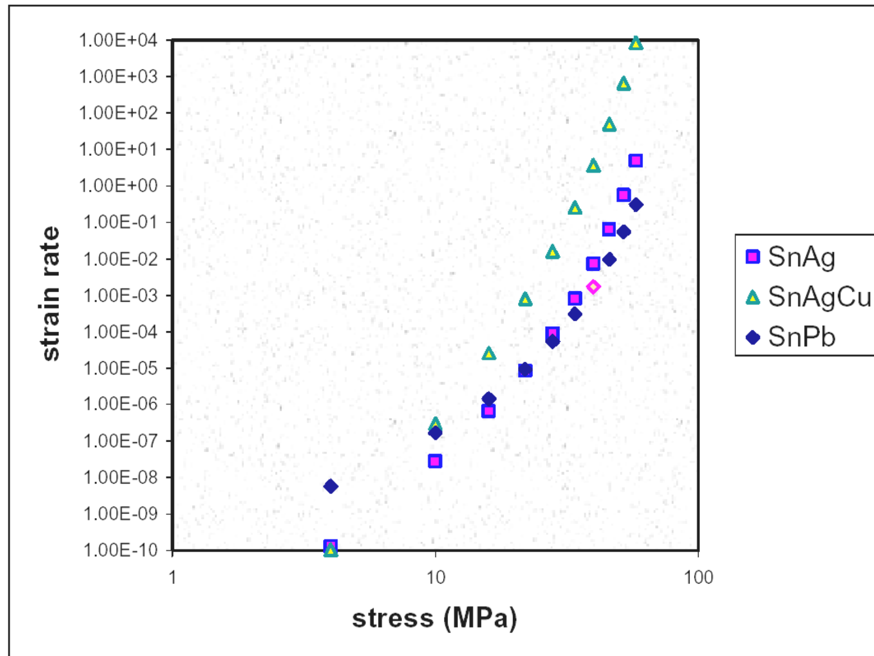

Figure 1.17 Creep properties of 3 different solders [3]

1.4.3 Effect of Cooling Rate on Microstructure and Creep Behavior

Different cooling rates produce different microstructures, thus also affecting the creep behavior of the alloys. Examination of the resulting microstructures revealed that the intermetallic compound Cu_6Sn_5 was finely dispersed in the matrix of β-Sn. Slower cooling rates result in the increased formation of Ag_3Sn and Cu_6Sn_5 intermetallics, while faster cooling rates inhibit their growth [35]. Wu, et al. [36] investigated the tensile creep behavior of eutectic Sn-0.7Cu alloy at three temperatures ranging from 303~393K and steady state creep rates covering six orders of magnitude (10^{-3} -10^{-8} s^{-1}) over a stress range of $\sigma/E = 10^{-4} – 10^{-3}$. The study indicated that the creep rates are controlled by dislocation-pipe diffusion in the tin matrix because the creep data at all temperatures can be fitted by a single straight line with a slope of 7 after normalizing the steady-state rate and the effective stress [36].

During service, microelectronic solder joints are typically exposed to aggressive thermo-mechanical cycling (TMC) conditions with high homologous temperatures and large strain ranges [3] and thus the microstructures of solder joints can undergo rapid strain-enhanced coarsening. Nottay et al. [3] developed a new constitutive model for

solder creep incorporating the effect of microstructural coarsening in order to accurately predict joint reliability. He also indicated the different mechanism of microstructural coarsening between Pb-free solders and Pb-Sn eutectic solder. The microstructure of eutectic Pb-Sn solders in typical microelectronic joints consists of equiaxed grains of Pb-rich and Sn-rich phases, both of which coarsen. This mostly affects the diffusional creep component. In contrast, the microstructure of Sn-Ag-Cu solders typically consist of dispersed intermetallics in a β-Sn matrix and the primary coarsening comes from the rapid coarsening of the finely dispersed intermetallic particles, which is likely to affect the dislocation creep component [3].

Huang, et al. [32] reported that accelerated microstructural coarsening during thermo-mechanical deformation can be attributable to the generation of excess vacancies due to the combined effect of the local hydrostatic stress state (σ_h) and the instantaneous inelastic strain rate (ε). A greater tensile σ_h and a higher ε enhance the local vacancy concentration in the solder, thereby augmenting the diffusive flux and hence the coarsening kinetics. Dispersed intermetallic particles in a lead-free solder alloy are known to undergo substantial strain-enhanced coarsening, and are thus subject to a commensurately increase in the creep rate, during thermal mechanical cycling. Conrad, et al. [34] observed from microstructure pictures [34] that the second phase particles coarsened significantly with progressive aging process.

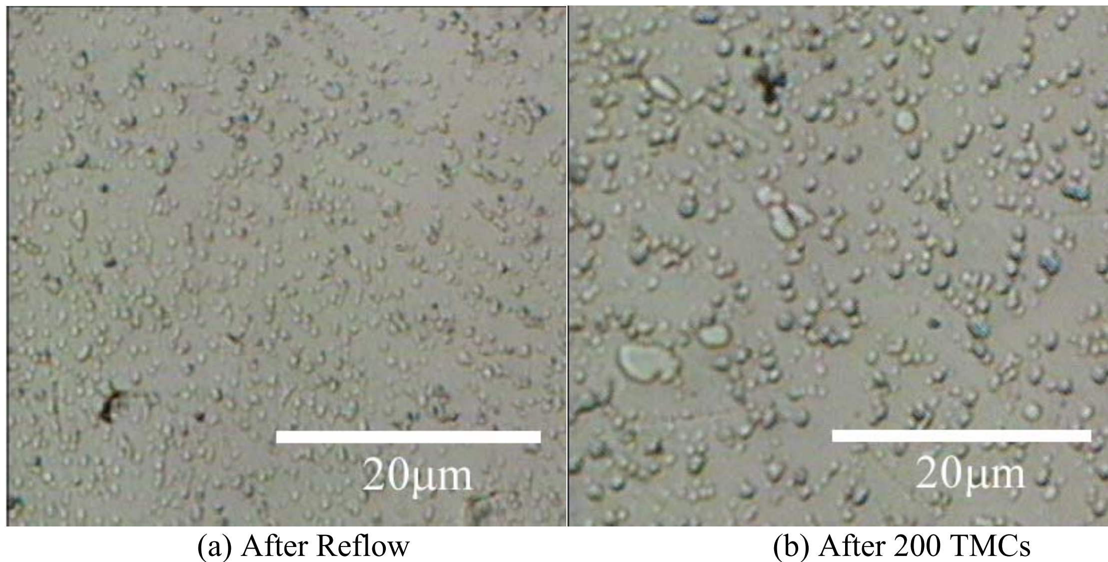

(a) After Reflow (b) After 200 TMCs

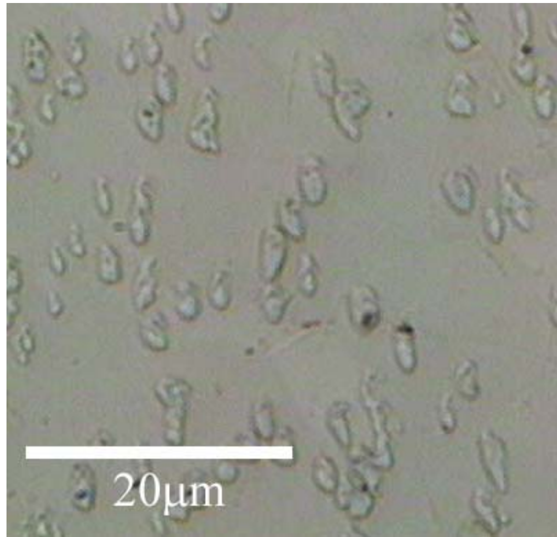

(c) After 1200 TMCs

Figure 1.18 Microstructure of a flip-chip joint of Sn-4.7Ag-1.7Cu [34]

An increase in cooling rate has been shown to result in a decrease in the secondary dendrite size, as well as in the secondary dendrite arm spacing [40]. Rapid solidification decreases the time available for diffusion, resulting in a finer dendrite microstructure. The secondary dendrite arm spacing is related to the solidification time by: [62]

$$SDAS = kt_s^{\,m} \quad (1.4)\ [62]$$

where SDAS denotes the secondary dendrite arm spacing, t_s is the solidification time, and k and m are constants that depend on the composition of the material.

Ochoa et al. [40] found that increasing the cooling rate also decreased the strain-to-failure of the solder. He observed the fracture surface of a water-cooled sample exhibited significant cavity growth, which appeared to originate from decohesion of the Sn-rich dendrites (Figure 1.19 (a)). Furnace cooled samples showed a fibrous morphology due to extensive co-deformation of the Sn-rich and Ag_3Sn phases in the eutectic (Figure 1.19 (b)) [40].

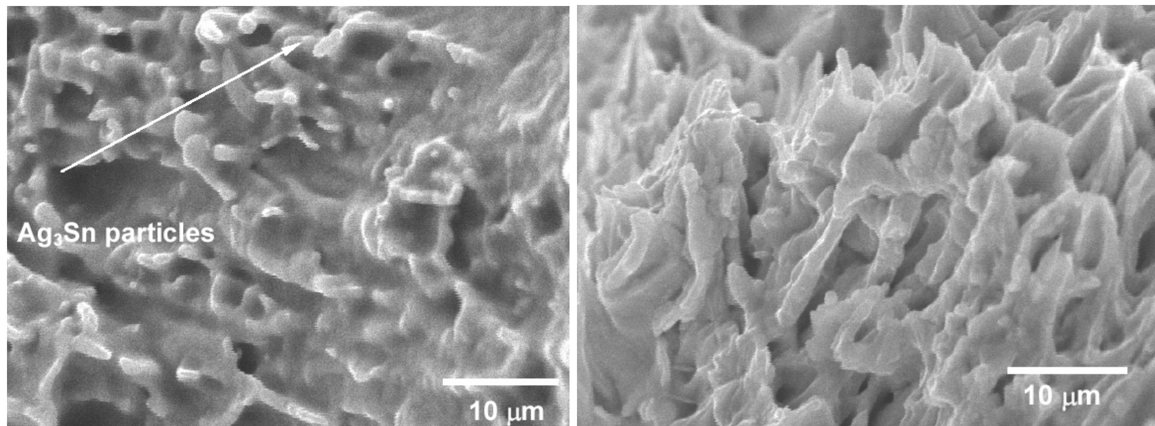

Figure 1.19 Fracture surface for (a) water cooling, (b) furnace cooling [40]

1.5 Effect on Microstructure and Mechanical Properties of Adding a Quaternary Element Metal to the Sn-Ag-Cu Alloy System

Previous research revealed that adding a quaternary element such as bismuth, boron or other metal to the Sn-Ag-Cu alloy system refines the intermetallic particles and increases solidification, thus improving the mechanical properties of the alloy [48, 56, 58, 59]. However the effect of a quaternary element on mechanical properties and microstructure is not clearly understood. More research work needs to be done for the investigation of adding a quaternary element to the existing lead free solder system (for example Sn-Ag-Cu).

Qi, et al. [56] added different amount of Bi (1% and 3% wt) to Sn-3Ag-0.5Cu solder in order to study the microstructure evolution and the growth kinetics at different aging times and the morphology of intermetallic compounds (IMC) changed from a scallop-like shape to planar. The IMC was formed at the solder joint interface when lead free solder reacted with the Cu layer on substrate. The mean thickness of the IMC layer in the solder joints increased with aging time and decreased with increasing Bi contents. McCormack (1994) found that with the addition of Zn to eutectic Sn-Ag, the Zn was incorporated into the Ag_3Sn precipitates, refining the microstructure and tending to suppress the formation of Sn dendrites, while making the Ag_3Sn precipitates finer and more spherical. Ye, et al. [48] found that adding boron particles to Sn-3.5Ag-0.5Cu provided heterogeneous nucleation sites during solidification and therefore refined the microstructure.

CHAPTER 2

Tensile Property Measurement And Microstructure Analysis For Sn-Ag-Cu Lead Free Solders As A Function Of Composition

2.1 Introduction

While the electronics industry appears to be focusing on Sn-Ag-Cu as the alloy of choice for lead free electronics assembly, the exact composition varies by geographic region, supplier and user. Add to that dissolved copper and silver from the printed circuit board traces and surface finish, and there can be significant variation in the final solder joint composition. In this chapter, the results and discussion of a systematic study of the mechanical and microstructural properties of Sn-Ag-Cu alloys with Ag varying from 2wt% to 4wt% and Cu varying from 0.5wt% to 1.5wt%, are presented in detail [28].

Various sample preparation techniques (water quenched, oil quenched and water quenched followed by reflow) were explored and the resulting microstructure compared to that of a typical reflowed lead free chip scale package (CSP) solder joint. The sample preparation techniques used and the comparative microstructures are presented in this chapter. The tensile strength, 0.2% yield strength and the ultimate tensile strength were measured for the range of alloys at conditions of as-cast, aged for 100h at 125°C and aged for 250h at 125 ^{o}C. The results of this work provided the data needed to model the solder joint reliability for a range of Sn-Ag-Cu compositions, along with a baseline for evaluating the effects of subsequent quaternary additions.

2.2 Specimen Preparation

The solder alloy compositions investigated in this study covered Ag from 2.0~4.0 % and Cu from 0.5~1.5%, both by weight percent. Sn was the base metal for all the alloys. In the specimen preparation process, commercial tin shot (purity 99.99 +%, 3mm), silver shot (99.9 +%, 1-5mm) and copper shot (99.5+%, 0.5-0.8mm) were mixed according to the specified composition ratios (Table 2.1), and then combined with small quantities of flux (Kester Tacky Flux TSF-6522). The alloy mixture was placed in a fused-quartz crucible and heated 30°C above the melting point on a hot plate in an inert environment (vacuum was first applied and then the sample was purged with argon gas). The heating profile is shown in Figure 2.1. Table 2.1 shows the chemical composition of the solder alloys as measured by plasma emission spectroscopy. Plasma emission spectroscopy is the method commonly used to analyze the various elements in a sample, where the sample/analytic solution is passed through a plasma (high temperature ionized gas) source, thereby exciting the outer orbital electrons of the analytic with simultaneous emission of electromagnetic radiation (in the form of photons), which are analyzed spectrographically [63].

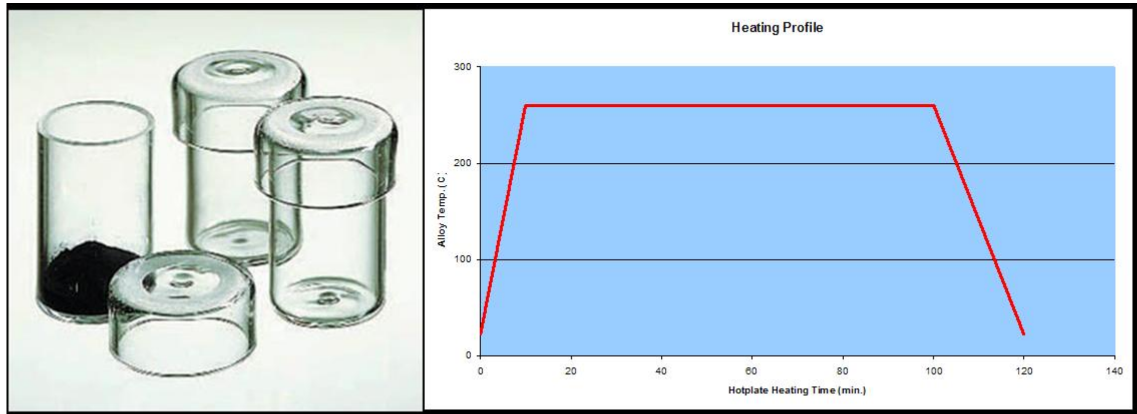

Figure 2.1 Heating profile for alloy melting

Table 2.1 Target Alloy Composition Matrix and Chemical Analysis

Alloy Chemical Composition		Target Cu (wt.%)			
		1.5%	1.2%	0.8%	0.5%
Target Ag (wt.%)	4%	94.7Sn3.9Ag1.4Cu	94.7Sn4.06Ag1.24Cu	95.23Sn3.92Ag0.85Cu	95.52Sn4.0Ag0.51Cu
	3.5%	95.2Sn3.4Ag1.4Cu	95.2Sn3.6Ag1.2Cu	95.64Sn3.5Ag0.86Cu	96.06Sn3.4Ag0.54Cu
	3.0%	95.6Sn3Ag1.4Cu	95.78Sn3Ag1.22Cu	96.28Sn2.9Ag0.82Cu	96.47Sn2.9Ag0.53Cu
	2.5%	96.23Sn2.47Ag1.4Cu	96.44Sn2.4Ag1.16Cu	96.6Sn2.5Ag0.8Cu	96.96Sn2.55Ag0.49Cu
	2.0%	96.58Sn2.02Ag1.4Cu	96.86S2.01Ag1.13Cu	97.28Sn2.02Ag0.8Cu	97.46Sn2.04Ag0.5Cu

The actual chemical analyses are shown in the table along with target composition, as indicated by row and column headings. The microstructure of alloy depends primarily on the cooling option and aging condition chosen. To date, two specimen preparation methods have generally been selected by previous researchers, namely the dog-bone bulk solder specimen, which has bigger physical dimensions than a solder joint, and the flip chip solder joint or lap joint specimens, which are used for shear tests [27, 28]. An advanced specimen preparation process has been developed using rectangular cross-section small glass tubes and a controlled vacuum system (Figure 2.2) [28]. The solder is melted in a quartz crucible (L=120mm, Φ=19mm) with a heating coil. A thermocouple and temperature control module are used to monitor and control the melting process temperature. After the temperature of the molten solder has maintained the desired temperature for 5 minutes the rectangular cross section glass tube connected to the controlled vacuum system is inserted into the molten solder and the molten solder is pulled into the glass tube. The glass tube is then immersed in oil or cold water

immediately after filling. Once the sample is cooled to room temperature, the specimen can be extracted due to the lower coefficient of thermal expansion of the glass compared to the solder (Figure 2.2). Figure 2.3 shows the dimensions of a specimen made by this process [22]. Compared with the dog-bone or casting specimens used by other researchers [3-5, 39], the thickness of the Auburn uni-axial specimen is close to that of a real CSP (0.25~0.5mm) and BGA (0.5mm) solder joints [16, 17]. This new specimen replicates the solder joint thermal history of typical electronic packages and also separates the specimen from the effects of other variables.

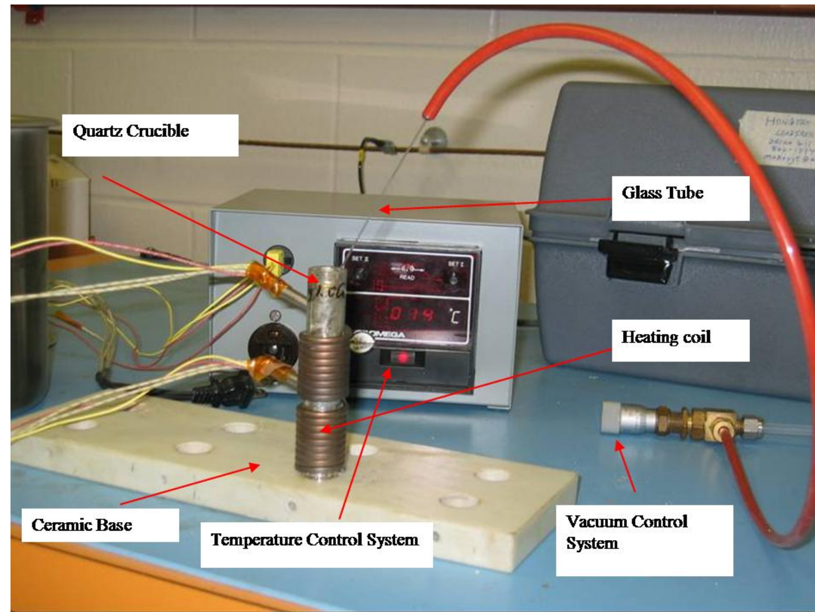

(a) Solder Melting System

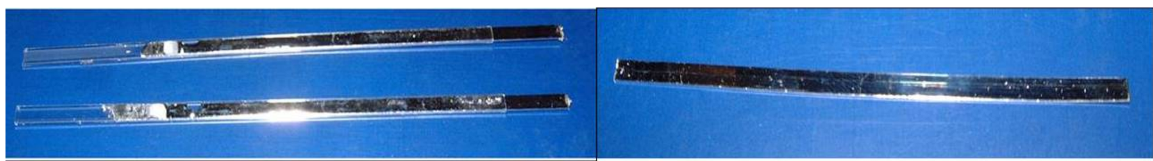

(b) Specimen solidified in glass tube (c) Specimen after removal from glass tube

Figure 2.2 - Solder Melting System and Specimen Preparation [22]

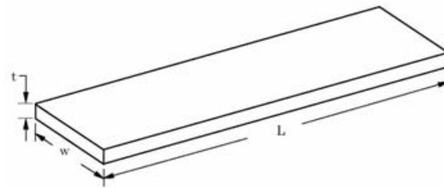

Figure 2.3 - Auburn Uniaxial Specimen [22]

2.3 Microstructure of the Sn-Ag-Cu System

2.3.1 Comparison of Microstructure for Different Cooling Options

The mechanical properties of alloy specimens depend on their microstructure. Hence, the challenge is to make a specimen which has a comparable microstructure to that of a real solder joint. The microstructure is mainly controlled by the specimen geometry and cooling profile [28]. In this study, the cooling options were: oil quenching; water quenching; and water quenching followed by a 248 ^{o}C (or 264 ^{o}C, based on the alloy composition) peak reflow temperature in a Heller 1800 reflow furnace (Figure 2.4 a, b, c, d). The resulting microstructures were compared with that of a comparable CSP solder joint (95.5Sn-4Ag-0.5Cu) reflowed using the CSP quick ramp profile (Figure 2.4 e).

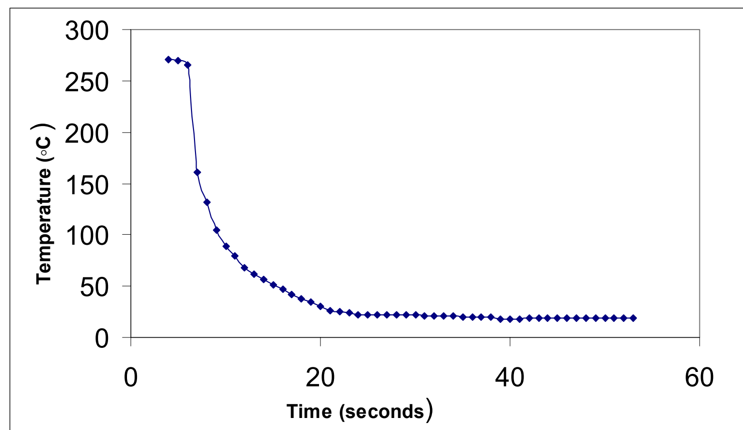

(a) Cooling curve by oil quench

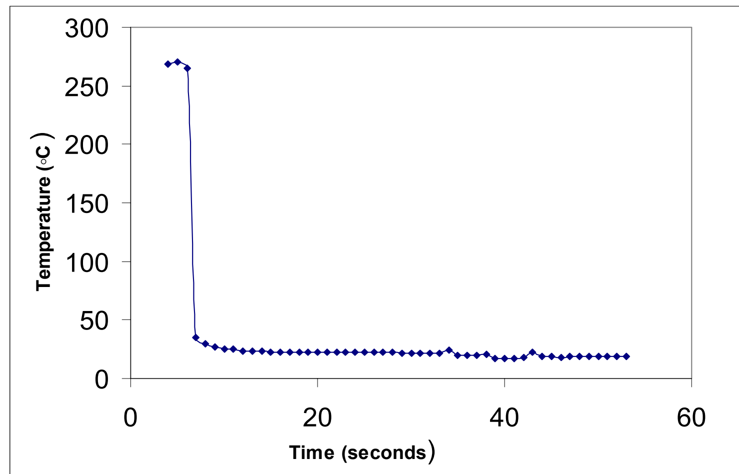

(b) Cooling curve by water quench

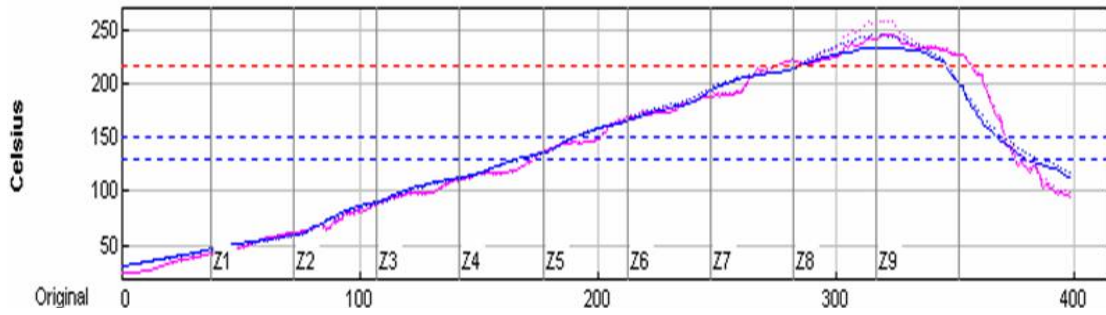

(c) Reflow profile 1 with reflow time (>217 ^{o}C): 84 sec, peak temp: 248°C

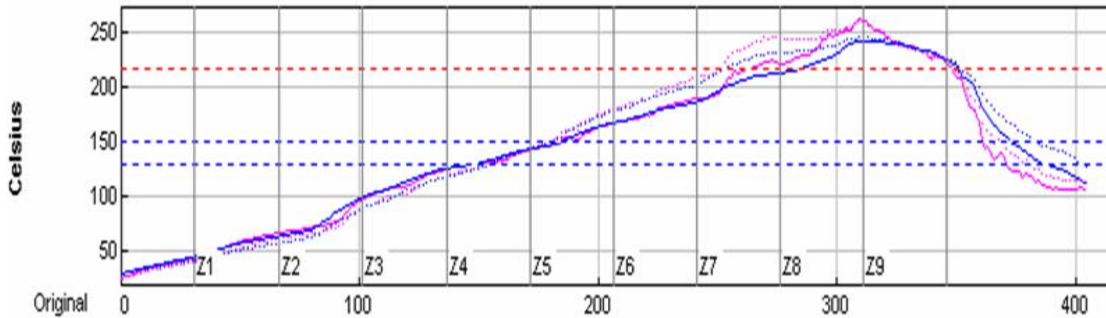

(d) Reflow profile 2 with reflow time (>217 ^{o}C): 86 sec, peak temp: 264°C

Red line: Temp of thermocouple within glass tube
Blue line: Temp of thermocouple between the glass tube and the fixture

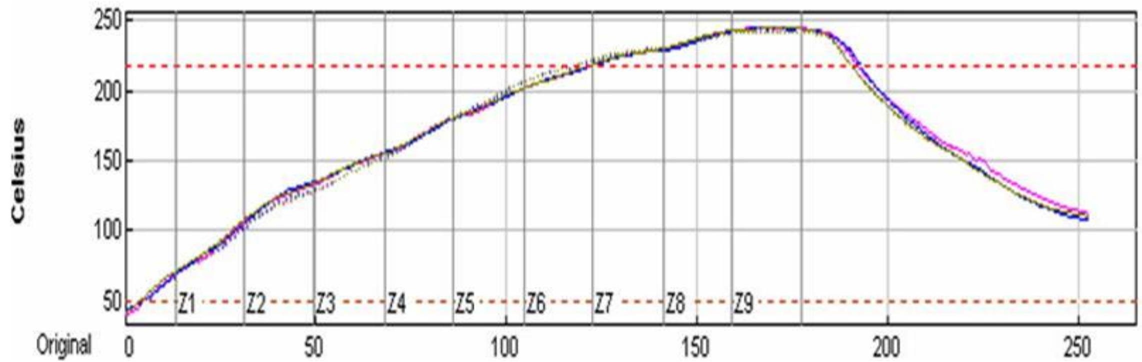

(e) CSP quick ramp reflow profile with reflow time (>217 ºC): 86 sec, peak temp: 264ºC

Figure 2.4 - Different cooling options for specimens and CSP reflow profile

Specimens for each of the different cooling options were cut, mounted, ground then polished with SiC papers, diamond paste and finally with Al_2O_3 paste to a 0.1 micrometer finish. High pressure water was used to clean the surface of the polished specimens after the final step, which proved effective in removing the tiny residues on the solder surface. After each step, the samples were dried by high pressure nitrogen gas. All samples were etched for a few seconds with 5% volume of hydrochloric acid in methanol. A scanning electron microscope (SEM) was used to analyze the microstructure.

Figure 2.5 (a) and (b) show the microstructure of alloy specimens 95.5Sn-4Ag-0.5Cu and 94.5Sn-4Ag-1.5Cu by water quenched cooling, which indicted the dense dendritic Sn with Ag_3Sn precipitates in a fine eutectic.

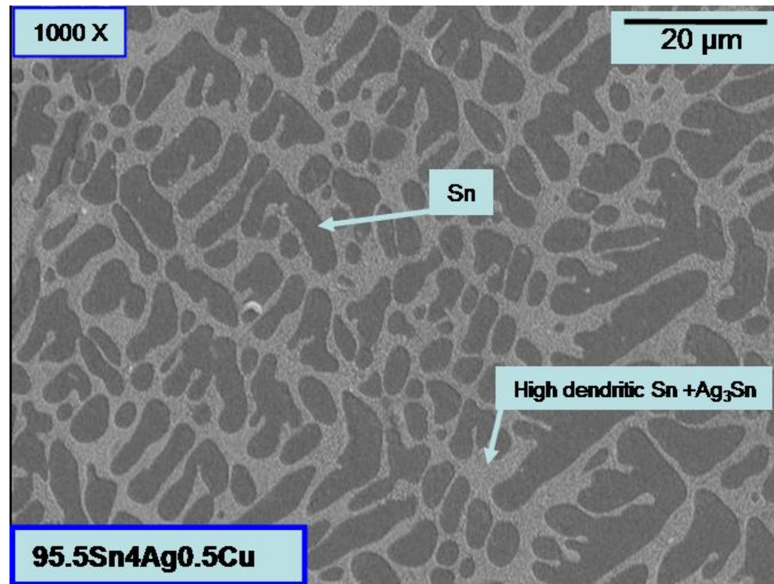

(a) Alloy 95.5Sn-4Ag-0.5Cu

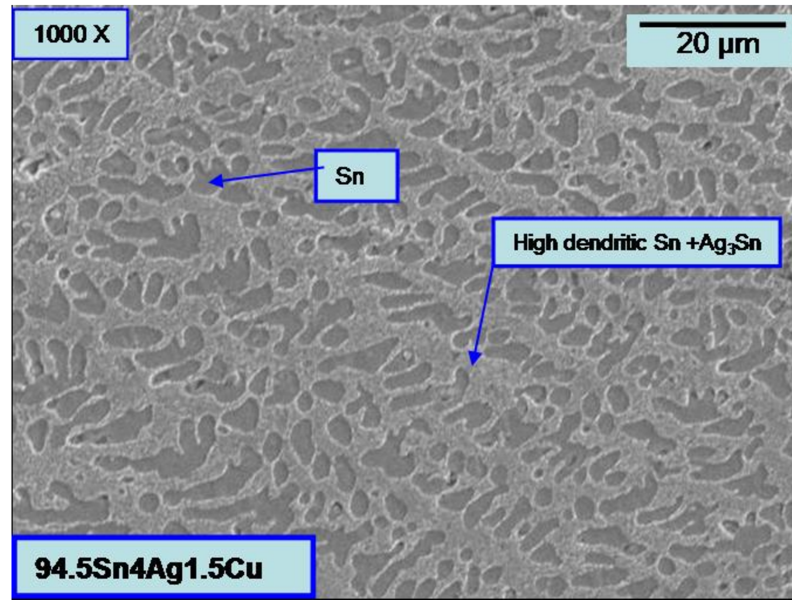

(b) Alloy 94.5Sn-4Ag-1.5Cu

Figure 2.5 SEM microstructure for water quenched specimens

The water quenched and then reflowed specimen was initially proposed to simulate the situation for the real solder joint in package assembly. In the water quenching then reflow cooling option, the specimen was attached to a specially designed fixture (Figure 2.6) at an inclined angle to allow the molten solder to flow to the tape-sealed bottom end and enable any gas bubbles to escape from the top end of the glass tube. In this way, the surface of the specimen was smooth compared to a specimen reflowed horizontally. Two different reflow profiles (Figure 2.4 (c) and (d)) were chosen for different alloy compositions based on the phase diagram (Figure 2.7). The microstructure of water quenched then reflowed specimens was essentially a pure Sn matrix with coarsened eutectic (Sn + Ag_3Sn) and Ag_3Sn precipitates (Figure 2.8 (a, c, d, e), although a small quantity of polygonal Cu_6Sn_5 precipitates were found in samples with a high Cu level content alloy (Figure 2.8(b)).

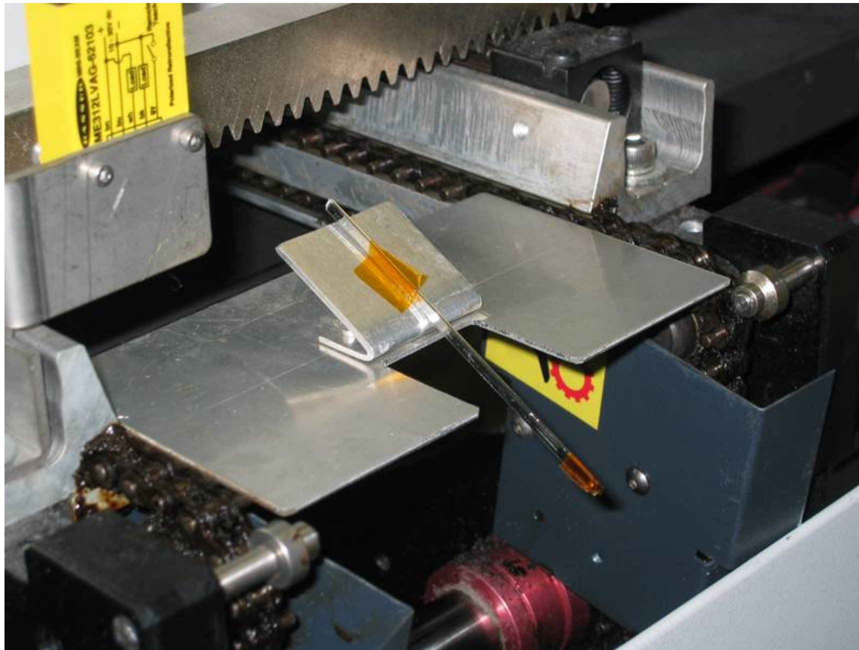

Figure 2.6 Specimen attached to fixture with inclined angle through reflow oven

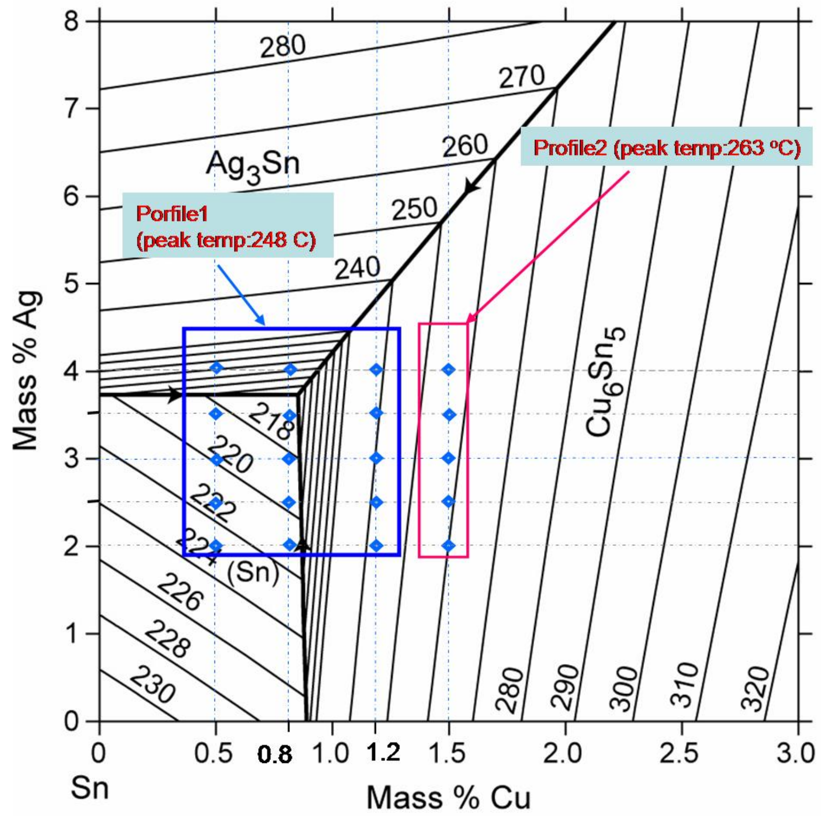

Figure 2.7 Sn-Ag-Cu Phase diagram in Sn-rich corner [11]

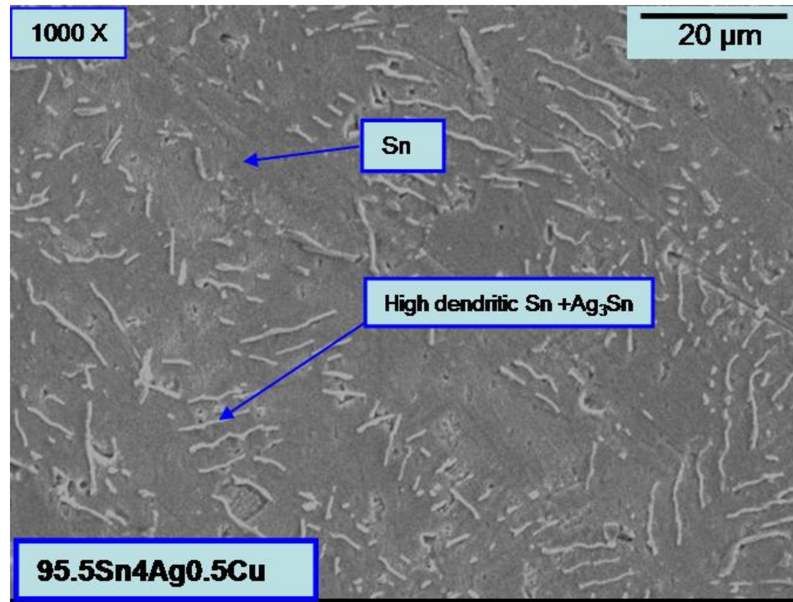

(a) Microstructure of 95.5Sn-4Ag-0.5Cu alloy by water quenched then reflowed

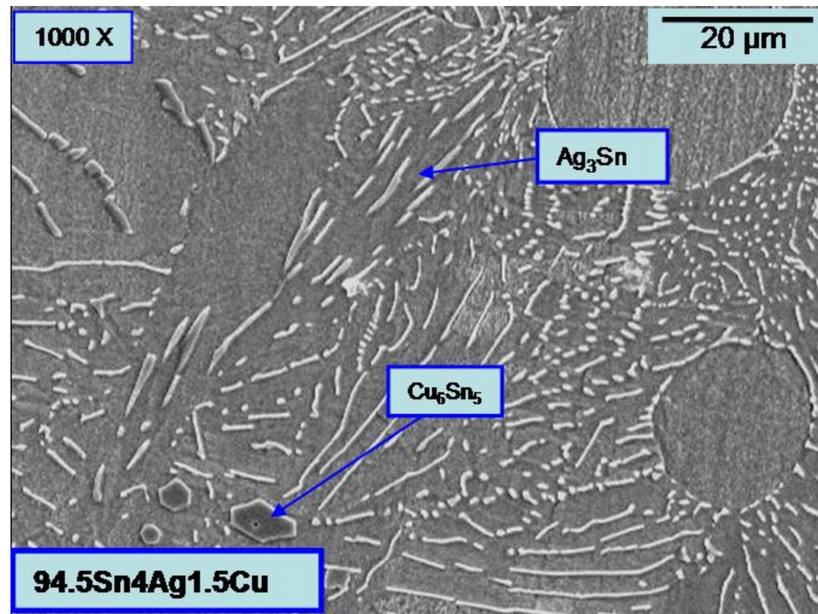

(b) Microstructure of 95.5Sn-4Ag-1.5Cu alloy by water quenched then reflowed

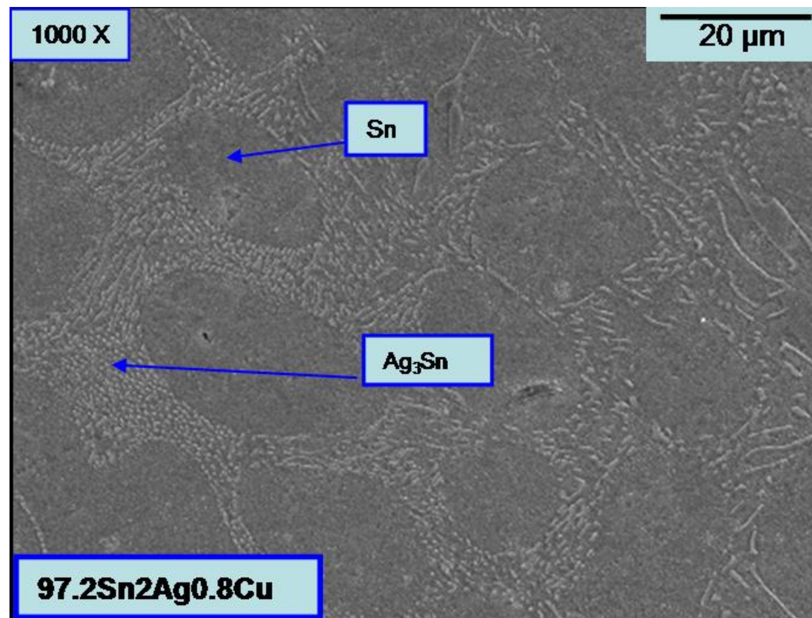

(c) Microstructure of 97.2Sn-2Ag-0.8Cu alloy by water quenched then reflowed

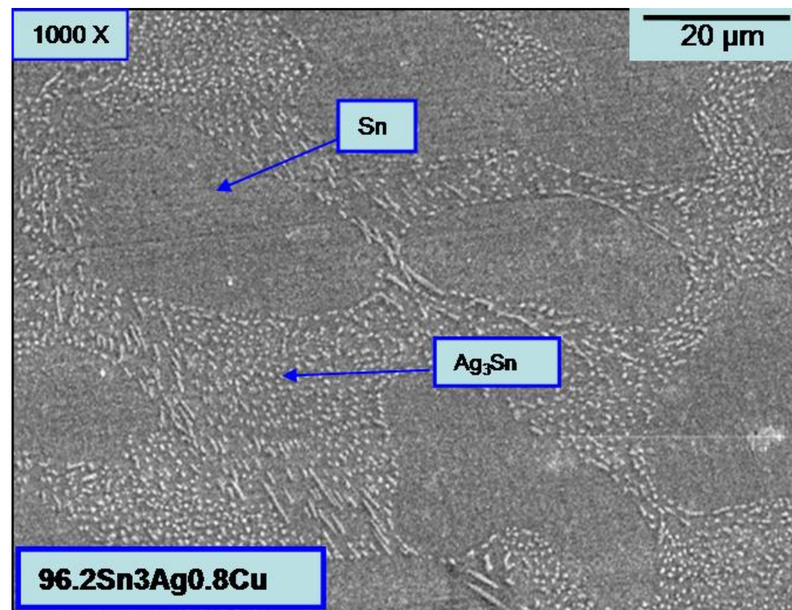

(d) Microstructure of 96.2Sn-3Ag-0.8Cu alloy by water quenched then reflowed

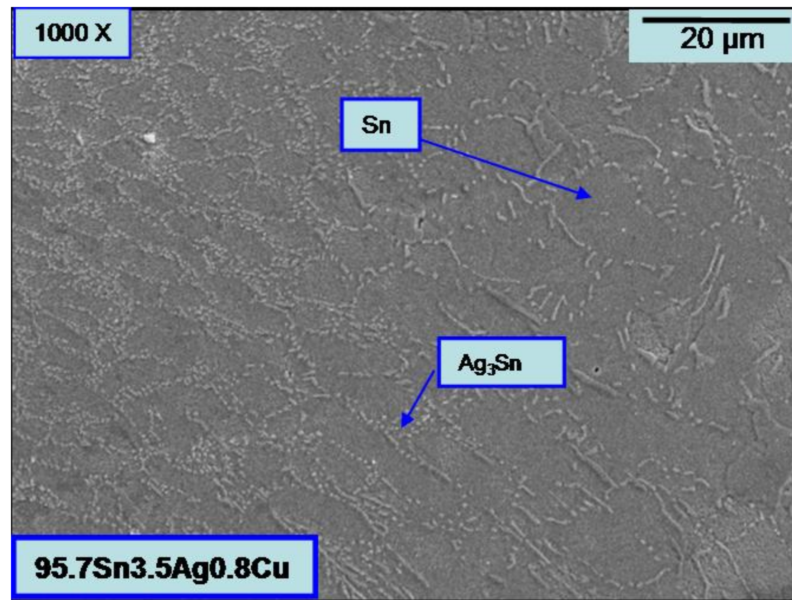

(e) Microstructure of 95.7Sn-3.5Ag-0.8Cu alloy by water quenched then reflowed

Figure 2.8 Microstructure for different alloy compositions by water quenched then reflowed

Figure 2.9 (a, b, c, d) show the SEM microstructure of oil quenched specimen for selected alloys. Figure 2.10 shows the cross section location of the CSP package by x-ray inspection, which ensured the section area was in fact from the middle cross section area of the solder joint. Figure 2.11 shows the SEM microstructure for the whole CSP solder joint, indicating uniform distribution of microstructure through the reflow process.

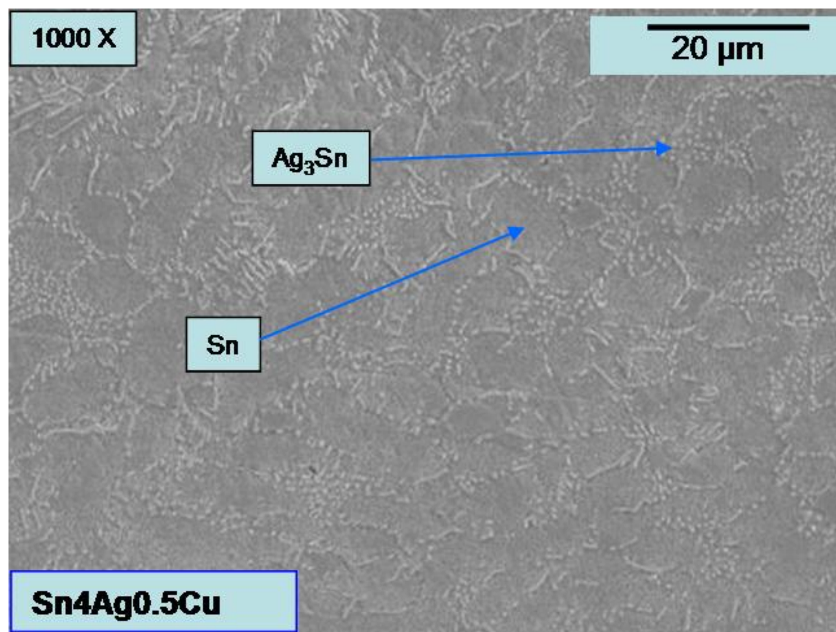

(a) Microstructure of 95.5Sn-4Ag-0.5Cu alloy by oil quenched

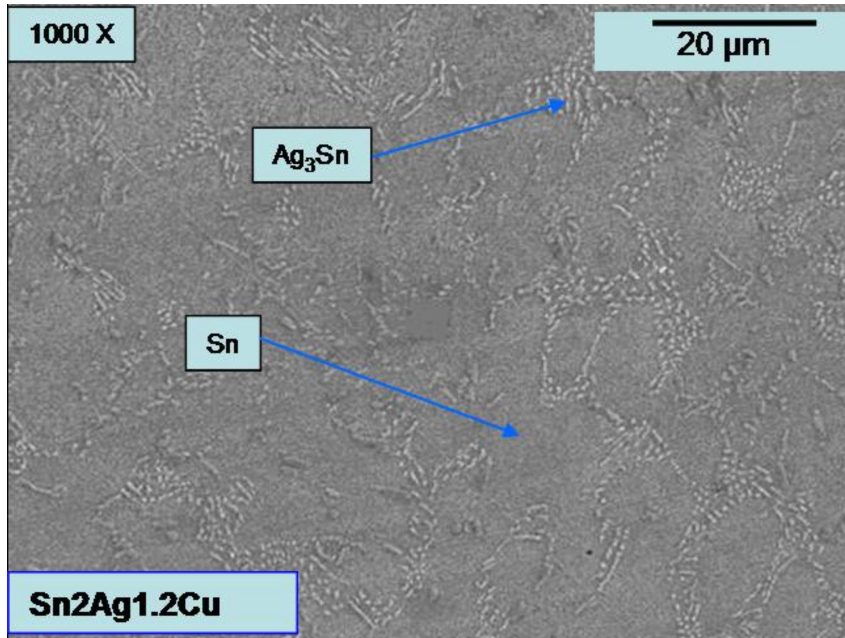

(b) Microstructure of 96.8Sn-2Ag-1.2Cu alloy by oil quenched

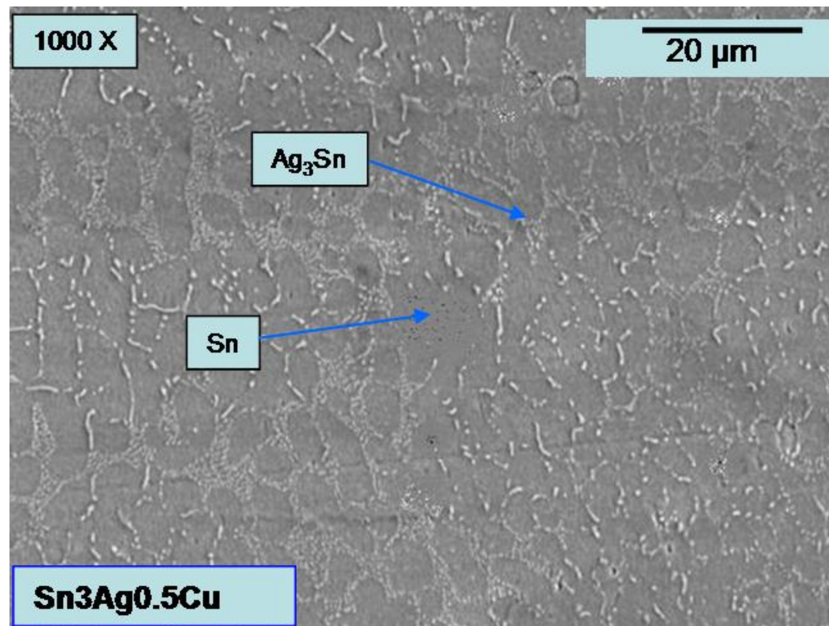

(c) Microstructure of 96.5Sn-3Ag-0.5Cu alloy by oil quenched

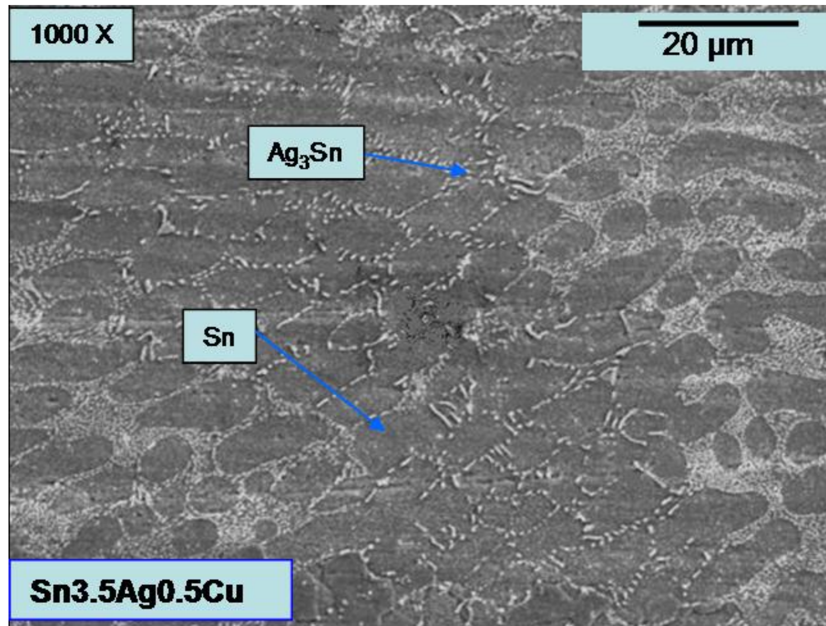

(d) Microstructure of 96Sn-3.5Ag-0.5Cu alloy by oil quenched

Figure 2.9 Microstructure for different alloy compositions by oil quenched

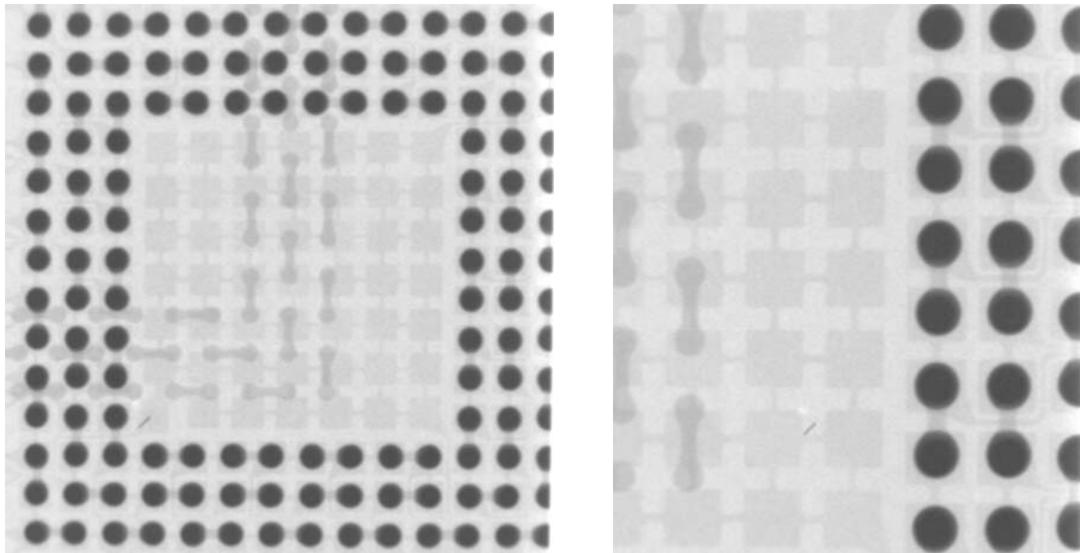
Figure 2.10 Cross section locations for CSP package

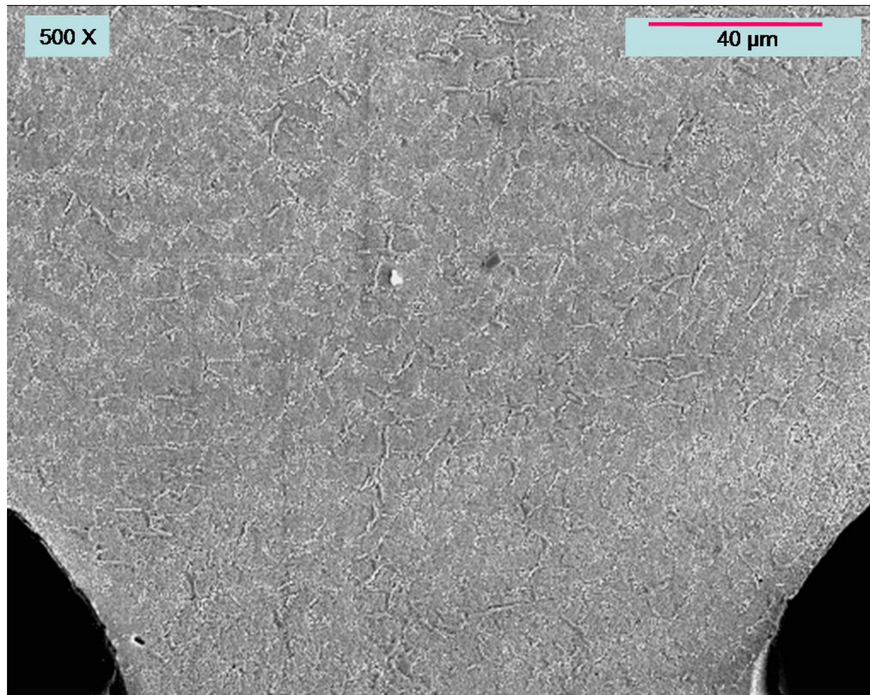

Figure 2.11 Microstructure of entire CSP solder joint

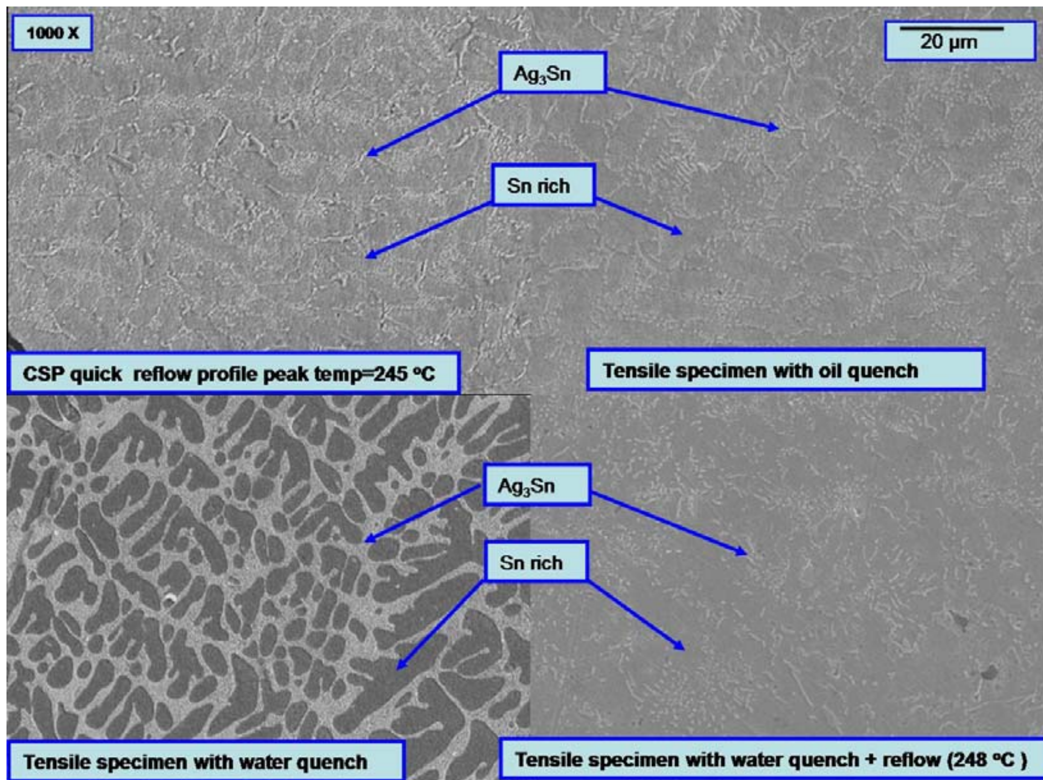

Figure 2.12 -Microstructure comparison between CSP solder joint and specimens with different cooling options for 95.5Sn-4Ag-0.5Cu

Figure 2.12 compares the SEM microstructures (95.5Sn-4Ag-0.5Cu) from the different cooling conditions with that of a CSP solder joint. With the aid of energy dispersion x-ray analysis (EDS), it is found that the dark areas are Sn rich phase and the bright areas, which are needle-like, elongated or spherical, are the Ag_3Sn intermetallic phase. Both the oil quenched specimen and CSP solder joint shown the eutectic region of Sn and moderately dispersed Ag_3Sn intermetallic surrounded by a dentritic Sn-rich phase. The microstructure of the water quenched specimen consisted of a mixture of eutectic regions of dense Ag_3Sn intermetallic within a tin rich matrix surrounding large equiaxed crystals of tin-rich solid solution [21]. The specimen made by water quenching followed by a reflow cycle had a more coarse tin eutectic structure, with irregular dispersed Ag_3Sn intermetallic precipitates. Based on the microstructure evaluation, the water quenched specimen shown had a finer microstructure than the CSP solder joint, while the specimen that was water-quenched followed by a reflow cycle showed a coarser microstructure than the CSP solder joint. The specimen prepared by oil quenching had the microstructure close to that of the CSP solder joint after reflow. Specimens fabricated by water quenching with reflow and oil quenching were used for the tensile test and oil quenched samples were used for creep tests.

The water quenched specimen (faster cooling rate) produced a finer grain size than did either the oil quenched specimen or the water quenched with reflow specimens, both of which had a slightly slower cooling rate. This phenomenon can be explained by applying nucleation and growth theory to the phase transformation [64]. The surface and bulk energies were put together to determine the overall change in energy ($\Delta G_{L\text{-}S}$) on production of a solid nucleus (Figure 2.13):

$\Delta G_{L\text{-}S} = \gamma_{SL}$ x surface area of nucleus + ΔG_V x volume of nucleus

For a spherical nucleus of radius r, this becomes:

$$\Delta G_{L\text{-}S} = 4\pi r^2 \gamma_{SL} + (4/3)\pi r^3 \Delta G_V \qquad (2.1)\ [64]$$

γ_{SL} is the solid-liquid interfacial energy per unit area,
r is radius of nucleus during solidification

$$\Delta G_V = G_S - G_L \qquad (2.2)\ [64]$$

while G_S and G_L are respectively the energy of a unit volume of solid and that of the volume of liquid that transformed to make a unit volume of solid.

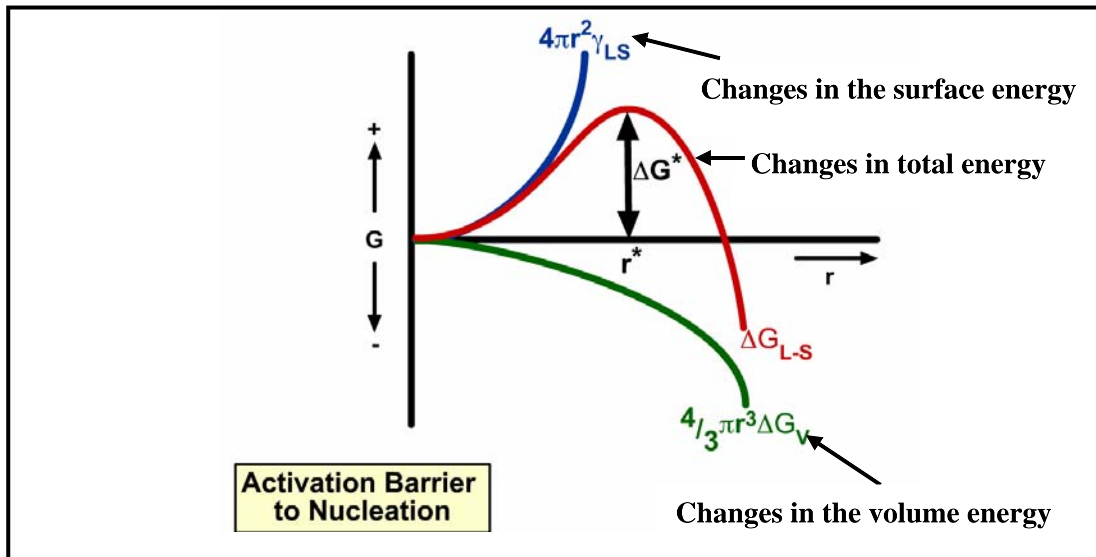

Figure 2.13 Free energy changes as a function of crystallization nuclei size [64]

Any nucleus that forms with a radius r less than r* is unstable and can reduce its energy by reverting to the liquid state. In contrast, any nucleus with a radius r greater than r* is stable and can reduce its energy by continuing to grow. As undercooling $\Delta T = T_M - T$ increases, the ΔG_V term becomes increasingly negative and so the values of both ΔG * and r* fall. Increasing the cooling rate (dT/dt) will increase ΔT_N (the value of ΔT at which stable nucleation actually occurs). This will make nucleation of grains faster and r* smaller, as well as slowing the growth of grains. Consequently, as dT/dt increases the mean grain size decreases and the faster cooling rate will thus produce a finer grain size [64].

2.3.2 Effect of Aging on Microstructure for Oil Quenched Specimens

The Sn-Ag-Cu alloy undergoes major microstructural changes during aging. Figure 2.14 (a) (b) (c) (d) shows the microstructure for the alloy of 95.5Sn-4Ag-0.5Cu initially as cast, after aging for 24h, 100h and 250h at 125 °C. The phase coarsening that occurs during aging is clearly visible, along with the intermallic needle-like or spherical particles that join to form the larger intermallic phase, which appears as platelets. As the Sn-Ag-Cu ternary eutectic consists of Ag_3Sn and very small quantity of Cu_6Sn_5 in a tin matrix, Ardell [47] determined that coarsening of rod-type eutectics can be described in the following equation. Here the rate-controlling process is a volume diffusion control:

$$r^3 - r_o^3 = \frac{6\gamma c_e D\Omega^2}{RT} \times \frac{u^3}{\xi} t \qquad (2.3)\ [47]$$

where r and r_o are the average rod radii at times t and 0 respectively, γ is the rod/matrix interfacial energy, Ω is the rod molar volume, c_e is the equilibrium solute concentration in the matrix, D is the diffusivity of the rate-controlling species, u and ζ depend on the rod

volume fraction. This expression can be altered to take into account the density of intermetallic rods, ρ, based on the assumption of that the volume fraction of the intermetallic rods is constant. c_e and D can be re-written as $c_e=C_0\exp(-Q_s/RT)$ and $D=D_0\exp(-Q_D/RT)$. The following equation represents the combination of these replacements:

$$\rho^{-3/2} - \rho^{-3/2} = \frac{K}{RT}\exp(\frac{Q_s + Q_D}{RT}) \qquad (2.4)\ [47]$$

where K is a constant, Q_s is the heat of solution for the rate-controlling species in the matrix and Q_D is the activation energy for diffusion of the rate-controlling species. The mechanical properties such as Young's modulus, the yield strength, etc. will decrease as microstructure coarsening takes place due to diffusion of the intermetallic rods under high temperature aging.

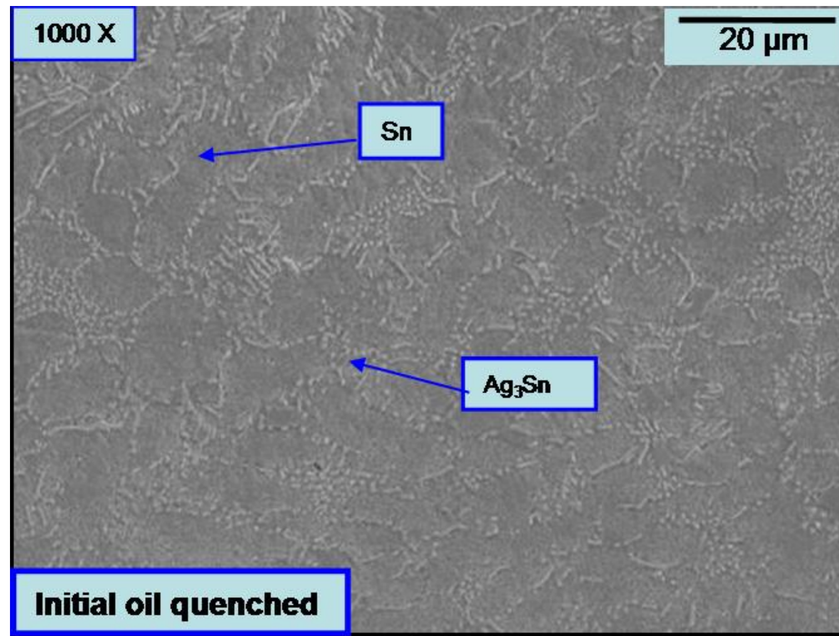

(a) Microstructure for 95.5Sn-4Ag-0.5Cu specimen as cast oil quenched

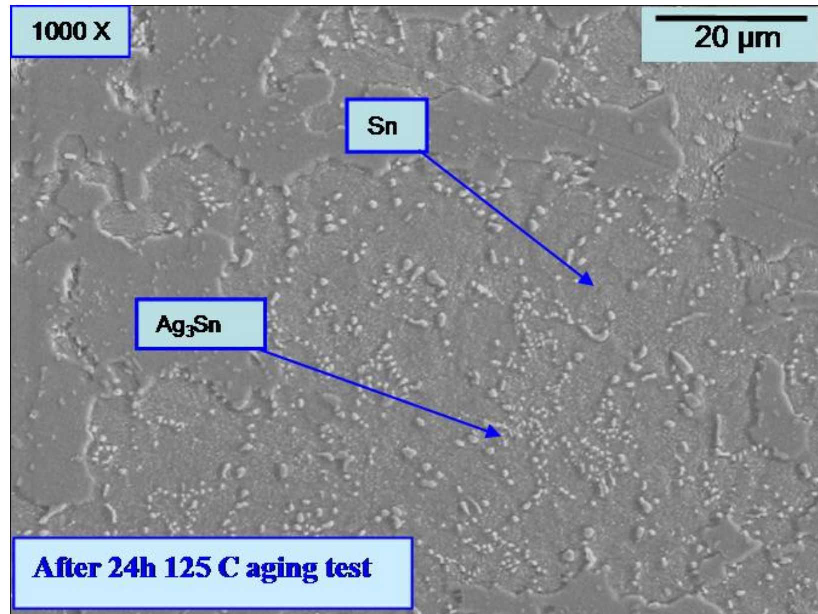

(b) Microstructure for 95.5Sn-4Ag-0.5Cu specimen after 24h at 125C aging

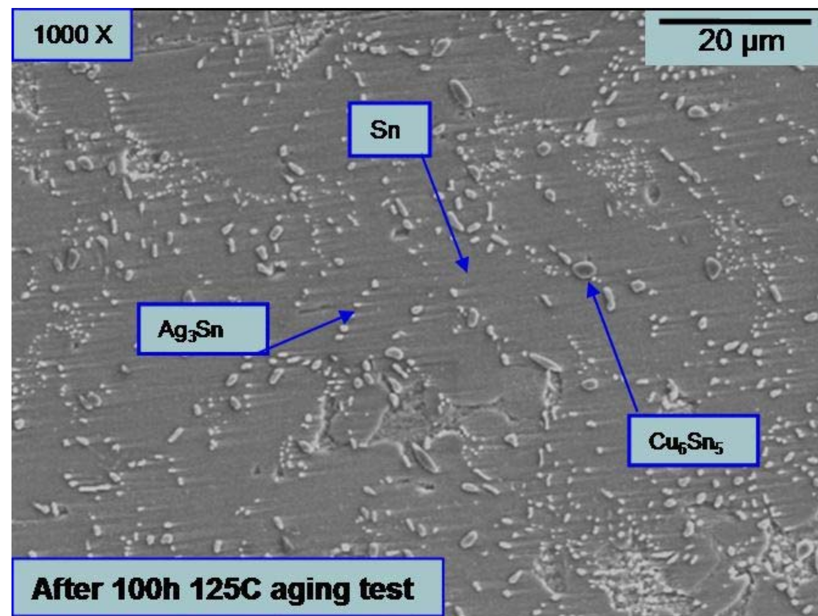

(c) Microstructure for 95.5Sn-4Ag-0.5Cu specimen after 100h at 125C aging

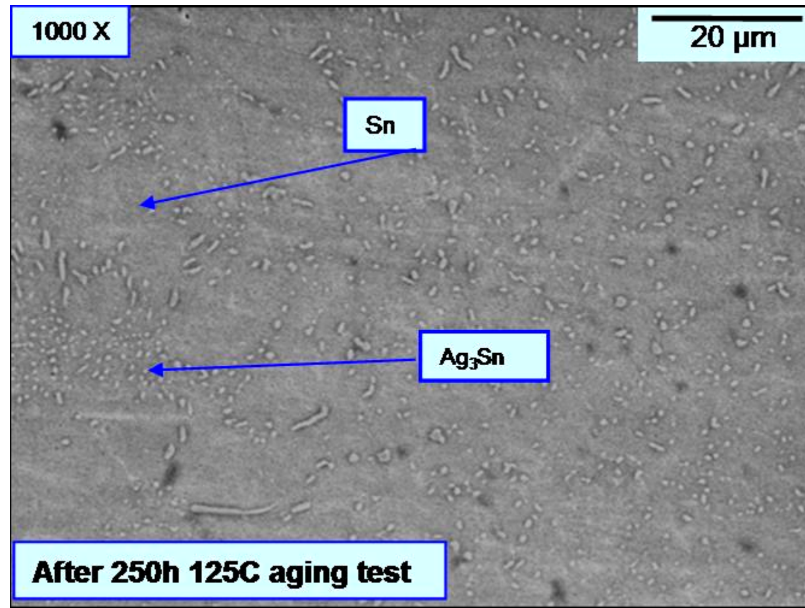

(d) Microstructure for 95.5Sn-4Ag-0.5Cu specimen after 250h at 125C aging

Figure 2.14 Microstructure change for Sn-4Ag-0.5Cu alloy with aging time

2.4 Tensile Properties of the SnAgCu System

2.4.1 Measurement of Tensile Properties

Although Young's modulus data was originally measured in a shear test, the relation $G=E/(2(1+\nu)$ [46] was employed by S. Wiese to convert the data into the Young's modulus. There are three methods for Young's modulus measurement: tensile testing, DMA and ultrasonic pulse [46]. In this research, tensile testing was selected for Young's modulus measurement.

Tensile tests were performed using the MT-200 tension/torsion thermo-mechanical test system made by Wisdom Technology Inc. shown in Figure 2.15. This system provides an axial displacement resolution of 0.1 micrometer and a rotation resolution of 0.001^{o}. The testing machine utilizes displacement control. Load and displacement data were recorded and used to determine the true stress/true strain curve. True stress and true strain were calculated from the engineering stress and strain based on the conventional constant volume assumption. Figure 2.16 indicates the Young's modulus, 0.2%-strain yield stress and ultimate tensile strength on a typical strain-stress testing curve measured at a strain rate of 10^{-3} s^{-1} at 25 ^{o}C.

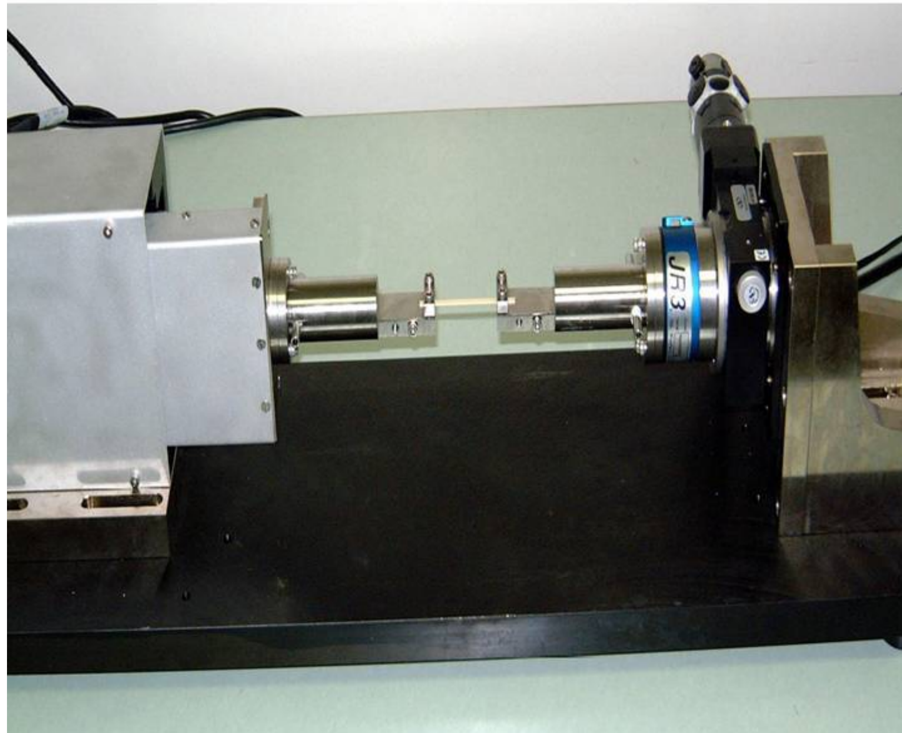

Figure 2.15 - Micro Tension Tester

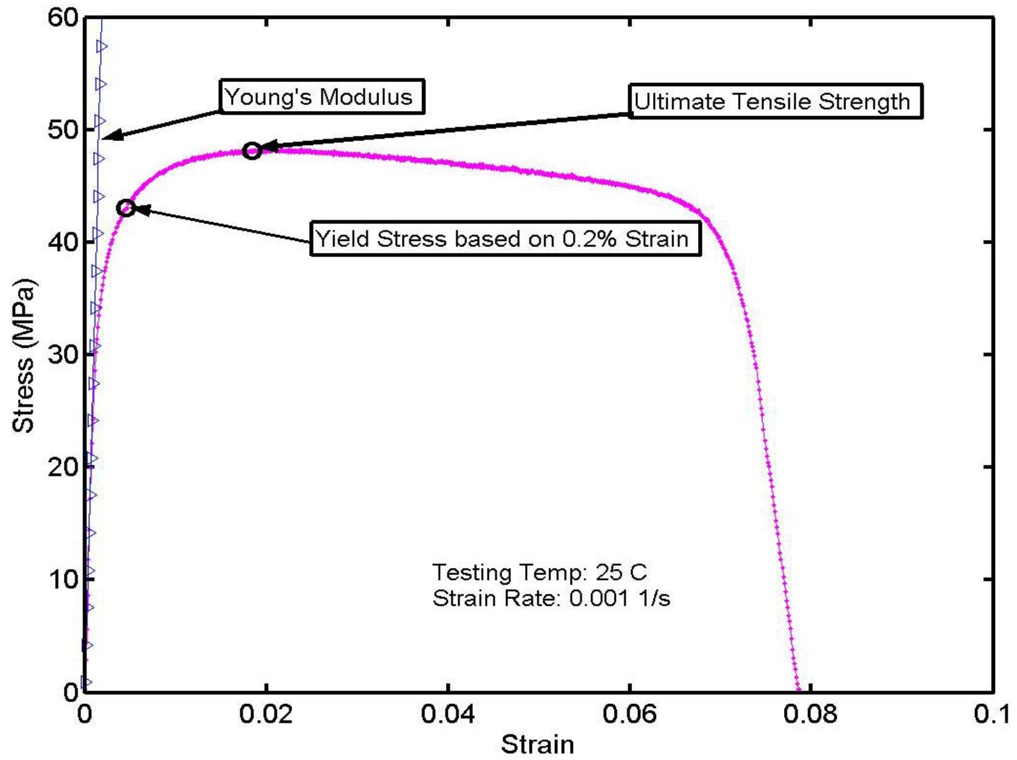

Figure 2.16 Tensile stress-strain curve for an oil quenched 96.5Sn-3.5Ag-1.5Cu sample

A series of stress-strain tensile test curves for 96.5Sn-3.5Ag-1.5Cu is shown in Figure 2.17 to represent the general test results. At least five specimens were tested for each alloy composition at each set of test conditions. Figure 2.16 shows that the tensile test data is in good agreement with the elastoplastic model for 96.5Sn-3.5Ag-1.5Cu. The elastoplastic model of lead free solder exhibits an elastic phase until a critical stress is reached (the yield point), after which plastic behavior becomes dominant. This model is normally used to predict the deformation of an alloy using the stress-stain curve.

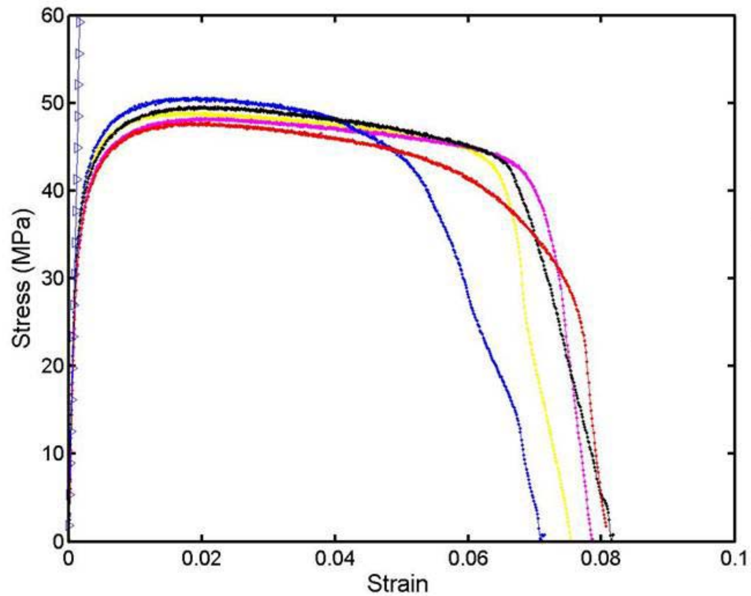

(a) Tensile measurement curves

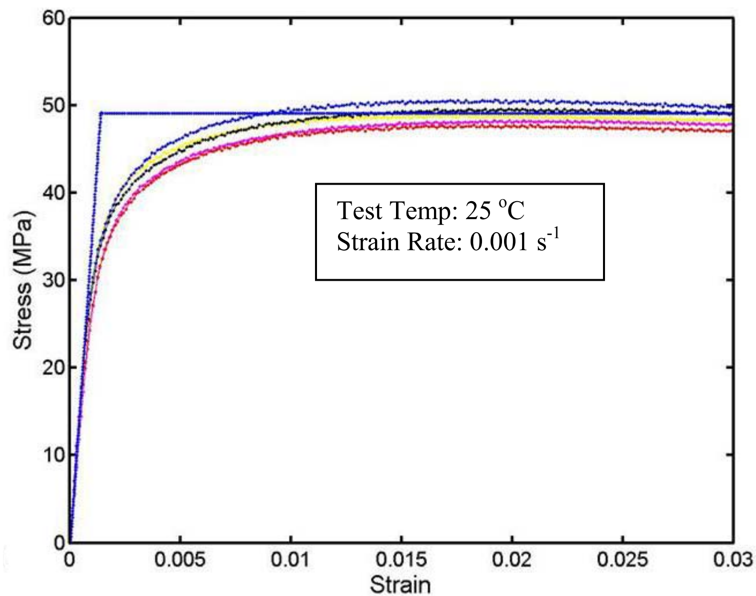

(b) Elasto-plastic model

Figure 2.17 Stress - strain tensile curve for oil quenched 96.5Sn-3.5Ag-1.5Cu samples

2.4.2 Tensile Properties as a Function of Alloy Composition for Water Quenched and Reflow Samples

Young's modulus, 0.2% strain yield stress and ultimate tensile strength were measured for all 20 selected alloy compositions (Table 2.1) in the as-cast condition using the water quenched with reflow cooling process. The distribution of tensile properties as a function of alloy composition is shown in Figure 2.18 (a, b, c). Young's modulus as a function of alloy composition (Ag=2%~4%, Cu=0.5%~1.5%) ranged from 31-40 GPa, which indicated significant differences in Young's modulus as a function of alloy composition. Generally, the Young's modulus increased with increasing copper wt%. The distribution of 0.2% strain yield stress and ultimate tensile strength as a function of alloy composition followed the same trend as Young's modulus, and both were significantly higher at higher levels of copper content.

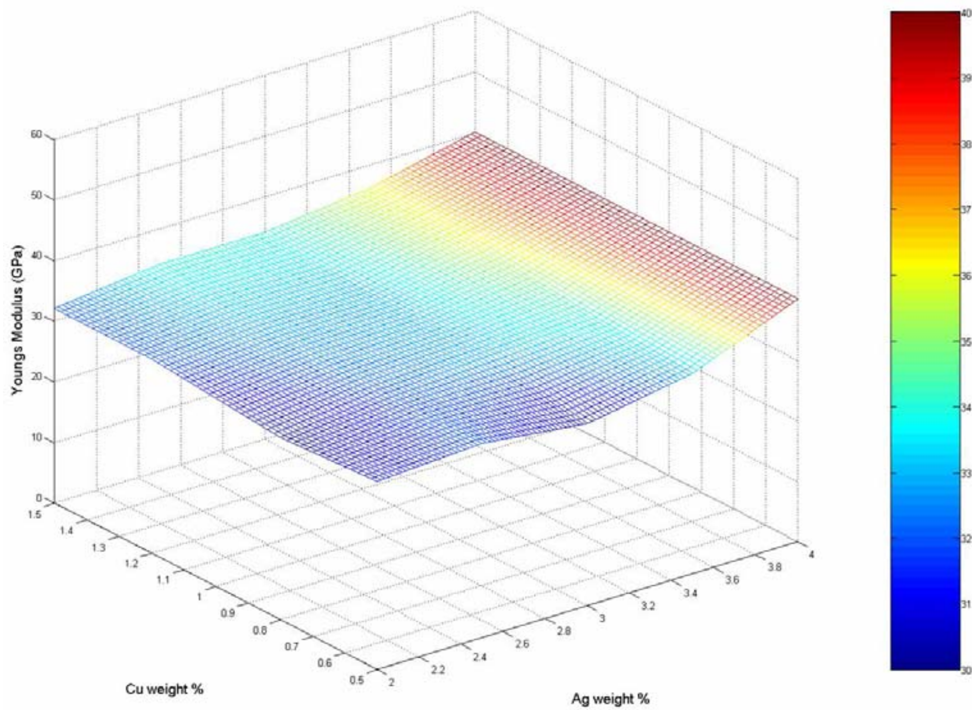

Figure 2.18(a) - Distribution of Young's modulus as a function of alloy composition

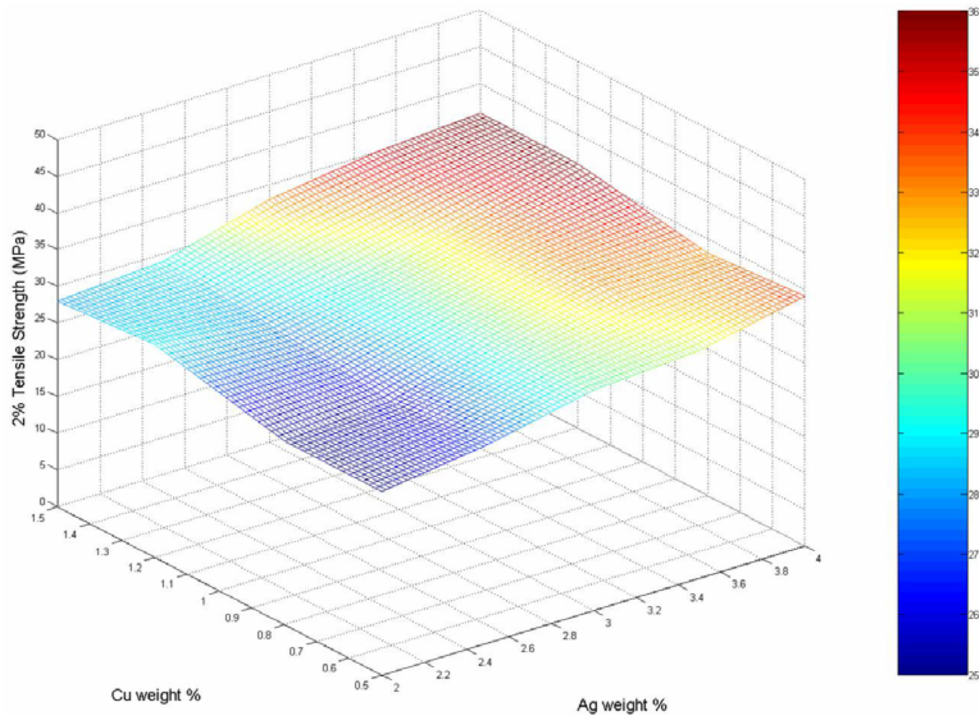

Figure 2.18(b) - Distribution of 0.2% tensile strength as a function of alloy composition

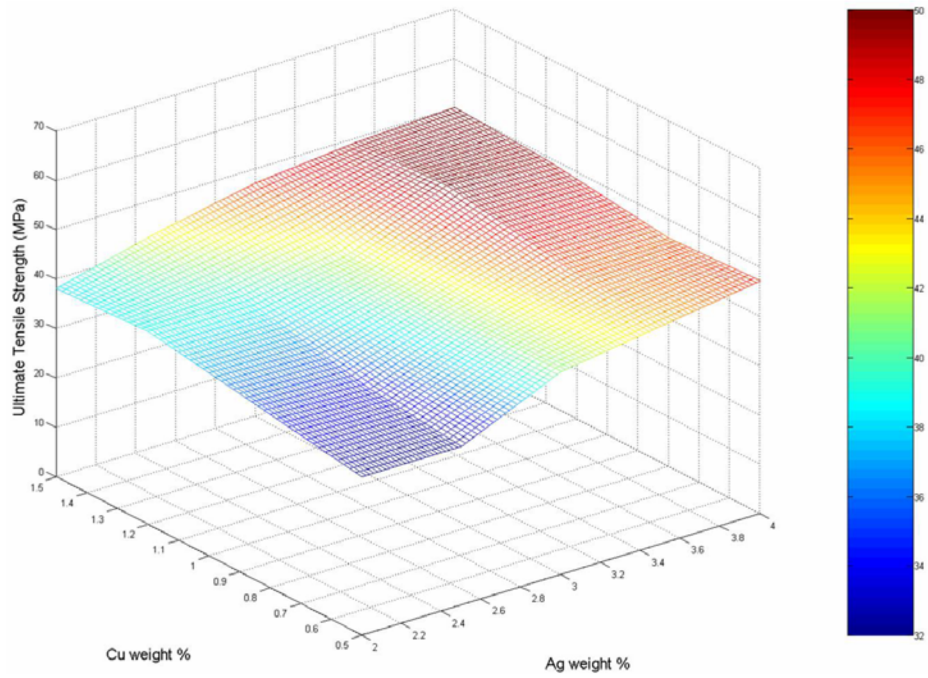

Figure 2.18(c) - Distribution of ultimate tensile strength as a function of alloy composition

2.4.3 Tensile Properties as a Function of Alloy Composition for Oil Quenched Samples

Young's modulus, 0.2% strain yield stress and ultimate tensile strength were measured for all 20 alloy compositions (Table 2.1) by oil quenched under three conditions (as-cast, aged for 100h at 125 ^{o}C, and aged for 250h at 125 ^{o}C). The distribution of tensile properties as a function of alloy composition and their change with aging time are shown in Figures 2.19~2.21. Young's modulus (Figure 2.19) as a function of alloy composition (Ag=2%-4%, Cu=0.5%-1.5%) as cast ranged from 37-41 GPa and decreased to 30-32 GPa after aging for 100 hours and 250 hours at 125 ^{o}C. There was no significant difference in Young's modulus as a function of alloy composition. After the initial decrease in modulus after 100 hours at 125 ^{o}C, there was only an insignificant change with further aging.

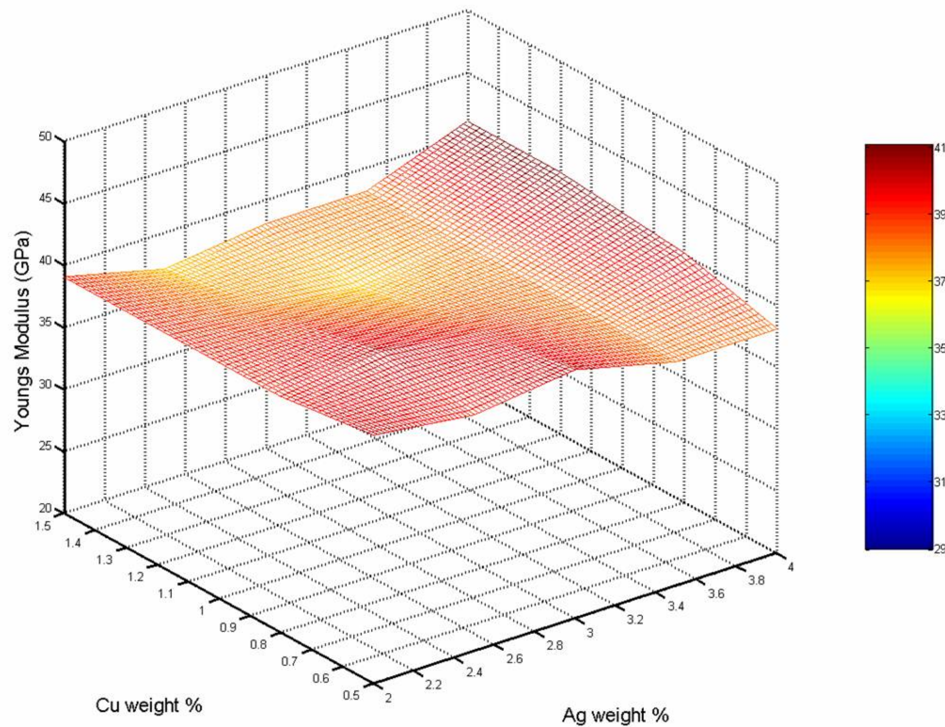

Figure 2.19(a) - Distribution of Young's modulus as a function of alloy composition (As-cast)

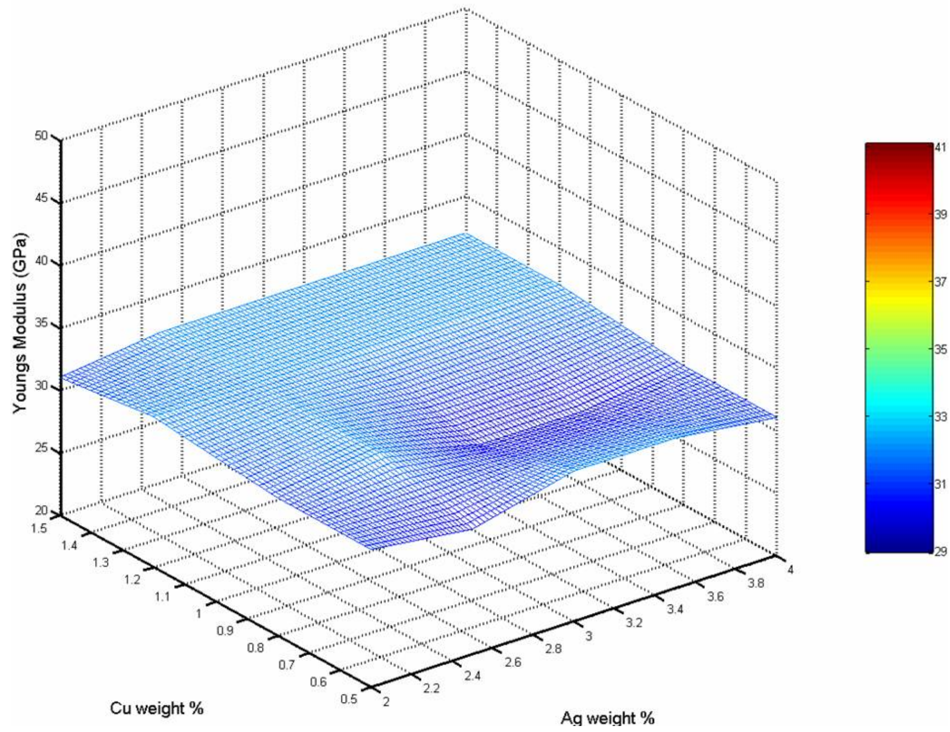

Figure 2.19(b) - Distribution of Young's modulus as a function of alloy composition (125 ^{o}C, 100h Aging)

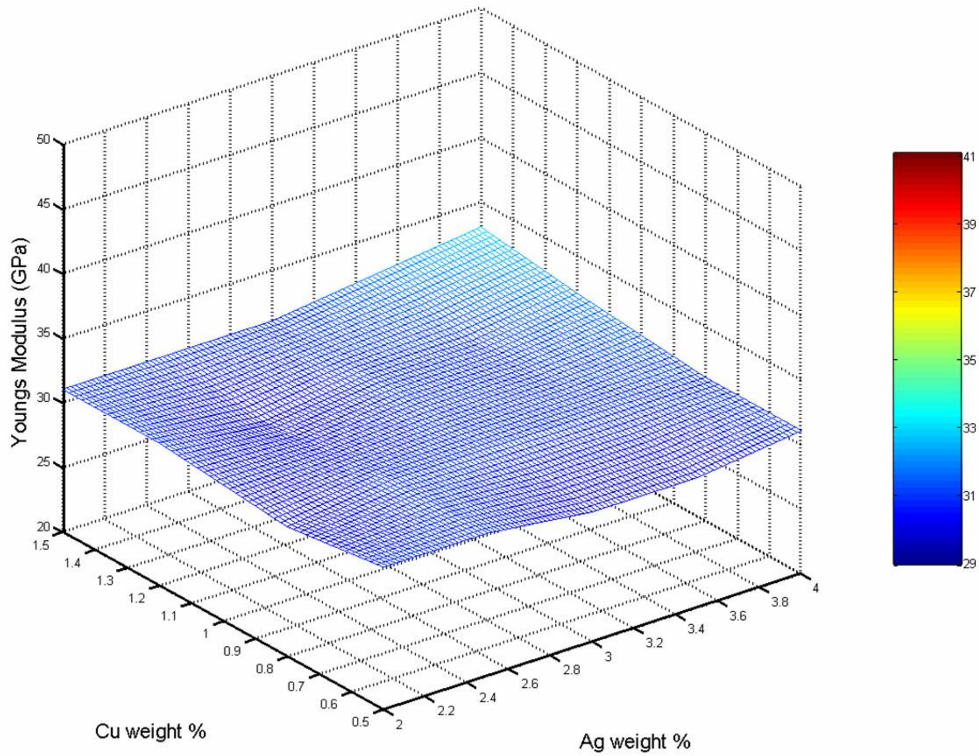

Figure 2.19(c) - Distribution of Young's modulus as a function of alloy composition (125 ^{o}C, 250h Aging)

The distribution of 0.2% strain yield stress (Figure 2.20) and ultimate tensile strength (Figure 2.21) as a function of alloy composition were more significant than the variation in Young's modulus; both were significantly higher with higher levels of silver and copper. The 0.2% strain yield stress was 56 MPa for the Sn-4Ag-1.5Cu alloy and 34 MPa for the Sn-2Ag-0.5Cu alloy. After 100h aging at 125 ^{o}C, the 0.2% strain yield stress for these alloys decreased to 32 and 23 MPa, respectively. The maximum ultimate tensile stress was 61 MPa for the Sn-4Ag-1.5Cu alloy and only 38 MPa for the Sn-2Ag-0.5Cu alloy (Figure 2.21(a)). After 100 hours of aging at 125 ^{o}C, the ultimate tensile stress for these two alloys decreased to 37 and 27 MPa, respectively. The absolute values of the yield stress and the ultimate tensile stress, as well as the difference between the values for the different alloy compositions, decreased during the aging process. As with the result for Young's modulus, there was no significant change in the 0.2% strain yield stress and the ultimate tensile stress distribution for the different alloys after 100 hours of aging at 125 ^{o}C.

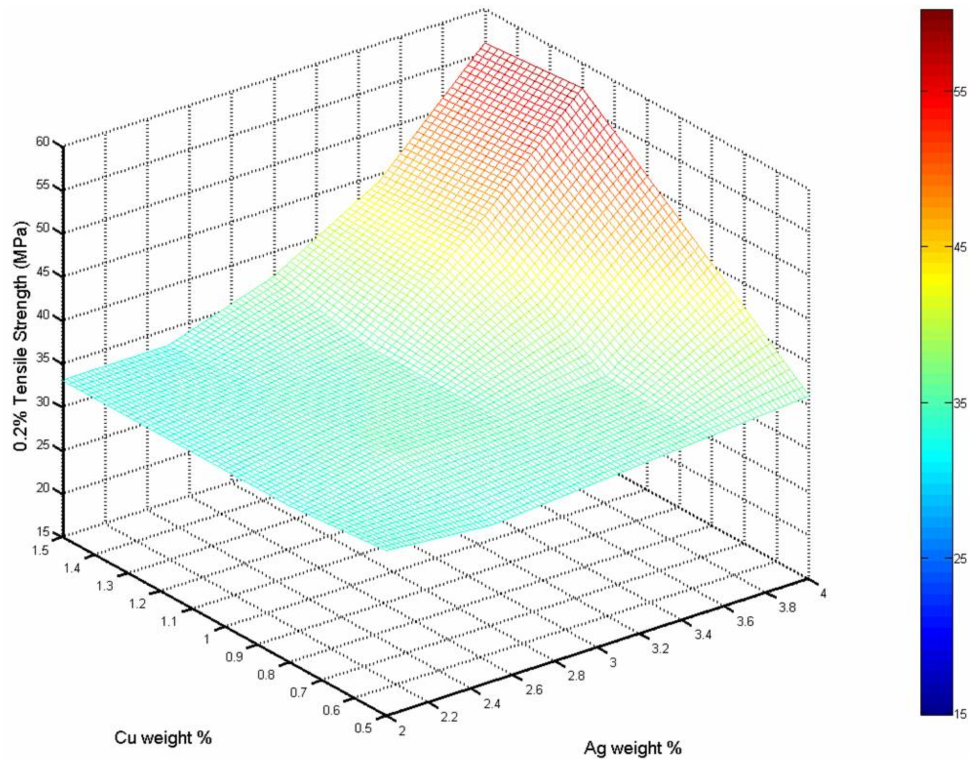

Figure 2.20(a) - Distribution of 0.2% strain yield stress as a function of alloy composition (as-cast)

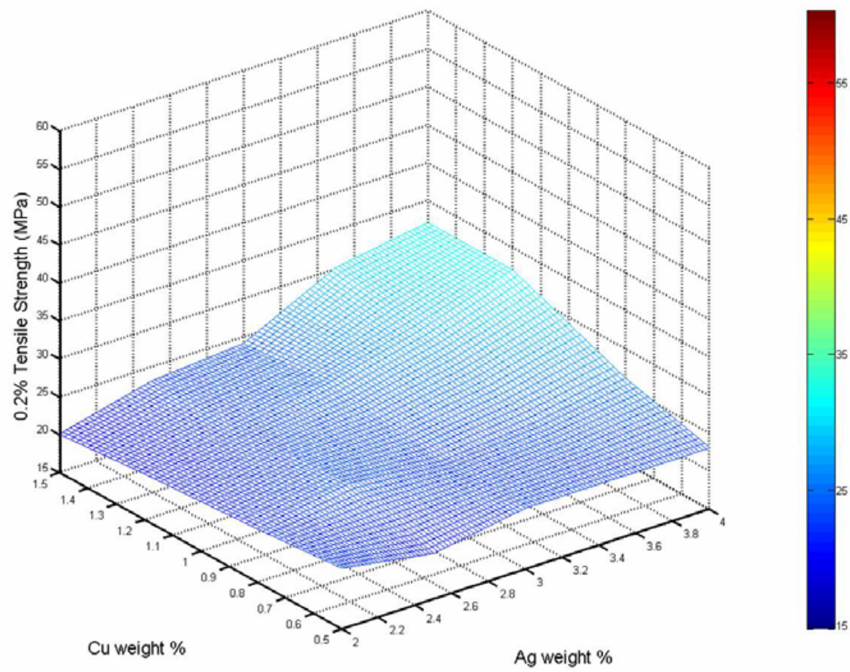

Figure 2.20(b) - Distribution of 0.2% strain yield stress as a function of alloy composition (125 ^{o}C, 100h aging)

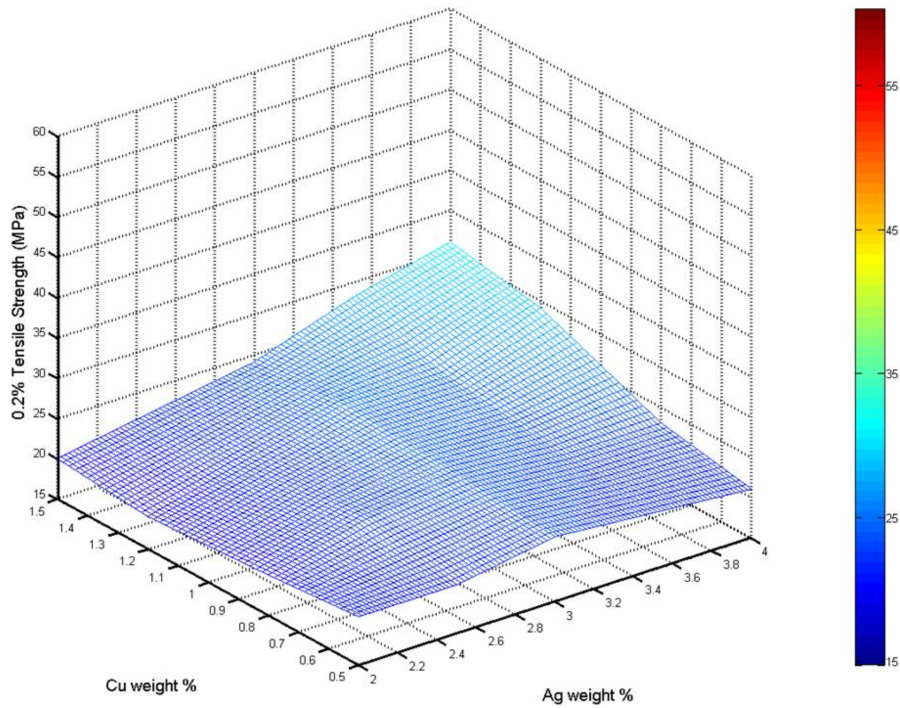

Figure 2.20(c) - Distribution of 0.2% strain yield Stress as function of alloy composition (125 ^{o}C, 250h aging)

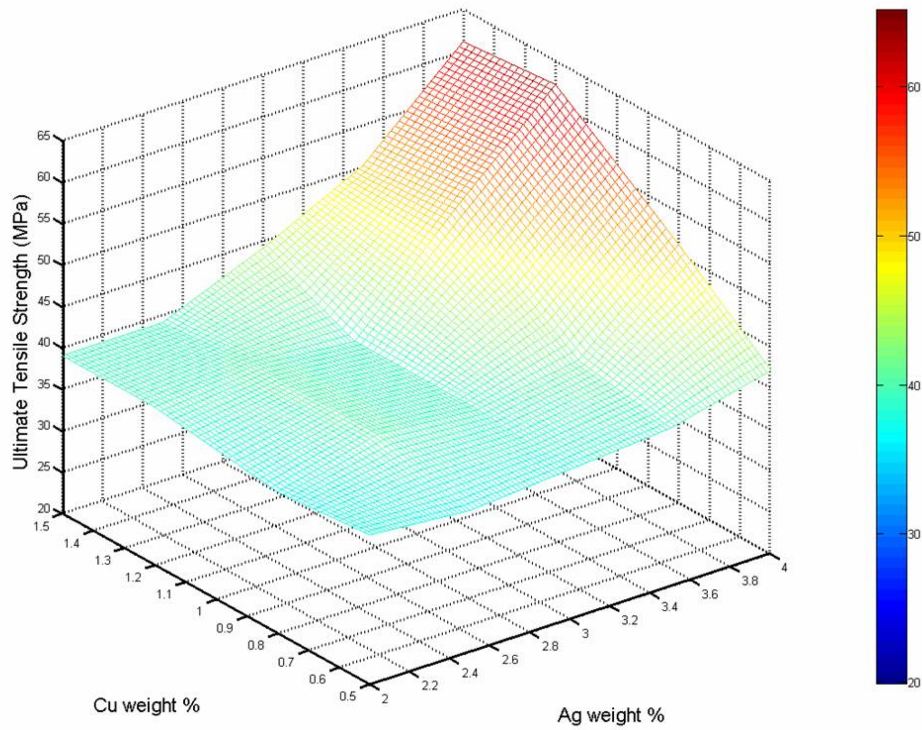

Figure 2.21(a) - Distribution of ultimate tensile strength as a function of alloy composition (as-cast)

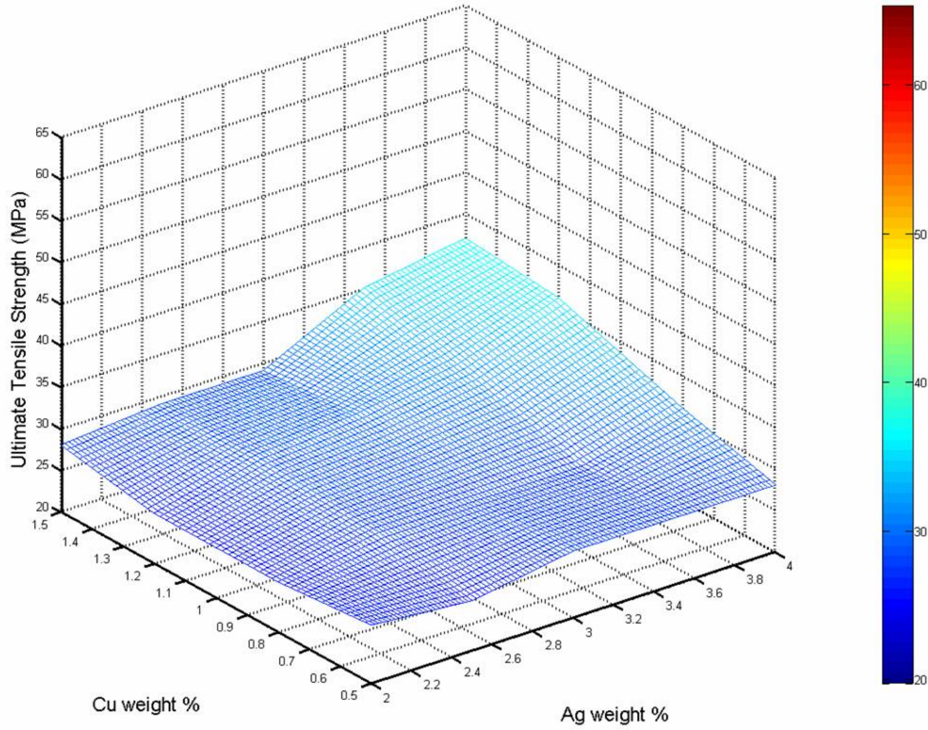

Figure 2.21(b) - Distribution of ultimate tensile strength as a function of alloy composition (125 °C, 100h aging)

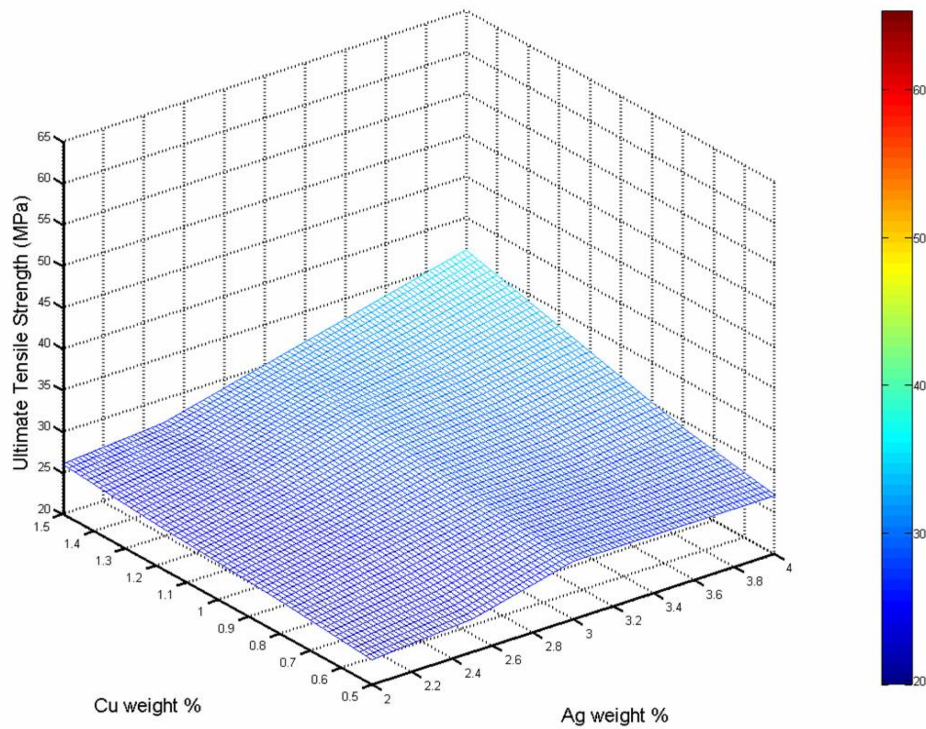

Figure 2.21(c) - Distribution of ultimate tensile strength as a function of alloy composition (125 ^{o}C, 250h aging)

Based on the significant drop between the initial as-cast condition and aging 100h at 125 ^{o}C condition, a test of the mechanical properties for samples aged 24h at 125 ^{o}C was performed to provide additional aging effects data. Sn-4Ag-1.5Cu, Sn-4Sg-0.5Cu, Sn-2Ag-1.5Cu, Sn-2Ag-0.5Cu, Sn-3.5Ag-0.8Cu were selected for this testing from the above initial Sn-Ag-Cu test matrix to represent the four corner levels and the middle point which is close to the eutectic composition. Figure 2.22 (a)-(e) shows the tensile properties measured for these alloys.

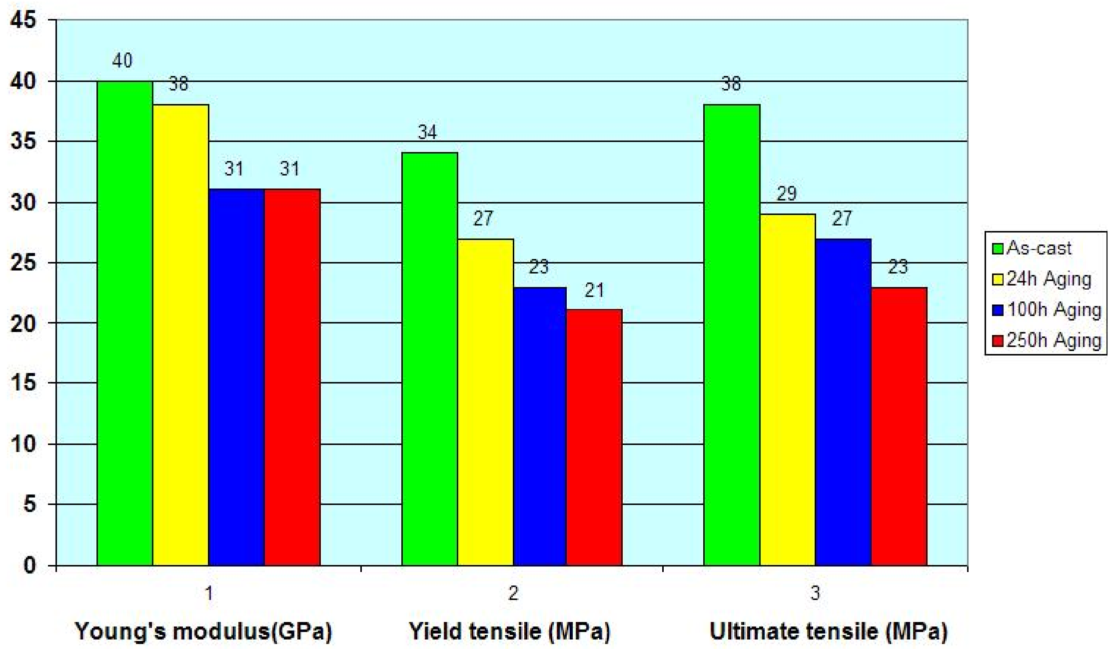

Figure 2.21(a) Tensile properties change with aging time at 125 C for Sn-2Ag-0.5Cu

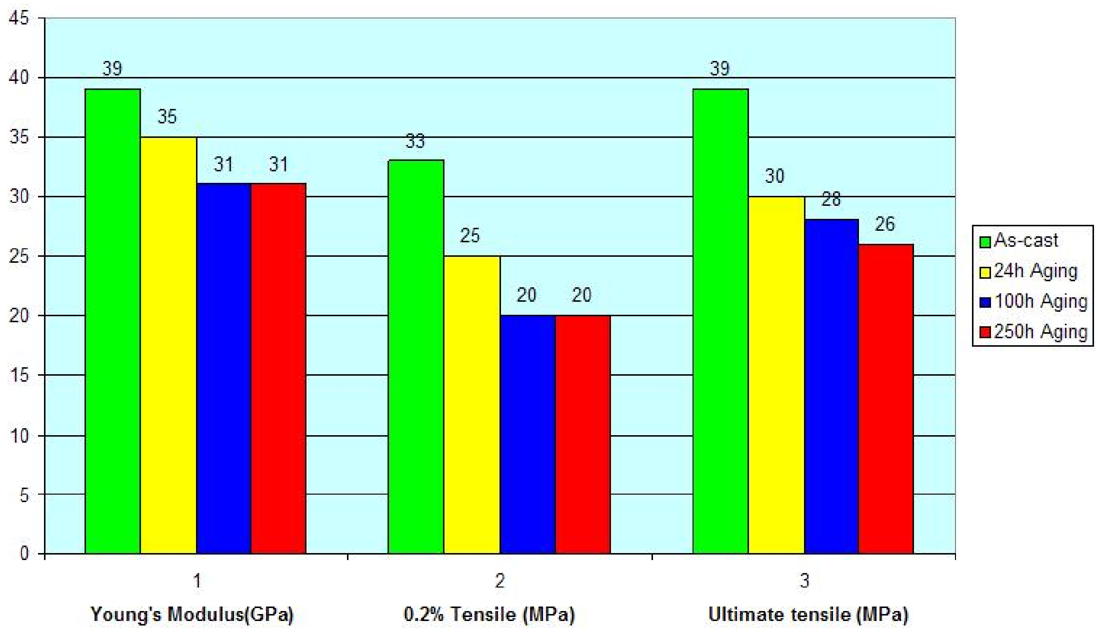

Figure 2.22 (b) Tensile properties change with aging time at 125C for Sn-2Ag-1.5Cu

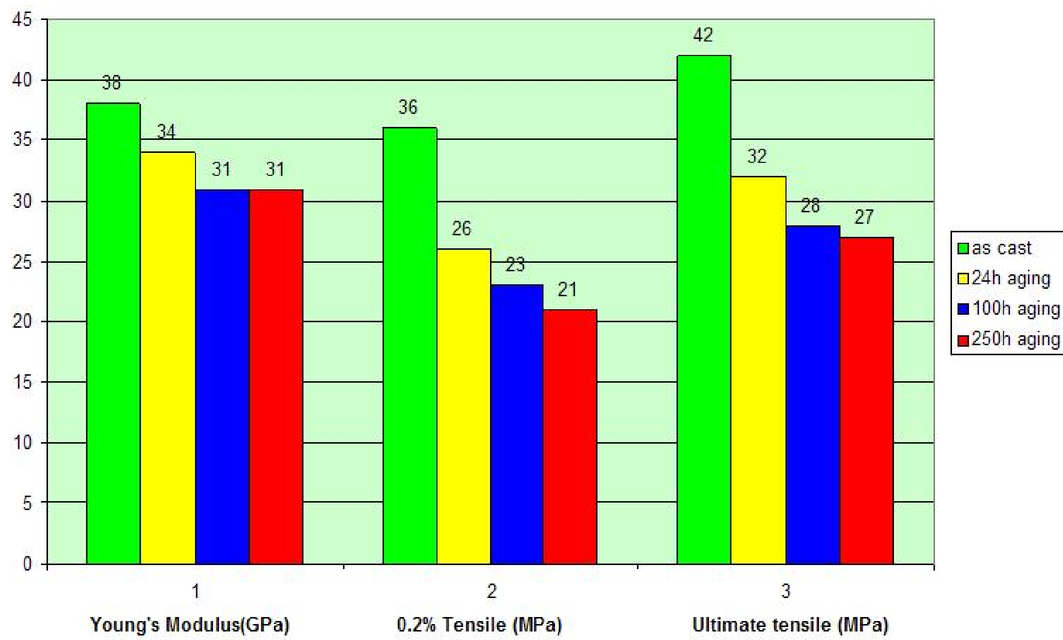

Figure 2.22 (c) Tensile properties change with aging time at 125C for Sn-4Ag-0.5Cu

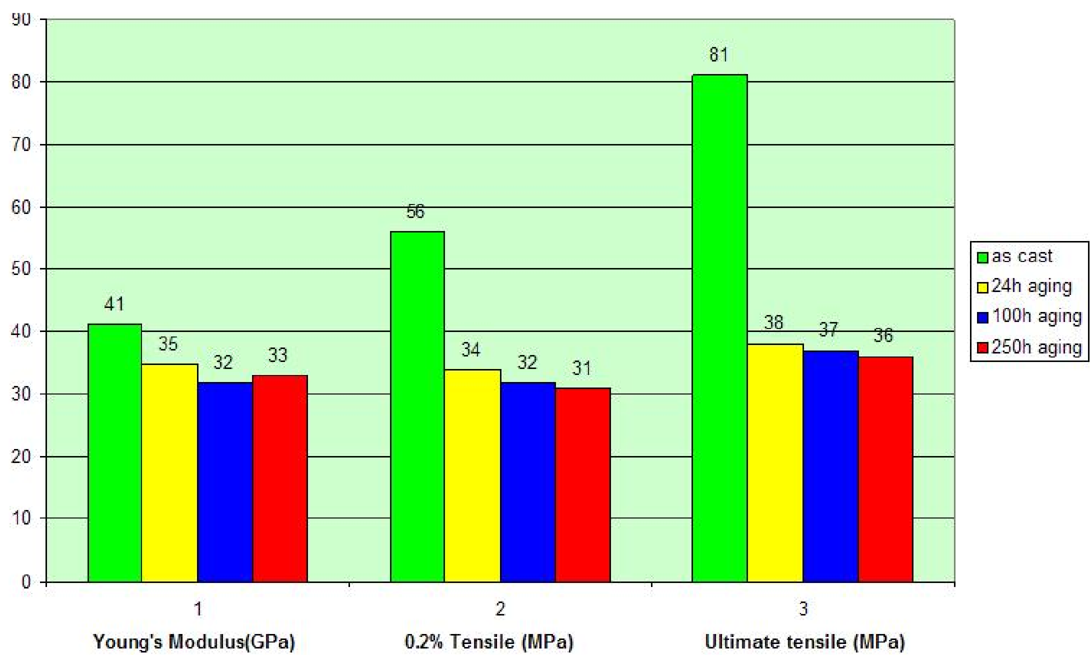

Figure 2.22 (d) Tensile properties change with aging time at 125C for Sn-4Ag-1.5Cu

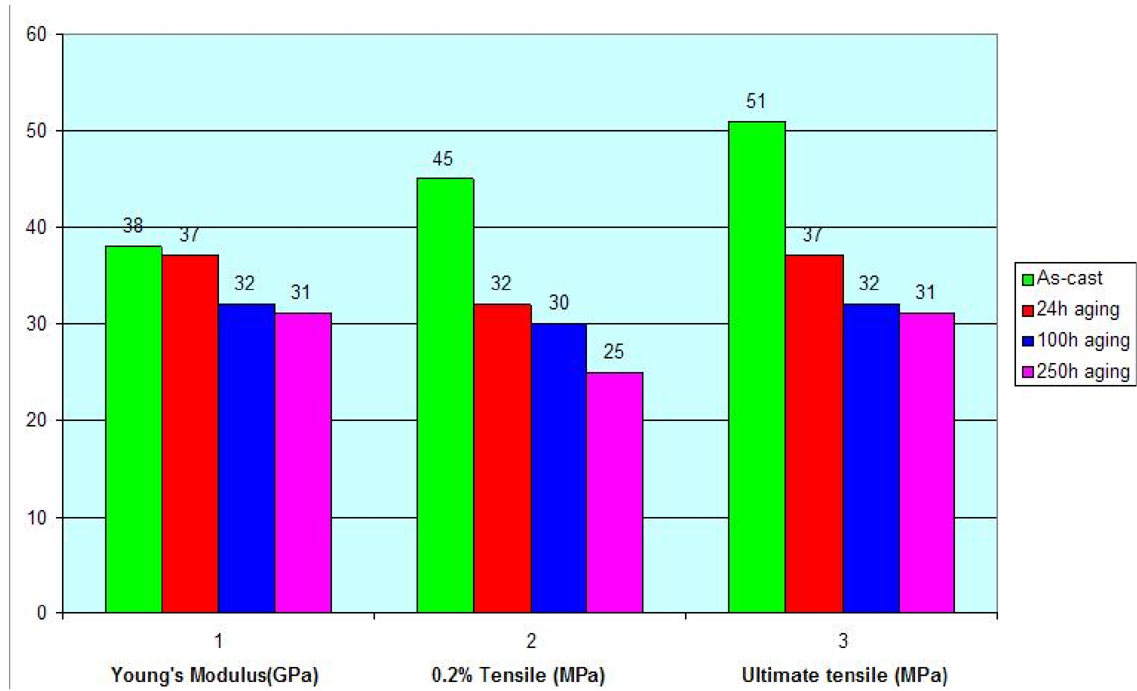

Figure 2.22 (e) Tensile properties change with aging time at 125C for Sn-3.5Ag-0.8Cu

In general, the tensile properties had already decreased significantly after 24 hours of aging at 125 ^{o}C. 0.2% yield strength and ultimate tensile strength decreased more than Young's modulus, especially for the alloys Sn-3.5Ag-0.8Cu and Sn-4Ag-1.5Cu. The origin of this degradation in tensile properties was confirmed by microstructure analysis, shown in Figure 2.14 (b), which revealed that there was already significant coarsening after only 24 hours of aging.

As the aging time increase, the microstructure changes from finer to coarser, and the grain size increases, resulting in decreased resistance to dislocation motion. The yield strength will decrease. Theoretically, grain growth during aging can reduce the grain boundary area, which reduces the overall energy in the alloy. Diffusion of atoms across the grain boundary is required for grain growth to occur. Consequently, the growth of grain boundaries is related to the activation energy for an atom to jump across the boundary. The Arrhenius equation [15] represents the relationship between the diffusion coefficient D and the temperature:

$$D = D_0 \exp\left(\frac{-Q}{RT}\right) \qquad (2.6)$$

where Q is the activation energy, R is the gas constant, T is the absolute temperature, and D_0 is a constant for a given alloy system. High temperature aging conditions will help to overcome the activation energy, increase the diffusivity and increase the size of grains [15].

2.5 Conclusions

The mechanical and microstructural properties of Sn-Ag-Cu alloys with Ag varying from 2wt% to 4wt% and Cu varying from 0.5wt% to 1.5wt% were systematically studied. A suitable specimen preparation process was developed using rectangular cross-section small glass tubes. Three sample preparation techniques (water quenched, oil quenched and water quenched followed by reflow) were studied and the oil quenched specimen microstructure was found to be comparable to that of a reflow soldered CSP solder joint.

The water quenched samples had a finer grain structure, while the water quenched and reflowed samples had a coarser grain structure compared to a CSP solder joint. Both the oil quenched specimens and CSP solder joint showed a eutectic region of Sn and moderately dispersed Ag_3Sn intermetallic surrounded by a dendritic Sn-rich phase.

For oil quenched specimens, Young's modulus as a function of alloy composition (Ag=2%~4%, Cu = 0.5% ~1.5%) ranged from 37-41 GPa and decreased to 30-32 GPa after aging for 100 hours and 250 hours at 125 ^{o}C. There was no significant difference in Young's Modulus as a function of alloy composition. After the initial decrease in modulus after 100 hours at 125 ^{o}C, there was only an insignificant change with further aging. Young's modulus ranged from 31-40 GPa for water quenched with reflow specimens, indicating that there was significant change as a function of alloy composition.

For the oil quenched specimens, the distribution of 0.2% strain yield stress and ultimate tensile strength as a function of alloy composition was more significant. Both were significantly higher for higher levels of silver and copper composition, gradually decreasing to the lowest value for low silver and copper compositions. The absolute value of yield stress and ultimate tensile strength both decreased during the high temperature aging process. The specimens obtained from water quenching with reflow exhibited the same trend but with different values compared with the specimens quenched by oil. The tensile properties for selected oil quenched alloy specimens were significantly lower after aging for 24 hours at 125°C. Yield strength and ultimate tensile strength decreased more than Young's modulus.

CHAPTER 3

Aging Effect On Creep Behavior of Sn-Ag-Cu Lead Free Solder System

3.1 Introduction

In this chapter, the creep test results and the effect of high temperature aging on creep properties are presented for the oil quenched samples. The creep data available in the literature for Sn-Ag-Cu ternary alloys is very limited. This hinders reliable predictions using finite element analysis of electronic assemblies [3]. The systematic analysis of creep properties over a wide range of Sn-Ag-Cu ternary alloy compositions after thermal aging is very important for finite element analysis (FEA) modeling. If the creep properties of the alloy change as a function of storage time at elevated temperatures, this must be included in the model for accurate predictions. Furthermore, there is little data available for strain rates less than 10^{-6} s^{-1}, stress levels less than 10 MPa and temperatures above 75°C, or combinations thereof [4]. However, the creep data at these conditions are very important as they represent the real stress conditions experienced by solder joints in electronic assemblies in service.

3.2 Creep Properties of Selected Lead Free Solders

The melting point of the alloys studied here were in the range of 490-513 K, exceeding the 0.5 T_m point at room temperature, 300 K, so creep processes are expected to dominate the deformation kinetics. The majority of the creep models utilized the stress and temperature dependence of steady state creep.

In this study, creep tests were performed with an MT-200 tension/torsion thermo-mechanical test system for selected alloy compositions (Sn-4Ag-1.5Cu, Sn-4Sg-0.5Cu, Sn-2Ag-1.5Cu, Sn-2Ag-0.5Cu, Sn-3.5Ag-0.8Cu) for three conditions: as-cast; aged for 100 hours at 125 °C; and aged for 250 hours at 125°C. The compositions of Sn-4Ag-1.5Cu, Sn-4Sg-0.5Cu, Sn-2Ag-1.5Cu, and Sn-2Ag-0.5Cu represent the four corners of the alloy range previously characterized for tensile properties, while the Sn-3.5Ag-0.8Cu alloy represents a mid-point and is close to the eutectic composition of the SnAgCu ternary alloy. Tests were conducted at three different temperatures (22 °C, 100 °C and 150 °C) at a range of constant stress levels (5-45MPa). The applied stress was selected to be below the yield stress. A thermal chamber was used for creep tests at different temperatures. The temperature of the specimen was monitored and controlled by a thermocouple placed close to the center of the specimen. Each test was continued until the minimum true strain rate was identified. As expected, the creep specimens failed earlier at high applied stress and had a long quasi-steady-state at low applied stress.

Figure 3.1 (a)-(c) shows the creep strain curve vs time for three testing temperatures. In the study, each experiment was run twice to verify the test data reliability. At each aging condition (eg. aging 100h at 125 °C), there were at least 9 creep

strain vs time curves generated from the experimental set up combination (3 temperature levels x 3 stress levels). Generally, high stress levels were selected for low temperatures, and low stress levels for high temperatures. Occasionally there were some scatter in the data for high stress levels because of tiny scratches at the surface of the specimens. There were a totally of 135 creep strain rate vs stress data sets (5 alloy compositions, each with 3 aging conditions (as-cast, 100h and 250h at 125 ^{o}C aging), and each aging condition with 9 creep strain vs time curves), which were conducted in order to evaluate the creep behavior of the Sn-Ag-Cu alloy system. Here, only creep strain vs time curves at one aging condition for one alloy composition [94.5Sn-4Ag-1.5Cu (100h, 125 ^{o}C aging)] are presented at three different testing temperatures (22 ^{o}C, 100 ^{o}C, 150 ^{o}C). Figure 3.1 (a) clearly shows that the extent of creep strain was small under an applied stress of 20 MPa and 25 MPa, although more significant strains were observed at a stress of 30 MPa at room temperature.

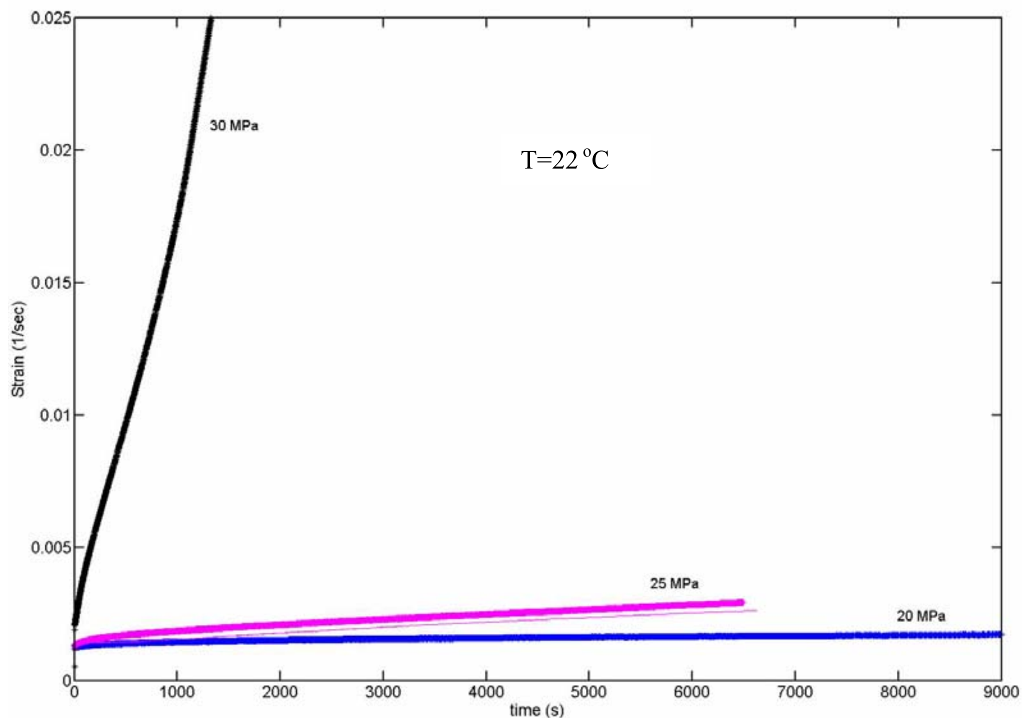

Figure 3.1 (a) Experimental creep strain vs time curves for 94.5Sn-4Ag-1.5Cu (100h, 125 ^{o}C aging) at T=22 ^{o}C

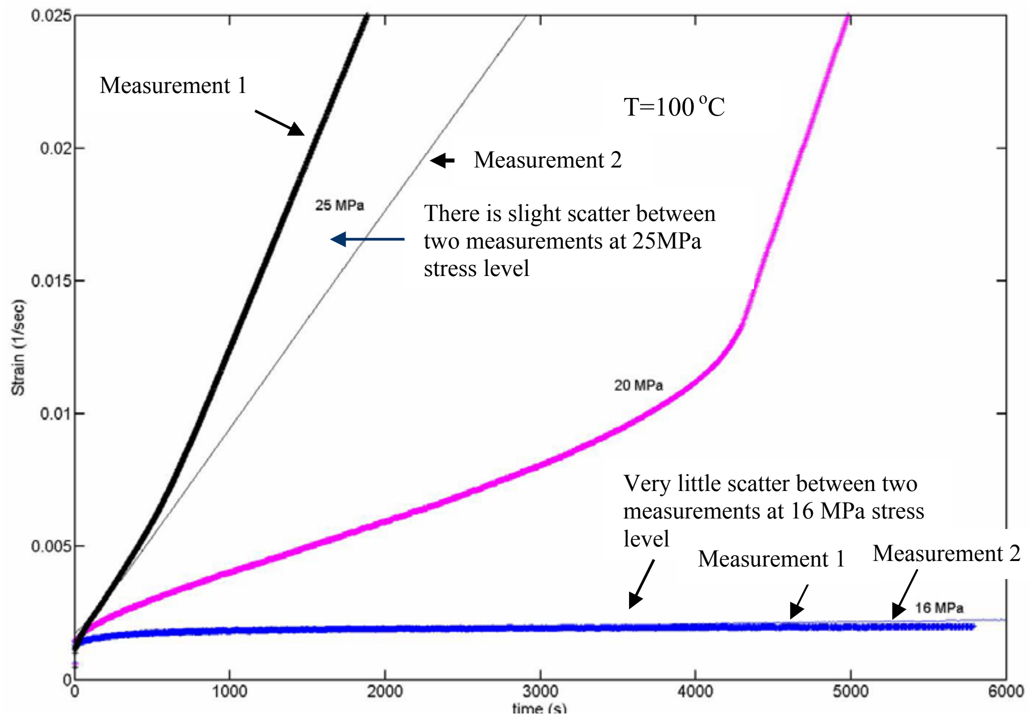

Figure 3.1 (b) Experimental creep strain vs time curves for 94.5Sn-4Ag-1.5Cu (100h, 125 °C aging) at T=100 °C

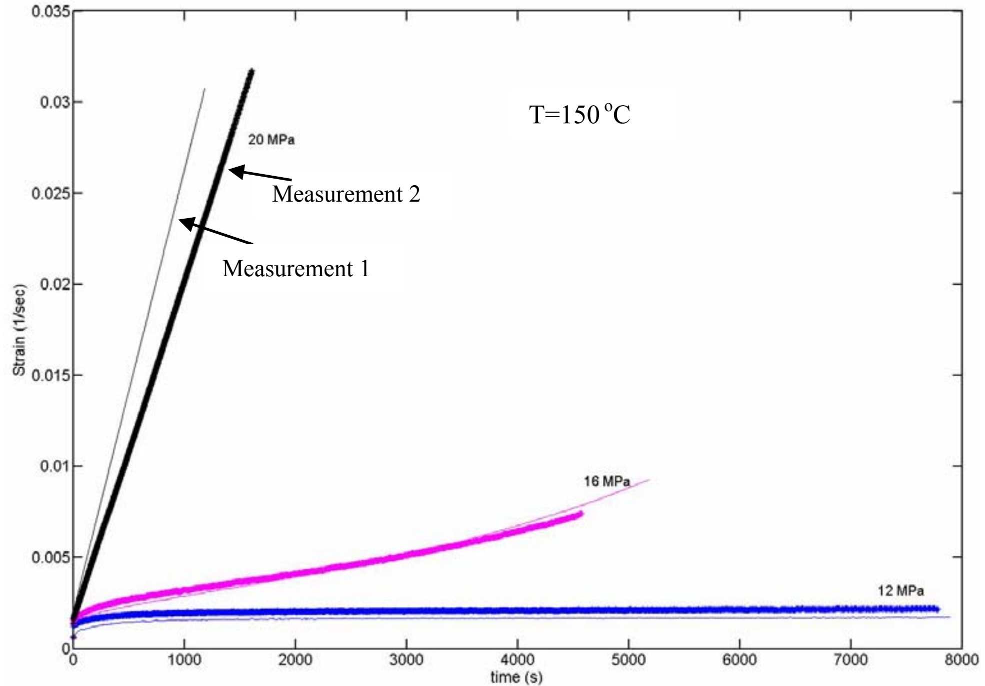

Figure 3.1 (c) Experimental creep strain vs time curves for 94.5Sn-4Ag-1.5Cu (100h, 125 °C aging) at T=150C

Figure 3.1 (b) and (c) show that the same strain range can be obtained at lower applied stress at higher testing temperatures (100 ^oC and 150 ^oC). At high stress levels (25MPa for 100 ^oC and 20MPa for 150 ^oC), there was slightly more scatter for the data curves, which was assumed to be due to the tiny defects on the surface of the specimen, while at low stress levels, this effect was minimized.

As a benchmark, this data was compared with reported reference creep data [4] and the results are shown in Figure 3.2, which shows the quasi-steady state creep rates plotted against applied stress in the log-log format. In general, the creep data from these sources are in the same range even though the sample dimensions, sample preparation and exact compositions vary. Comparing the specimen information from Table 3.1, there is a significant difference between the cross-section dimensions: Schubert et al. [5] used a sample of 3mm x 3mm versus the 11.28 mm x 13 mm diameter samples used by Kariya et al. [6]. The new specimens developed at Auburn have a 3mm x 0.5 mm rectangular cross section, which is compatible in thickness to the typical thicknesses of 0.5 mm for BGA and 0.25~0.5 mm for CSP solder joints. Moreover, the different cooling options used for specimens by the different researchers resulted in different microstructures. The data comparison can is useful in verifying the feasibility and reliability of the new experimental specimens developed at Auburn compared to those used by other research scientists'.

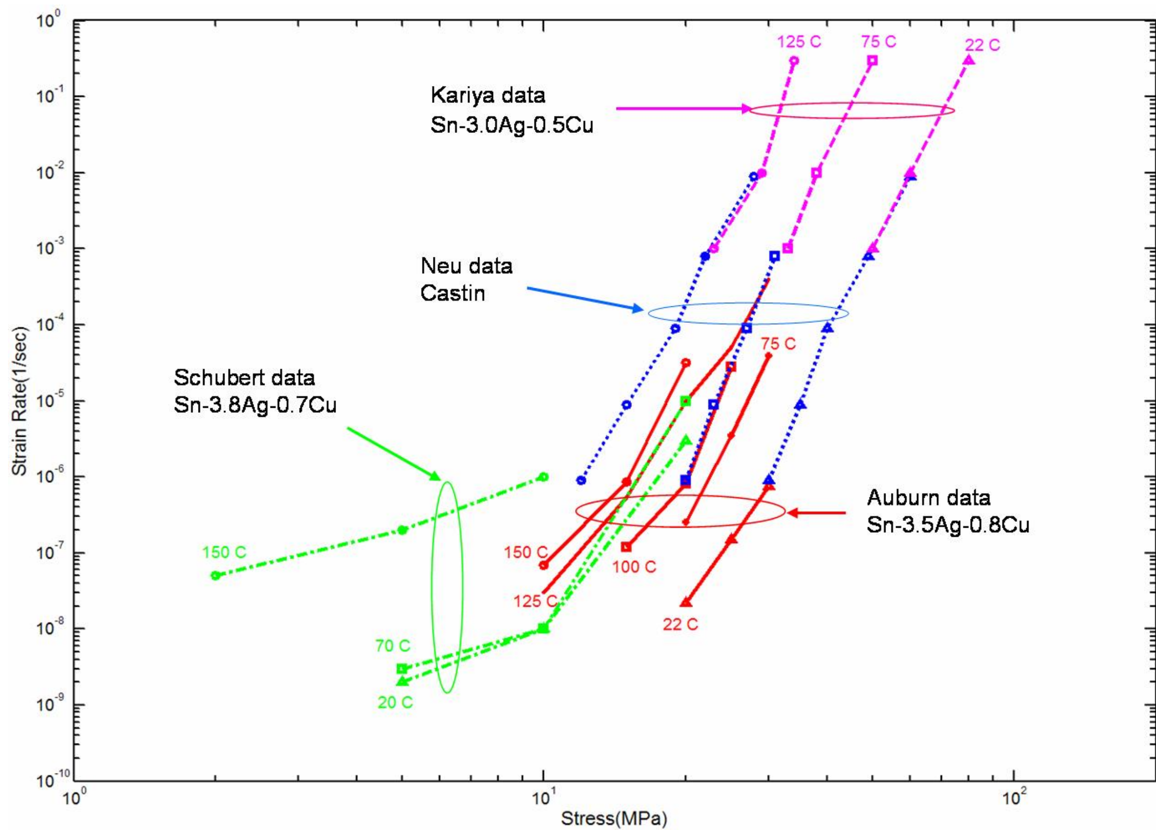

Figure 3.2 - Comparison of Auburn experiment data with published creep data for alloy compositions near Sn-Ag-Cu eutectic point [4]

Table 3.1 - Comparison of creep specimens between Auburn University and other researchers

Source	**Alloy Composition**	**Specimen shape**	**Specimen/Gauge length**	**Cross-section**	**Specimen treatment**
Auburn Univ.	95.7-Sn-3.5Ag-0.8Cu	Uniaxial rectangular	70mm/50mm	3mm x 0.5mm rectangular	Oil quench
Schubert et al. [5]	95.5.-Sn3.8Ag-0.7Cu	Dog-bone	60mm/30mm	3mm x 3mm	Not reported
Neu et al. [53]	96.2Sn-2.5Ag-0.8Cu-0.5Sb	Cylinder	127mm/12.7mm	13mm square	Air-cooled
Karriya et al. [53]	95.5Sn-3.8Ag-0.7Cu 96.5Sn-3.0Ag-0.5Cu	Dog-bone	60mm gauge	11.28mm square	Water quenched

The strain vs stress creep curves for the five selected alloy compositions at the different aging conditions are shown in Figures 3.3-3.5 for test temperatures of 22 ^{o}C, 100°C and 150 ^{o}C, respectively. The strain range is from 10^{-3} to 10^{-8}, while stress is in the range of 5-50 MPa. In general, the creep curves shift from right to left as the testing temperature increases, indicating that the creep resistance decreases as the test temperature is increased for all five alloy compositions. Comparing the five alloy compositions, the creep resistance decreases as the aging time increases. Sn-4Ag-1.5Cu has the highest creep resistance and Sn-3.5Ag-0.5Cu ranks second. The creep resistance for Sn-2Ag-0.5Cu, Sn-4Ag-0.5Cu and Sn-2Ag-1.5Cu are similar and lower.

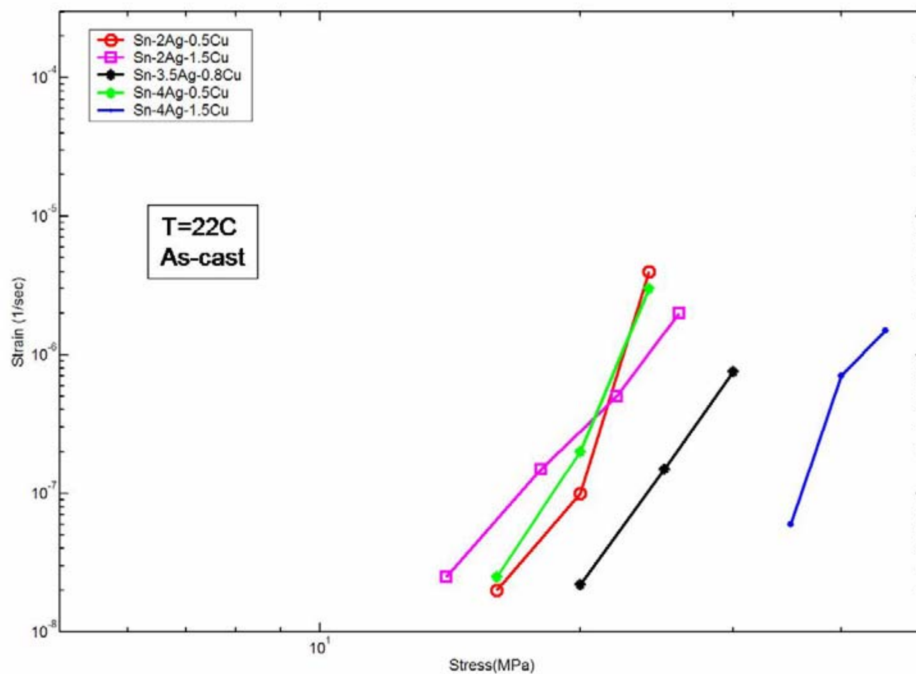

Figure 3.3 (a) Comparison of creep data at T=22°C (as-cast)

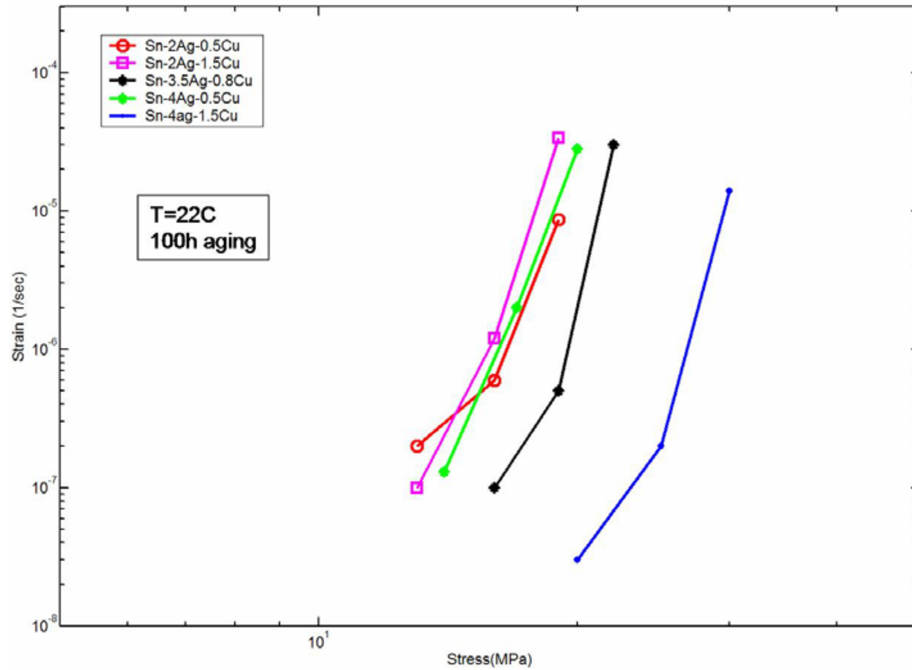

Figure 3.3 (b) Comparison of creep data at T=22°C (100h aging at 125°C)

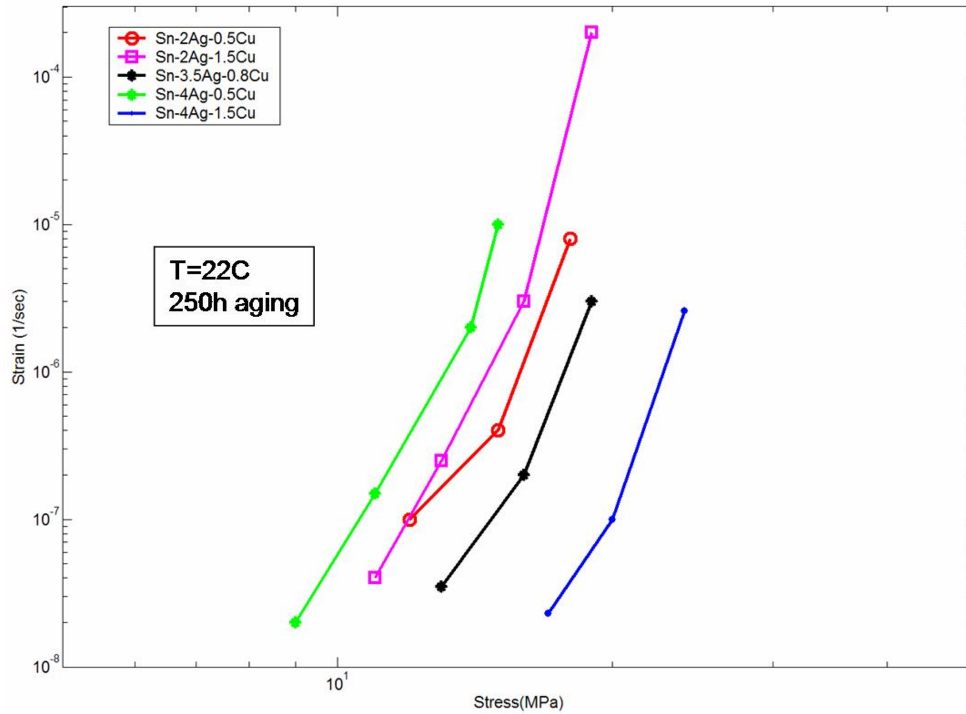

Figure 3.3 (c) Comparison of creep data at T=22 °C (250h aging at 125°C)

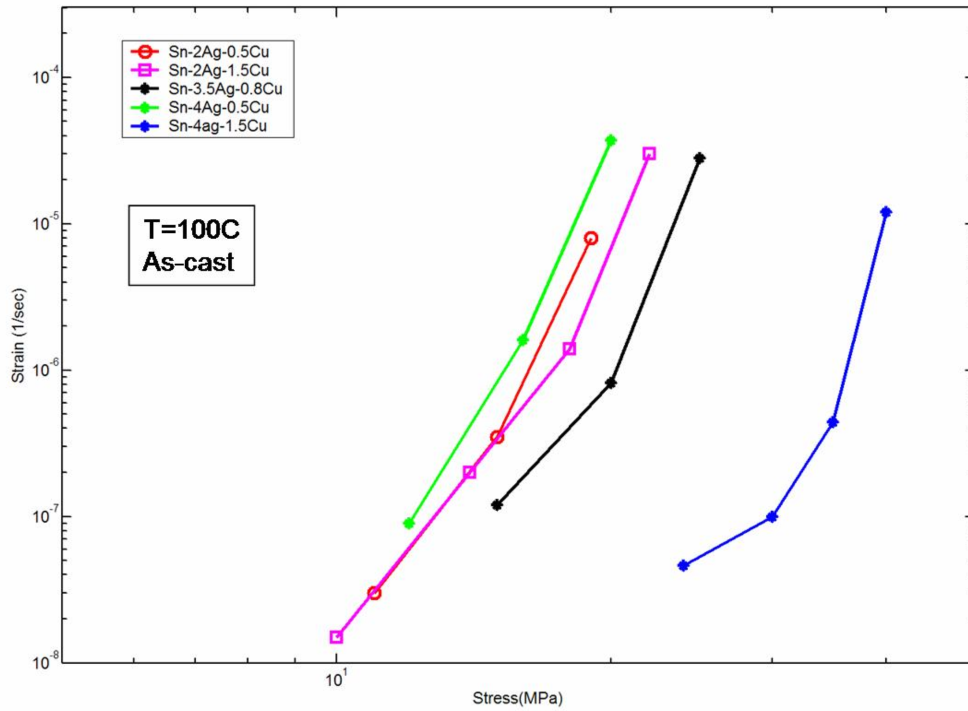

Figure 3.4 (a) Comparison of creep data at T=100°C (as-cast)

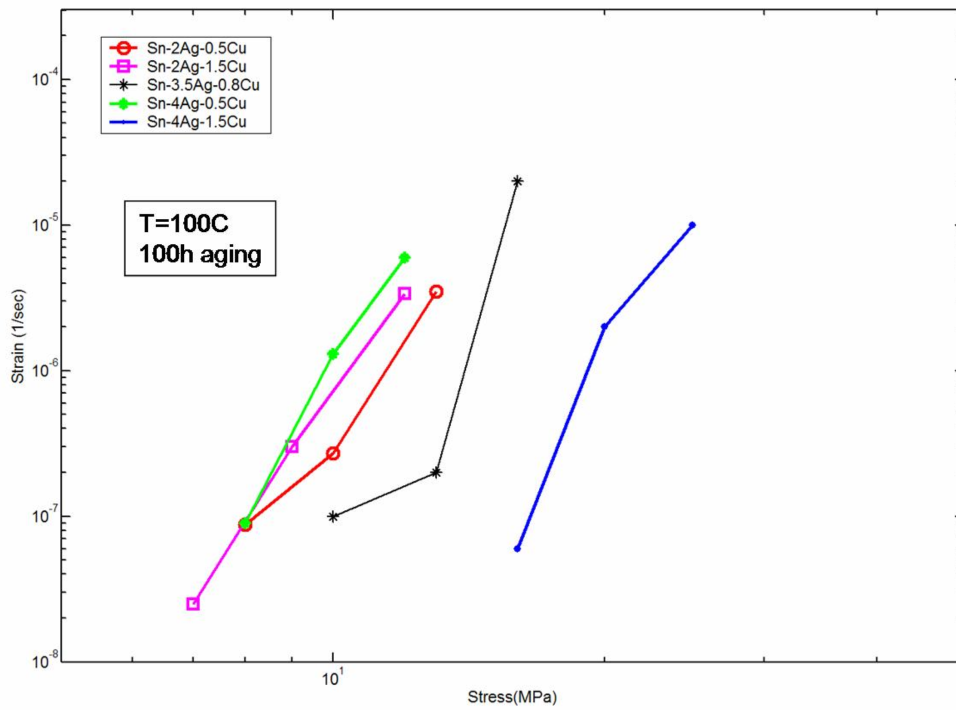

Figure 3.4 (b) Comparison of creep data at T=100°C (aging 100h at 125°C)

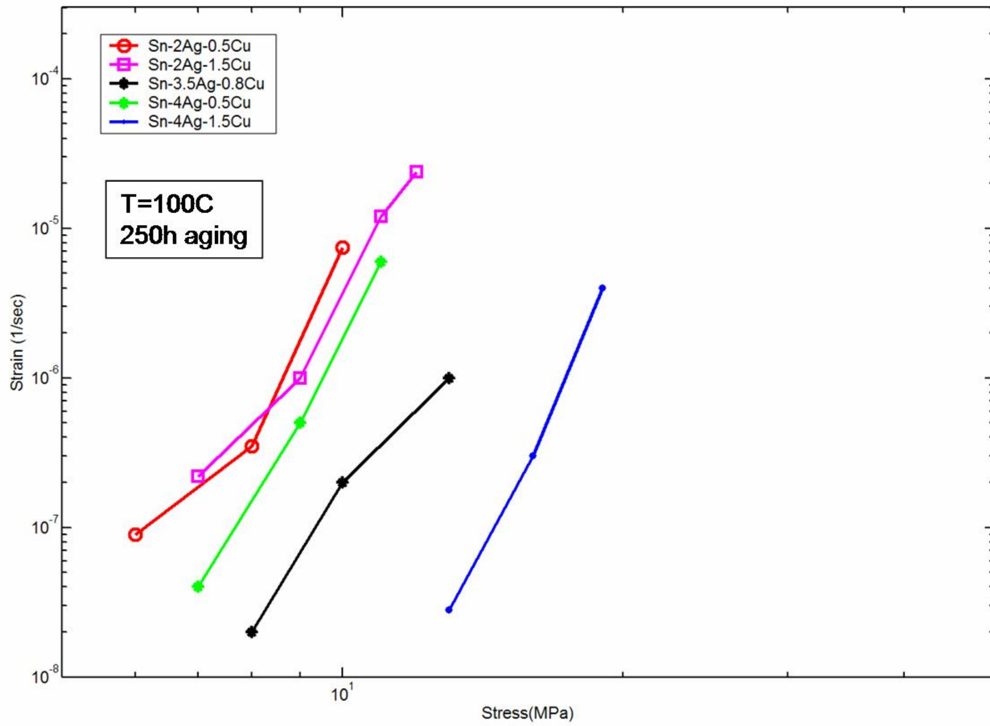

Figure 3.4 (c) Comparison of creep data at T=100°C (aging 250h at 125°C)

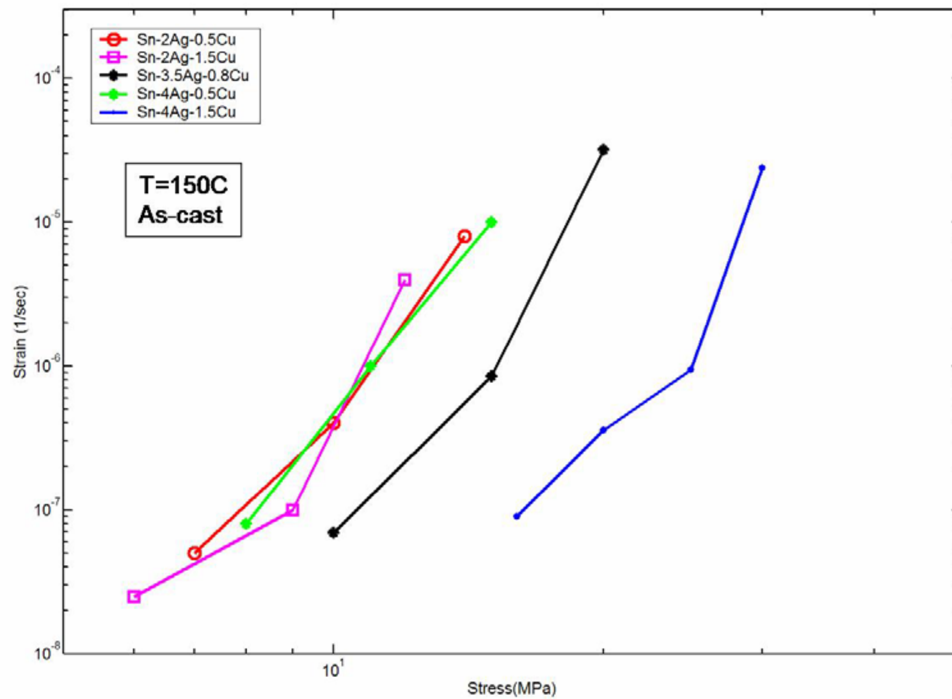

Figure 3.5 (a) Comparison of creep data at T=150°C (as-cast)

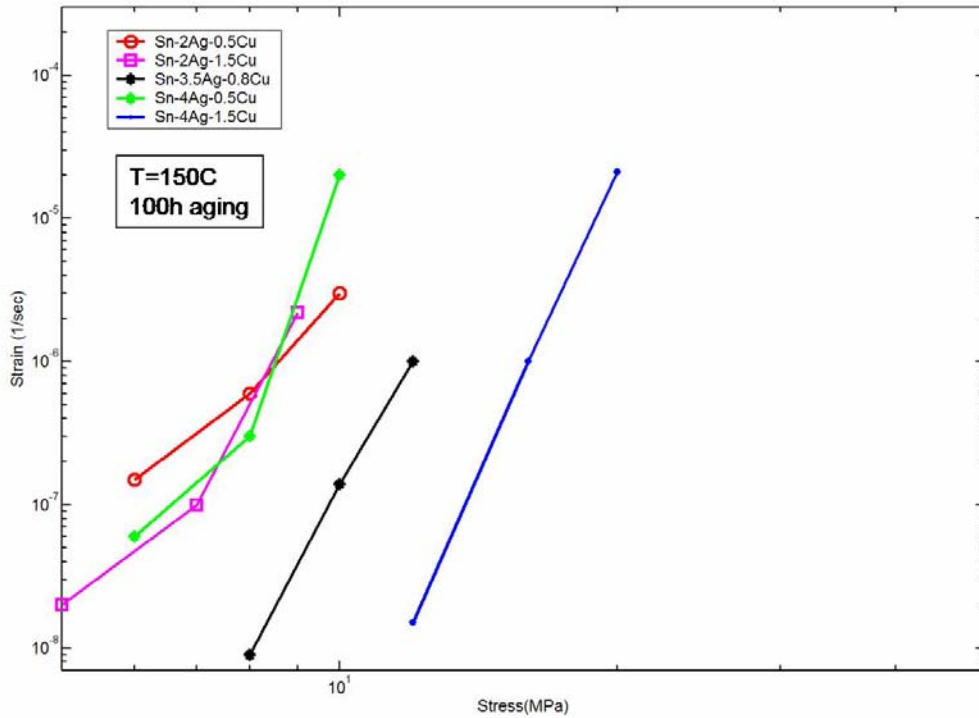

Figure 3.5 (b) Comparison of creep data at T=150°C (aging 100h at 125°C)

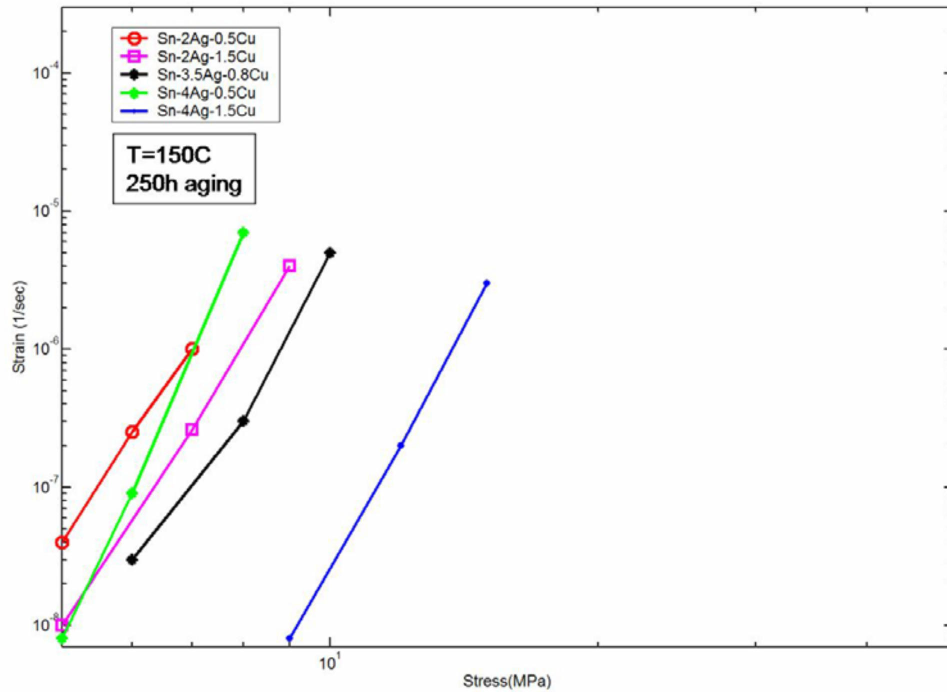

Figure 3.5 (c) Comparison of creep data at T=150°C (aging 250h at 125°C)

3.3 Creep Constitutive Models

The quasi-steady state creep constitutive model can be simply characterized by a power law relationship,

$$\dot{\varepsilon} = A\sigma^n e^{\frac{-Q}{RT}} \quad (3.1)$$

where the quasi-steady state creep strain rate is $\dot{\varepsilon}$, A is a material constant, σ is the applied stress, n is the stress exponent, Q is the creep activation energy, R is the universal gas constant, and T is absolute temperature [6]. The activation energy, Q, and the stress exponent, n, depend on the creep mechanism, and have different values at different temperatures and levels of applied stress. Equation (3.1) describes a linear relationship in logarithmic coordinates between the creep strain rate and the applied stress for a specified temperature. However, the simple power-law model cannot describe the non-linear experimental creep curves over large stress ranges. A hyperbolic-sine power-law relationship has been proposed and found to predict the observed behavior at low and high stresses [10, 11, 12]. At low and medium stresses, the creep strain rate depends on stress to the power n. At high stresses, the strain rate is an exponential function of stress [3].

$$\dot{\varepsilon} = C[\sinh(\alpha\sigma)]^n \exp\left(-\frac{Q}{RT}\right) \quad (3.2)$$

where C is a materials constant and α is the stress coefficient. Equation 3.2 can be represented by equation 3.3 in logarithmic terms:

$$\ln\dot{\varepsilon} = \ln C + n\ln[\sinh(\alpha\sigma)] - Q/RT \quad (3.3)$$

The parameters C, n, and Q can be determined from the coefficients of a multi-variable linear-regression analysis. The steady state creep data for all the selected alloy composition at three aging conditions (as-cast, and 100h and 250h at 125 ^{o}C) were fitted to equation (3.2). The fitted creep model parameters for the alloy compositions are given in Table 3.2.

Taking the Sn-4Ag-0.5Cu alloy as an example, the curve-fitted hyperbolic-sine creep model is given below to represent as-cast, aging 100h at 125 ^{o}C, and aging 250h at 125 ^{o}C:

$$\dot{\varepsilon} = 0.17[\sinh(0.14\sigma)]^{4.2} \exp\left(-\frac{55}{RT}\right) \quad (3.3\text{ a})$$

$$\dot{\varepsilon} = 0.04[\sinh(0.21\sigma)]^{4.4} \exp\left(-\frac{54}{RT}\right) \quad (3.3\text{b})$$

$$\dot{\varepsilon} = 0.0051[\sinh(0.25\sigma)]^{5.6} \exp\left(-\frac{55}{RT}\right) \quad (3.3\text{c})$$

Table 3.2 Creep model parameters for selected alloy compositions at different aging conditions

Aging conditions	Alloy compositions	Hyperbolic-sine power-law model parameters			
		C	α	n	Q (kJ/mole)
As-cast	Sn-4Ag-1.5Cu	0.48	0.05	5.9	53
	Sn-4Ag-0.5Cu	0.17	0.14	4.2	55
	Sn-2Ag-1.5Cu	2.1	0.09	5.6	55
	Sn-2Ag-0.5Cu	0.3	0.19	4.0	66
	Sn-3.5Ag-0.8Cu	1.46	0.09	4.9	60
100h at 125 ^{o}C	Sn-4Ag-1.5Cu	1.6e-3	0.14	4.9	55
	Sn-4Ag-0.5Cu	0.04	0.21	4.4	54
	Sn-2Ag-1.5Cu	0.014	0.25	4.1	55
	Sn-2Ag-0.5Cu	1.42	0.2	4.6	65
	Sn-3.5Ag-0.8Cu	6.54E-4	0.27	4.3	60
250h at 125 ^{o}C	Sn-4Ag-1.5Cu	5.7E-4	0.2	4.2	54
	Sn-4Ag-0.5Cu	5.1E-3	0.25	5.6	55
	Sn-2Ag-1.5Cu	1.4E-2	0.27	4.3	55
	Sn-2Ag-0.5Cu	8	0.2	4.8	66
	Sn-3.5Ag-0.8Cu	8.68E-2	0.22	4.2	60

Figure 3.6 shows the calculated data using the above creep model equations. The model is in good agreement with the experimental data for the different test temperatures. The fitted value of parameters C and α varied with alloy composition at different temperature and aging times. The value of α determined for the selected alloy compositions is in the range 0.05~0.19, which compares to the value of 0.005 for 95.5Sn-3.9Ag-0.6Cu obtained by Vaianco [41]; 0.037 for 95.5Sn-3.8Ag-0.7Cu obtained by John [7]; 0.185 for 95.5Sn-3.8Ag-0.7Cu by Schubert [6]. The high value of α suggests that the creep behavior exhibits an increased sensitivity to stress. There was no significant difference for the n value between as-cast and 100h at 125 ^{o}C aging condition, but slightly high for 250h at 125 ^{o}C aging condition. Based on the experimental data, n is in the range of 4.2 - 5.6 for the tested alloy compositions. The small change of stress exponent value for the entire stress level implies a weak power-law break down phenomenon [41]. By comparison, the strong power-law break down behavior observed with Sn-Pb solder indicated by values of n in the range of $2<n<8$ because there is significant change of n value on the entire stress level [6]. The range of activation energy, Q, for the selected alloy composition samples is 53-66 kJ/mol, which generally indicates a grain-boundary or interface-related, short-circuit (or fast) diffusion mechanism [41]. Vaianco et al [41] reported creep fitted results for 95.5Sn-3.9Ag-0.6Cu with n=4.2, Q=54 kJ/mol; John et al [7] reported their fitted results for alloy 95.5Sn-3.8Ag-0.7Cu with n=5.1, Q=65 kJ/mol, and Schubert et al [6] reported n=3, Q=39 kJ/mol for alloy 95.5Sn-3.8Ag-0.7Cu. The microstructure of Sn-Ag-Cu is characterized by precipitates that are

dispersed in the β-tin matrix, which leads to higher creep resistance due to the precipitation strengthening [46].

Strain rate (1/s)

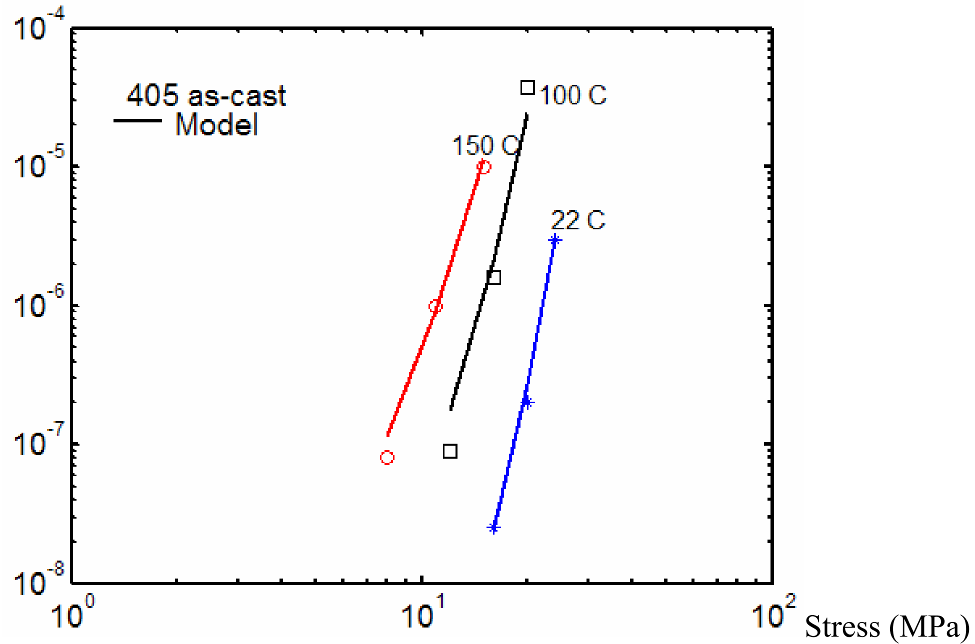

Figure 3.6 (a) Comparison of model and experimental creep data at as–cast conditions

Strain Rate (1/s)

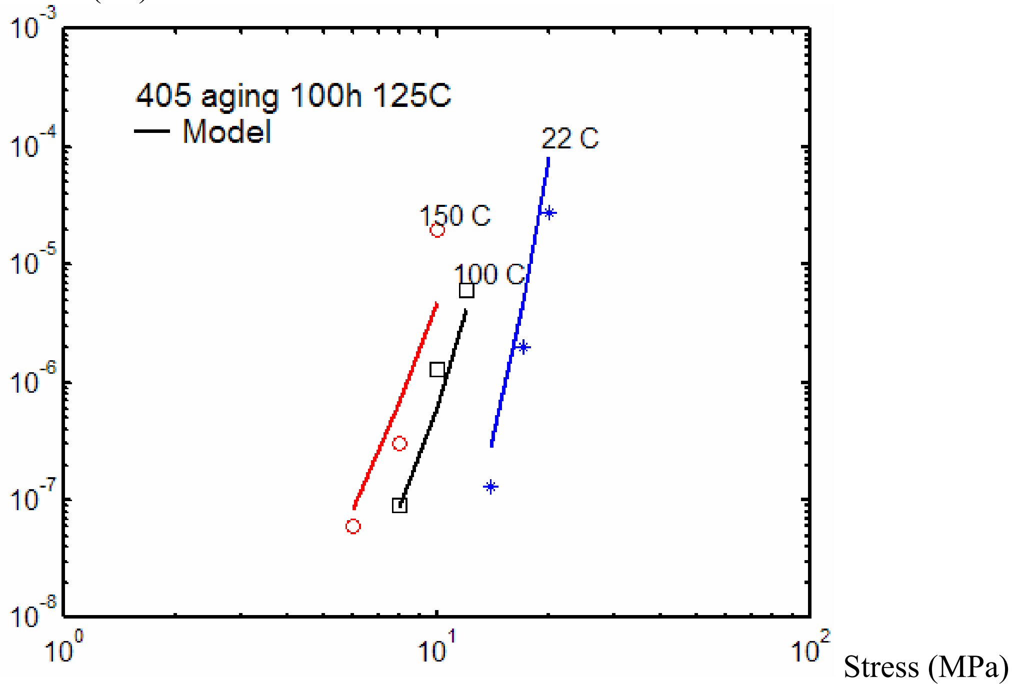

Figure 3.6 (b) Comparison of model and experimental creep data for aging100h at 125°C

Strain Rate (1/s)

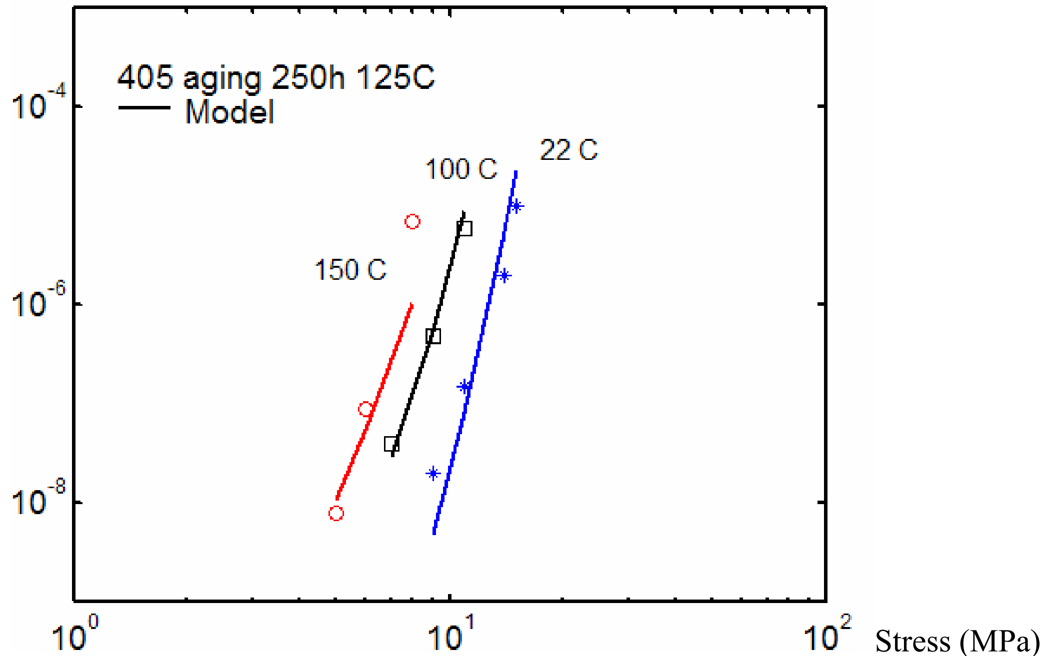

Figure 3.6 (c) Comparison of model and experimental creep data for aging 250h at 125°C

3.4 Creep Fracture Analysis for Selected Sn-Ag-Cu Alloy

3.4.1 Creep Fracture Surface Analysis

Creep strain is the result of thermally activated dislocation motion and/or the movement of vacancies and atoms, resulting in the elongation of the material [3]. The reliability of solder joints will depend on the behavior of solder and the number of dislocations increased during plastic deformation. However, because dislocations are a natural part of crystalline materials, only applied stress can be controlled as the dependent factor in the experiment. An understanding of plastic deformation and the relationship between dislocations and applied stress will reveal how these effects influence the reliability related to the properties of the material. Microstructural evolution provides important information for practical applications [39].

In this research, each creep test stopped when the steady state creep rates was identified. Under a small applied stress it will take longer to produce a creep fracture failure so only a few specimens had creep fracture failures under either high applied stress level or high testing temperature. The creep fracture analysis was only conducted on these few specimens. The selected specimens were attached vertically on a supporting plate in order to process the SEM microstructure pictures. Analysis of the fracture surface was conducted to provide a basic understanding of the creep deformation at different testing temperatures, aging times and alloy compositions. Significant cavity growth was

observed due to decohesion of Sn-rich dendrites from the eutectic regions (Figure 3.7). The fine morphology of Ag_3Sn particles was also pulled out from the matrix [40].

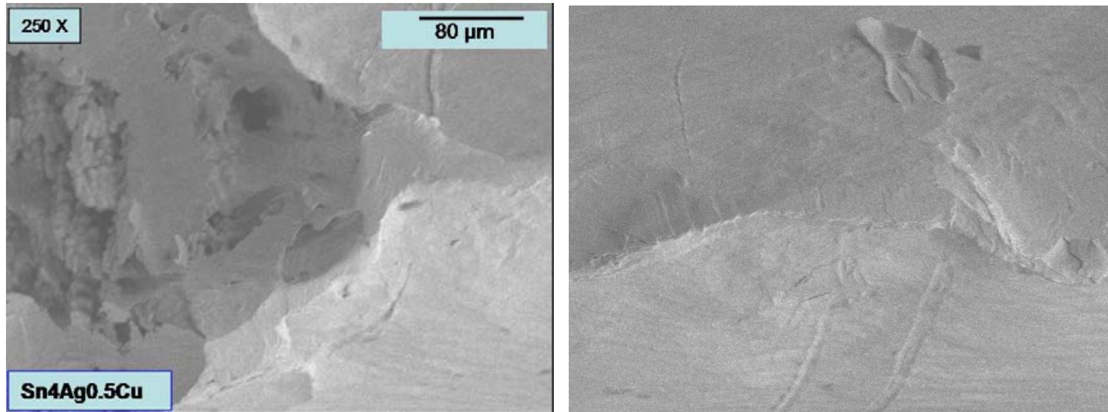

Figure 3.7 (a) Sn-4Ag-0.5Cu at 150°C, 100h aging with 10MPa stress creep (250x)

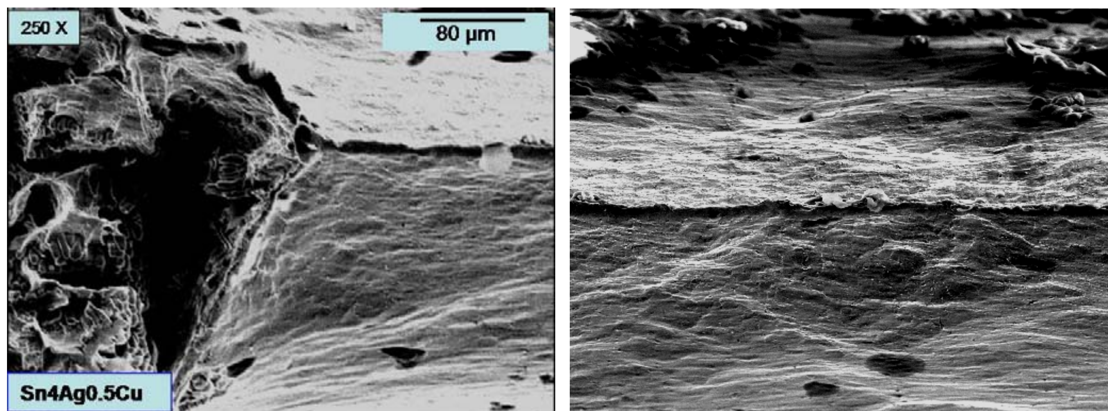

Figure 3.7 (b) Sn-4Ag-0.5Cu at 150°C, 100h aging with 8MPa stress creep

Figure 3.7 shows the creep fracture surface for Sn-4Ag-0.5Cu tested at 150 ^{o}C after 100h (125 ^{o}C) aging under 10MPa and 8MPa stress levels. Both samples include cavities created at the initial break point of the creep specimens, while breaks also occurred at the middle section of the specimens. There is no significant difference for creep fracture between these two stress level creeps. Ochoa, et al. [40] indicated that the flow stress of Sn-rich regions was much lower than the flow stress of eutectic regions at higher testing temperatures, so the fracture will preferentially occur at grain boundaries in the Sn-rich regions. Figure 3.8 shows the creep fracture surface for Sn-4Ag-1.5Cu at 100 ^{o}C as cast with 40MPa stress level and after 100h aging with 20MPa stress levels. There is a smooth surface in Figure 3.8(a) compared with the rough cavity in Figure 3.8(b), indicating more shear deformation of the specimen after aging. Figures 3.9(a) and (b) show the creep fracture surfaces for the alloy Sn-3.5Ag-0.8Cu under the initial aging

condition (as-cast) with different testing temperatures and stress levels. The SEM microstructures revealed that there are tough surfaces at the initial cavity break area and the break line in the middle of the specimen along the failure direction.

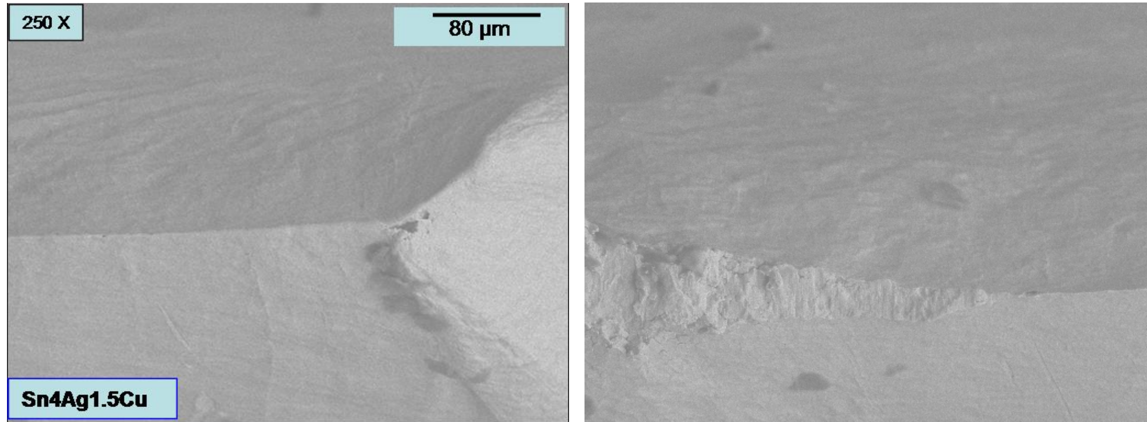

Figure 3.8 (a) Sn-4Ag-1.5Cu at 100°C as-cast with 40MPa stress creep

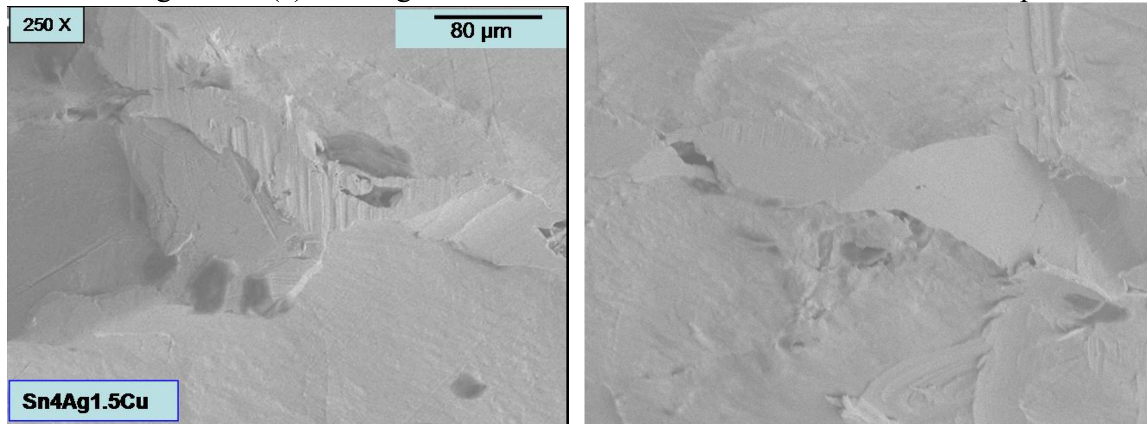

Figure 3.8 (b) Sn-4Ag-1.5Cu at 100°C after 100h aging with 20MPa stress creep

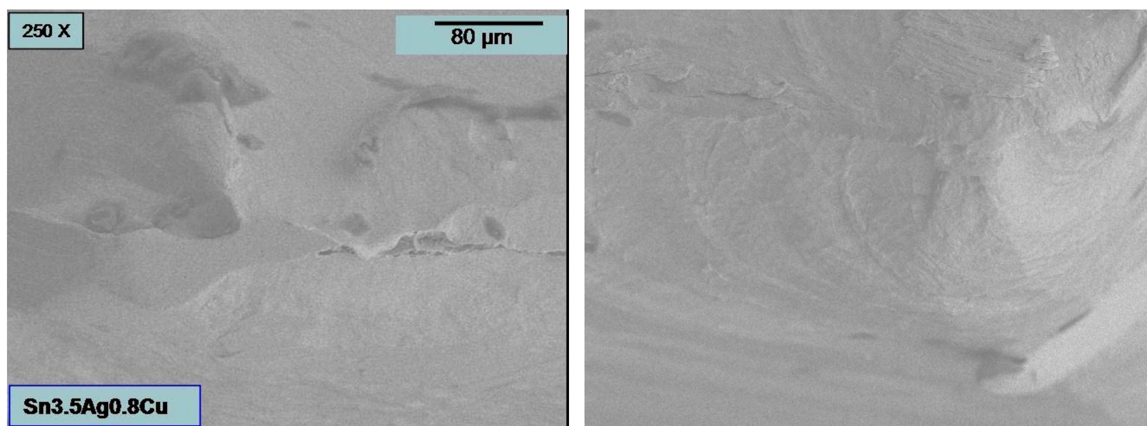

3.9 (a) Sn-3.5Ag-0.8Cu at 100°C of as-cast with 30MPa stress creep

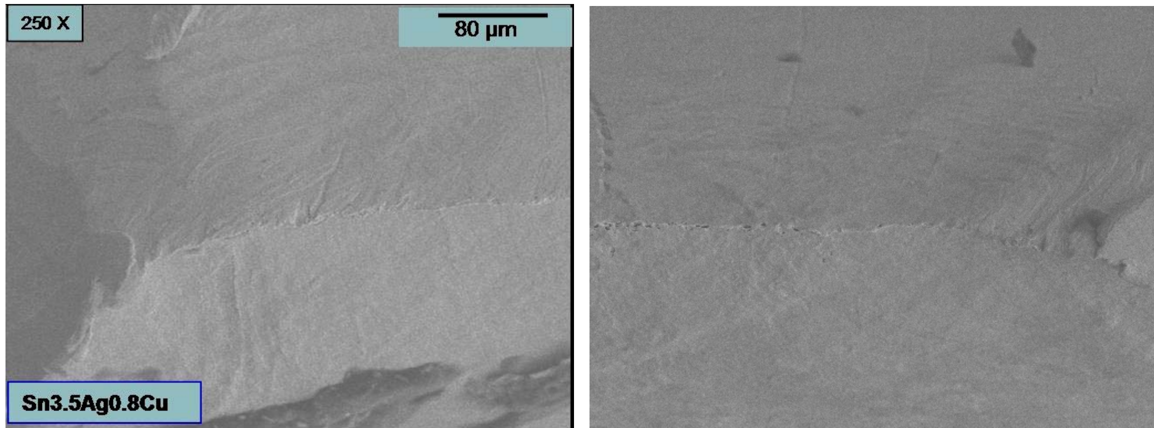

3.9 (b) Sn-3.5Ag-0.8Cu at 150°C of as-cast with 25MPa stress creep

3.4.2 Creep Fracture Cross-Section Analysis

After fracture surface evaluation, the few available specimens were cut along the direction longitudinal to the fracture surface (Figure 3.10). Each specimen was mounted in epoxy and then polished with successive SiC papers, diamond paste and finally with Al_2O_3 paste to a 0.1 micrometer finish. Specimens were etched for a few seconds with 5% volume of hydrochloric acid in methanol to reveal their phase compositions. A scanning electron microscope (SEM) was used to reveal the microstructure. These microstructures showed the effects of both the creep deformation and the test temperature environment.

Figure 3.10 Cut line for cross-sectioning of creep fracture specimens

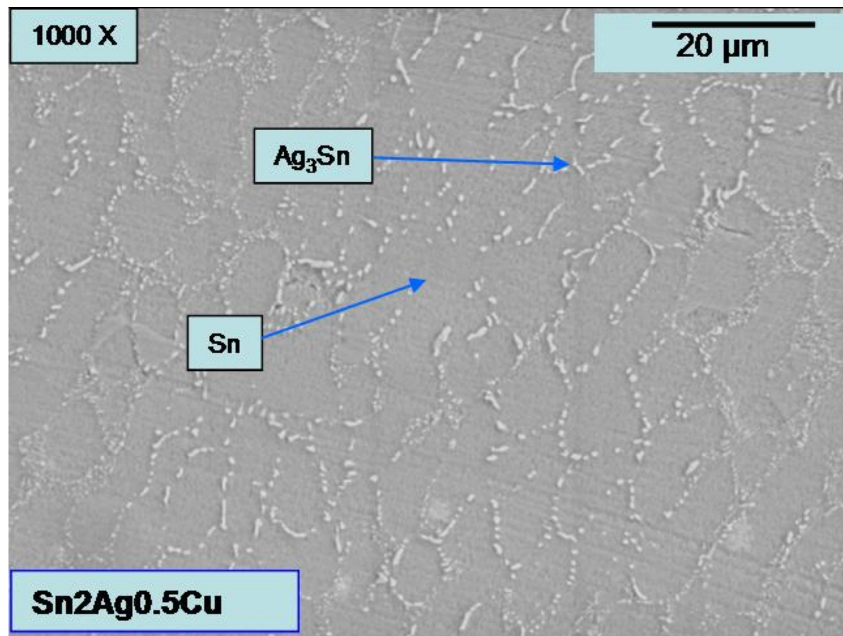

Figure 3.11 (a) Sn-2Ag-0.5Cu testing temp:100°C; creep stress:13MPa; aging:100h

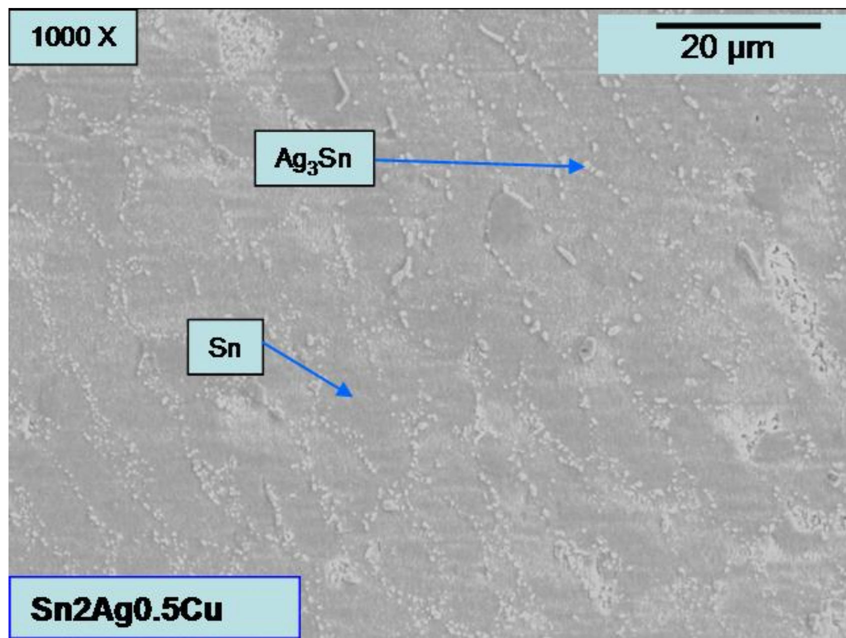

Figure 3.11 (b) Sn-2Ag-0.5Cu testing temp:150°C; creep stress:10MPa; aging:100h

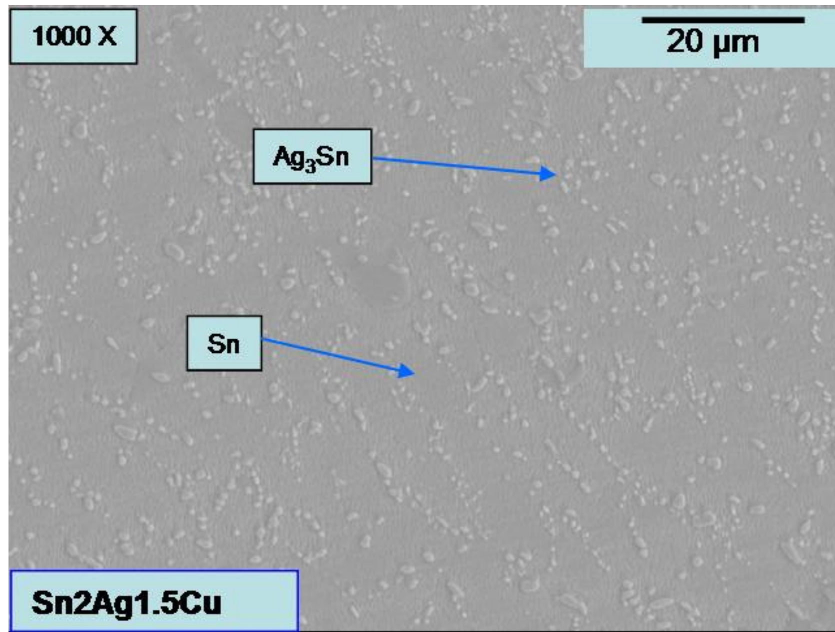

Figure 3.12 Sn-2Ag-1.5Cu testing temp:150°C; creep stress: 9MPa, aging:100h

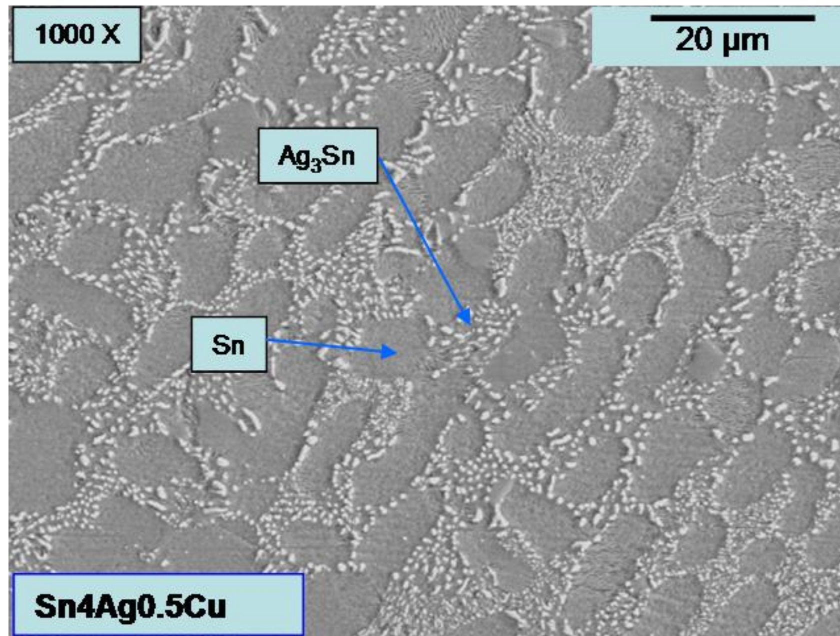

Figure 3.13 Sn-4Ag-0.5Cu testing temp:150°C; creep stress: 15MPa; aging: As-cast

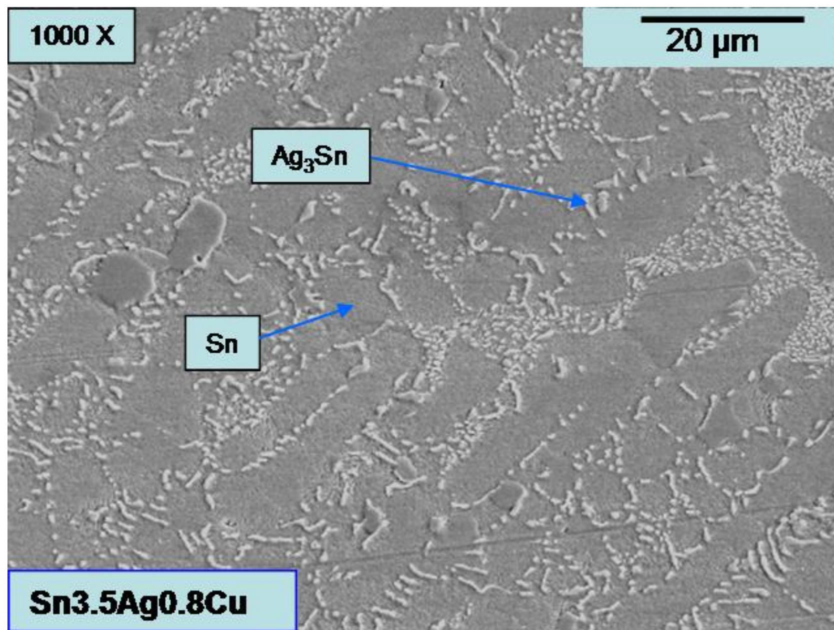

Figure 3.14 Sn-3.5Ag-0.8Cu testing temp:150°C; creep stress: 25MPa; aging: As cast

Figure 3.11(a) and (b) show the microstructures of Sn-2Ag-0.5Cu after 100h aging at slightly different test temperatures and stress levels. Figure 3.12 shows the microstructure of Sn-2Ag-1.5Cu after 100h aging at 150 °C with 9 MPa stress level. Figure 3.13 and 3.14 show the microstructure of Sn-4Ag-0.5Cu and Sn-3.5Ag-0.8Cu at initial as-cast at 150 °C with different stress levels. SEM images and Energy Dispersive Spectroscopy (EDS) analysis revealed the common findings that the microstructure after creep fracture was composed of a tin rich area surrounded by a eutectic area with dispersed Sn_3Ag precipitates and β-Sn. In the initial as-cast aging condition (Figure 3.13 and 3.14) the microstructure was shown to have some condensed dendritic structure, which was related to higher creep resistance in creep data measurements, while after 100h (125 °C) aging time the intermetallic particles tended to coarsen [Figure 3.11 (a),(b) and 3.12], which was related to the decreased creep resistance as aging time increased.

3.5 Conclusion

The tensile creep behavior was investigated at three temperatures (22 °C, 100 °C 150 °C) for five selected alloy compositions (Sn-4Ag-1.5Cu, Sn-4Sg-0.5Cu, Sn-2Ag-1.5Cu, Sn-2Ag-0.5Cu, Sn-3.5Ag-0.8Cu) as-cast, after aging at 125 °C for 100 hours and after aging at 125 °C for 250 hours. The creep resistance decreased as the testing temperature increased for all alloy compositions. For each alloy composition, the creep resistance decreased as the aging time at 125 °C increased. Sn-4Ag-1.5Cu had the highest creep resistance and Sn-3.5Ag-0.5Cu ranked second, while the curves for Sn-2Ag-0.5Cu, Sn-4Ag-0.5Cu and Sn-2Ag-1.5Cu were similar.

A hyperbolic-sine power-law creep constitutive model was developed to provide an acceptable description for all selected alloy compositions at different aging conditions over wide applied stress ranges. Comparison of the hyperbolic-sine creep model data for the selected Sn-Ag-Cu alloys showed that the stress exponent n varied from 4.1 to 5.9, while the activation energy Q varied from 53 kJ /mol to 66 kJ/mol.

The creep fracture surface and cross-section analysis on a few selected specimens by SEM and EDS were conducted to reveal the fracture mechanism after creep fracture. The SEM images of fracture surface indicated the presence of a tough shear surface at the initial cavity break area and the break line in the specimen along the failure direction. SEM pictures of the cross section for creep fracture specimens indicated similar microstructures, composed of a dendritic tin rich area surrounded by a eutectic area with dispersed Sn_3Ag at initial as-cast aging condition, which was related to higher creep resistance in creep data measurements. The microstructure tended to coarsen after aging, which was related to a decreased creep resistance as aging time increased.

CHAPTER 4

Effect of Quaternary Element Bi on Mechanical Properties of Lead Free Solder

4.1 Introduction

In the search for acceptable substitutes for conventional Sn-Pb eutectic solder, Sn-Ag-Cu alloys are considered to be among the best candidates for lead free solders. However, there are still problems to be addressed including issues such as large and brittle intermetallic Ag_3Sn and Cu_6Sn_5 phases which may have a negative effect on the mechanical properties. Adding a quaternary element such as bismuth, boron or zinc to the Sn-Ag-Cu and Sn-Cu eutectic alloy systems is expected to improve the mechanical properties, increase the creep resistance, and refine the microstructure [48, 56, 59]. L. Ye compared the microstructure between Sn-3.5Ag-0.5Cu and Sn-3.5Ag-0.5Cu-0.5B . The research indicted the Ag_3Sn phase in B-containing alloy tends to be spherical and distributed more homogeneously because of boron particles providing nucleation sites during solidification and therefore refining the microstructure [48].

Shine found that adding Bi (0, 2.5, 4.8, 7.5, and 10 wt%) to Sn-3.5Ag resulted in finely dispersed Bi particles and irregular Ag_3Sn IMC around β-Sn globules [37]. The creep resistance of the Sn-3.5Ag alloys was best at 2.5% Bi, showing the smallest creep rate and maximum rupture time [37].

For this study, Sn-3.5Ag-0.8Cu was chosen as the baseline ternary alloy as it is close to the eutectic alloy composition. Commercial bismuth shot (purity 99.999+%, 1-5mm) was combined with tin shot (purity 99.99 +%, 3mm), silver shot (99.9 +%, 1-5mm) and copper shot (99.5+%, 0.5-0.8mm) to create 1% and 2% bismuth containing alloy. The melting process was the same as described in Chapter 2 for Sn-Ag-Cu alloy melting. The chemical analysis results are shown in Table 4.1.

Table 4.1 Chemical analysis for quaternary alloy composition Sn-Ag-Cu-Bi

Target Alloy composition (wt%)	Compositions by chemical analysis (wt%)			
	Sn	Ag	Cu	Bi
94.7Sn-3.5Ag-0.8Cu-1Bi	94.63	3.47	0.81	1.08
93.7Sn-3.5Ag-0.8Cu-2Bi	93.60	3.45	0.82	2.11

Tensile and creep tests were performed on both compositions which had been oil quenched, and the results compared with the properties of Sn-3.5Ag-0.8Cu at the corresponding conditions. The microstructure of Sn-3.5Ag-0.8Cu-1Bi and Sn-3.5Ag-0.8Cu-2Bi at different condition was also investigated using SEM and EDS in order to evaluate the relationship between mechanical properties and microstructure change.

4.2 Tensile Properties of Sn-3.5Ag-0.8Cu-1Bi and Sn-3.5Ag-0.8Cu-2Bi

Tensile tests were performed with an MT-200 tension/torsion thermo-mechanical

test system for Sn-3.5Ag-0.8Cu-1Bi and Sn-3.5Ag-0.8Cu-2Bi at different aging conditions. Figure 4.1 plots the Young's modulus, 0.2%-strain yield stress and ultimate tensile strength distribution for Sn-3.5Ag-0.8Cu-1Bi at a strain rate of 10^{-3}(1/s) at 25 ^{o}C.

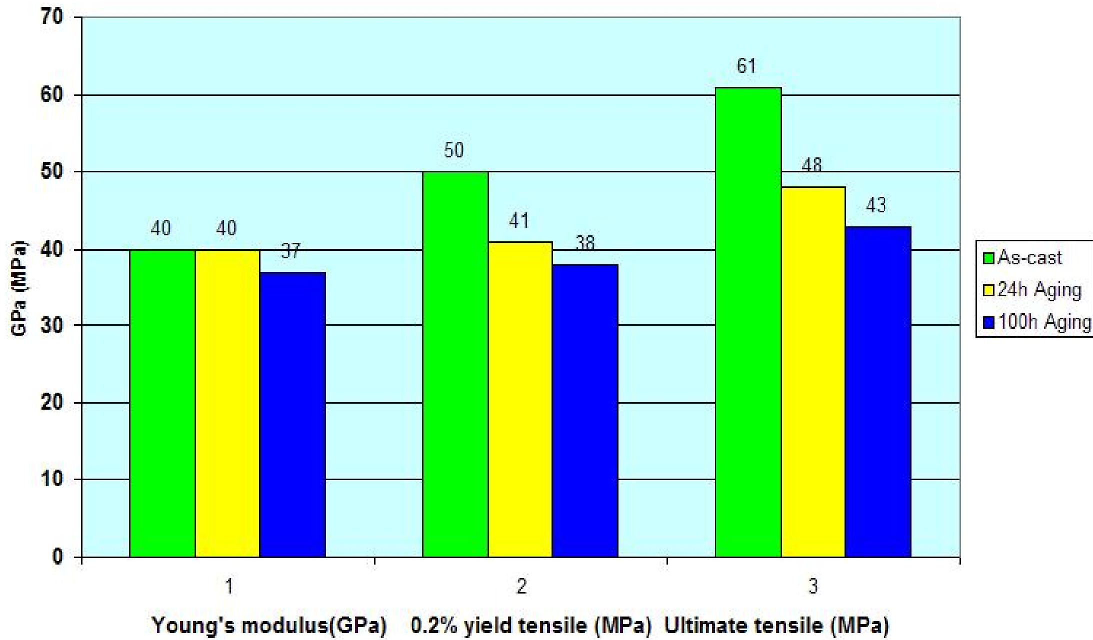

Figure 4.1 Tensile properties change with aging time for Sn-3.5Ag-0.8Cu-1Bi

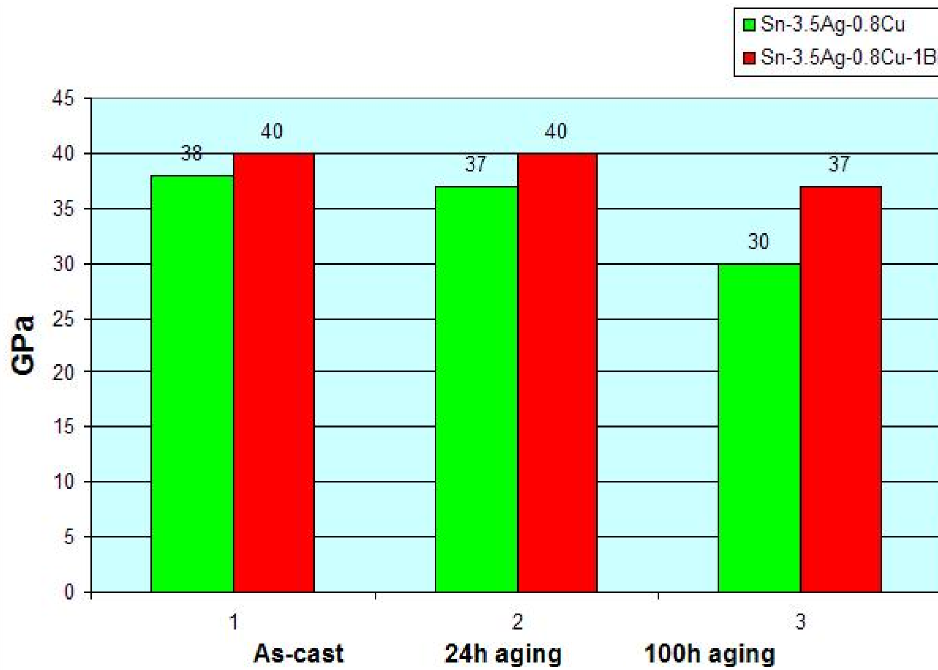

Figure 4.2 (a) Comparison of Young's modulus between Sn-3.5Ag-0.8Cu and Sn-3.5Ag-0.8Cu-1Bi

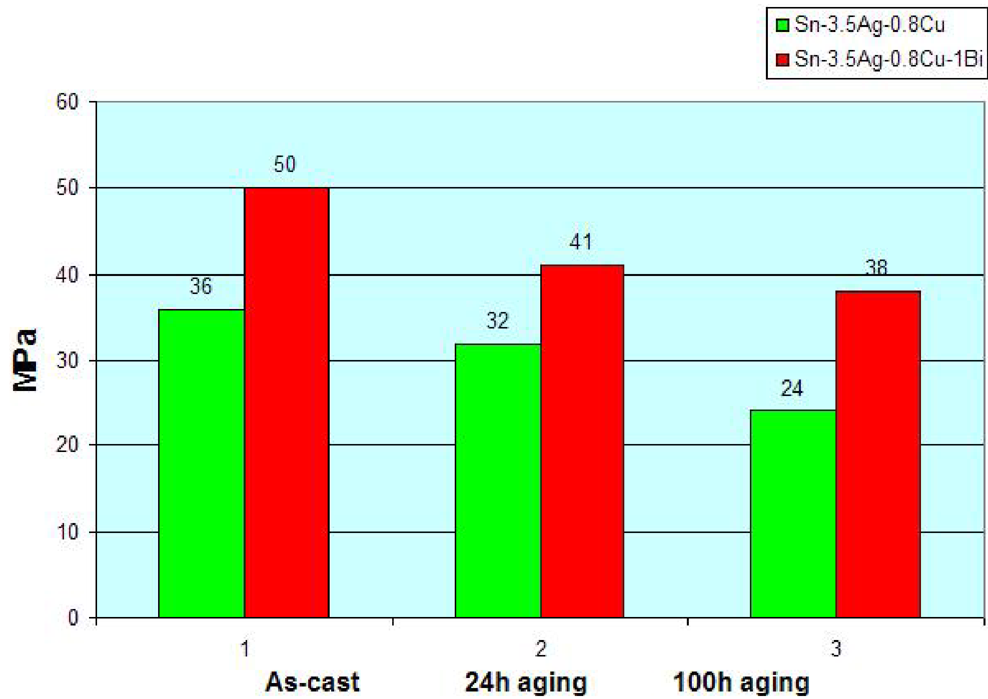

Figure 4.2 (b) Comparison of 0.2% yield strength between Sn-3.5Ag-0.8Cu and Sn-3.5Ag-0.8Cu-1Bi

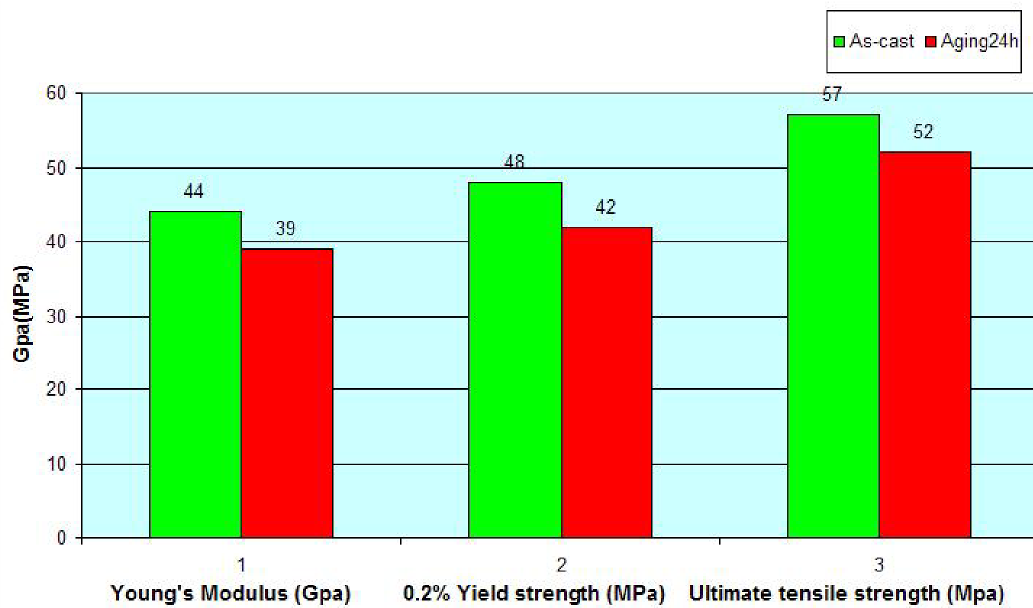

Figure 4.3 Tensile properties change with aging time for Sn-3.5Ag-0.8Cu-2Bi

Figure 4.2 (a) and (b) compare the Young's modulus and yield stress for Sn-3.5Ag-0.8Cu and Sn-3.5Ag-0.8Cu-1Bi, showing that there is no difference for the Young's modulus at initial as-cast and 24h aging, while the Young's modulus of Sn-3.5Ag-0.8Cu-1Bi is higher than Sn-3.5Ag-0.8Cu after 100h at 125 ^{o}C aging. The yield stress for Sn-3.5Ag-0.8Cu-1Bi are higher than those for Sn-3.5Ag-0.8Cu at as-cast, 24h aging and 100h aging. This means that adding Bi to the Sn-Ag-Cu alloy system improves the tensile properties of the Sn-Ag-Cu alloy. Other findings which are similar to earlier studies on the Sn-Ag-Cu alloy revealed that the tensile properties decrease as the aging time increases for both Sn-3.5Ag-0.8Cu-1Bi and Sn-3.5Ag-0.8Cu-2Bi, while the tensile properties with Bi-containing alloy do not decrease as much with aging as Sn-3.5Ag-0.8Cu (Figure 4.1-4.4). Adding Bi weight percent from 1% to 2% will have no significant improvement for tensile properties, while the experiment showed that the alloy Sn-3.5Ag-0.8Cu-2Bi tends to be brittle and broke earlier in the test.

4.3 Creep Behavior of Sn-3.5Ag-0.8Cu-1Bi and Sn-3.5Ag-0.8Cu-2Bi

Creep behavior was investigated at three temperatures (22 ^{o}C, 100 ^{o}C and 150 ^{o}C) for Sn-3.5Ag-0.8Cu-1Bi with three different aging times (as-cast, 24h, 100h) and for Sn-3.5Ag-0.8Cu-2Bi with two different aging times (as-cast, 24h). Creep data was plotted as a log-log graph of strain versus stress, as shown in figures 4.5 and 4.6. The creep resistance decreased as the testing temperature increased for both alloy compositions, and the creep data of both alloy compositions at 100 ^{o}C and 150 ^{o}C are very close and similar for all aging conditions, while the creep data at 22 ^{o}C was different for both alloy compositions. The creep data curves for Sn-3.5Ag-0.8Cu (Figure 4.4) were plotted as a baseline to compare the effect of adding bi element on the creep behavior.

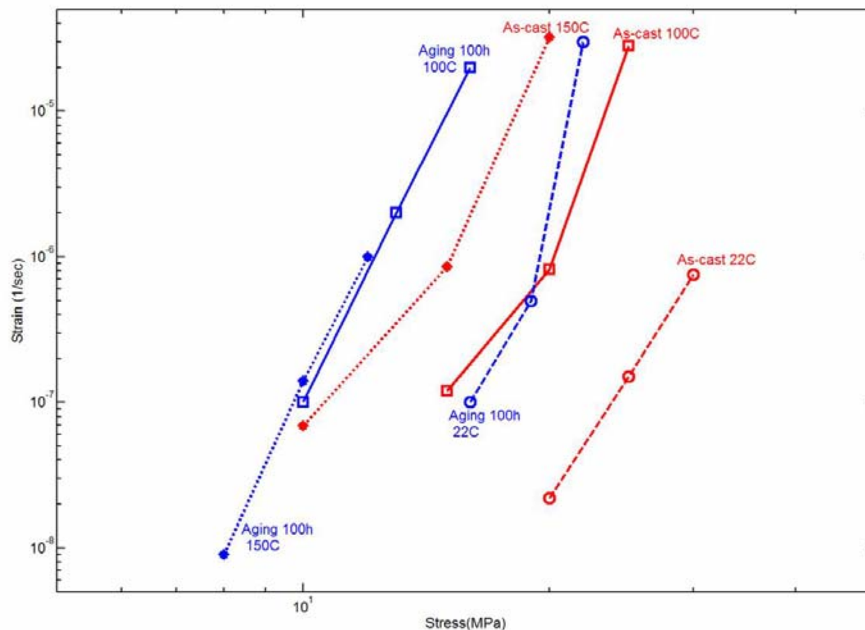

Figure 4.4 Comparison of creep data for Sn-3.5Ag-0.8Cu at different aging conditions and test temps

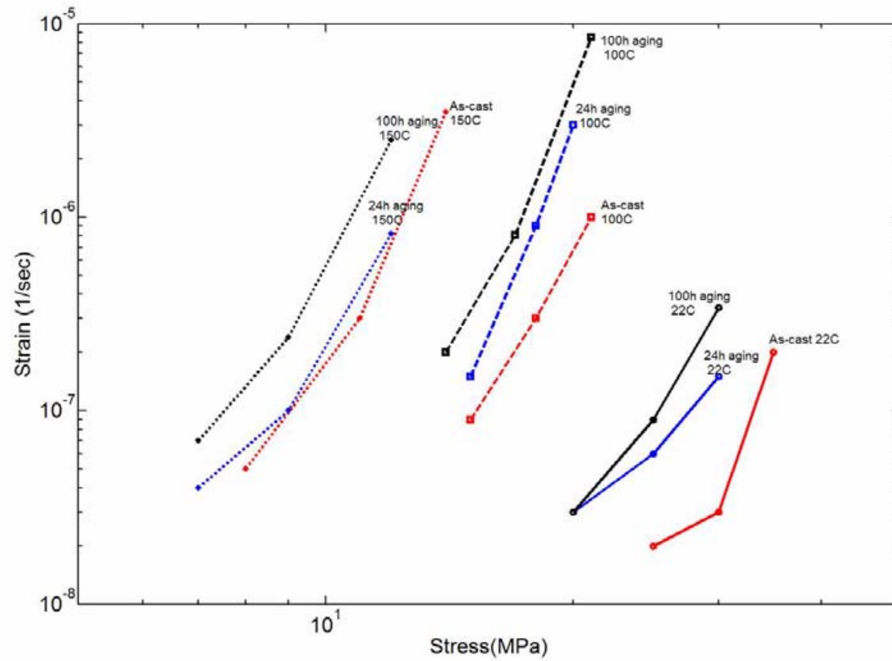

Figure 4.5 Comparison of creep data for Sn-3.5Ag-0.8Cu-1Bi at different aging conditions and testing temps

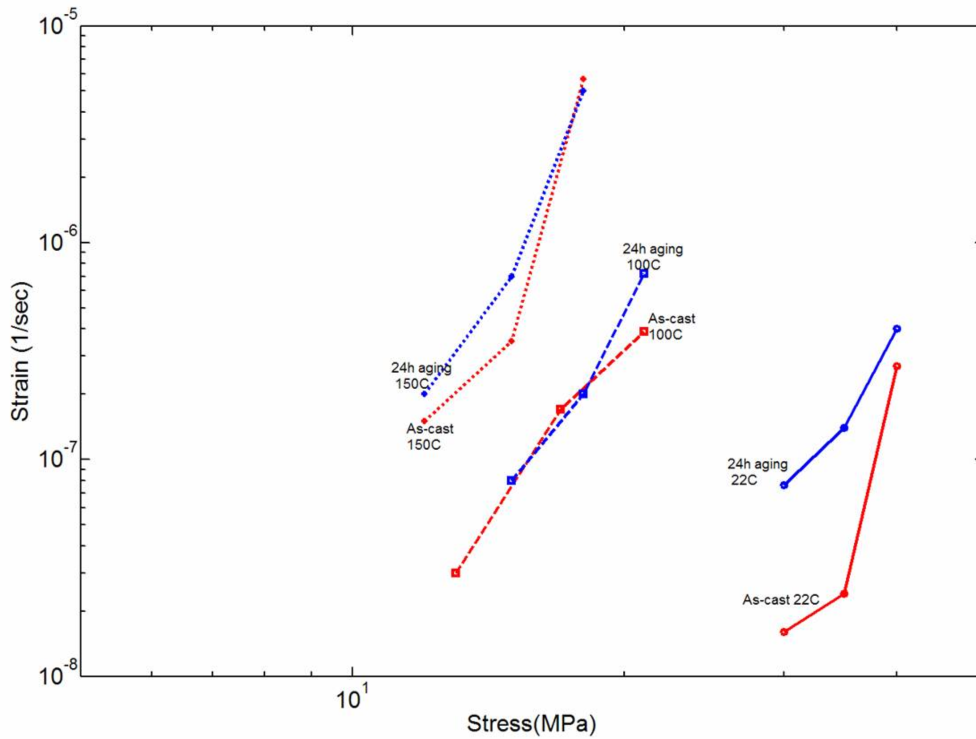

Figure 4.6 Comparison of creep data for Sn-3.5Ag-0.8Cu-2Bi at different aging conditions and testing temps

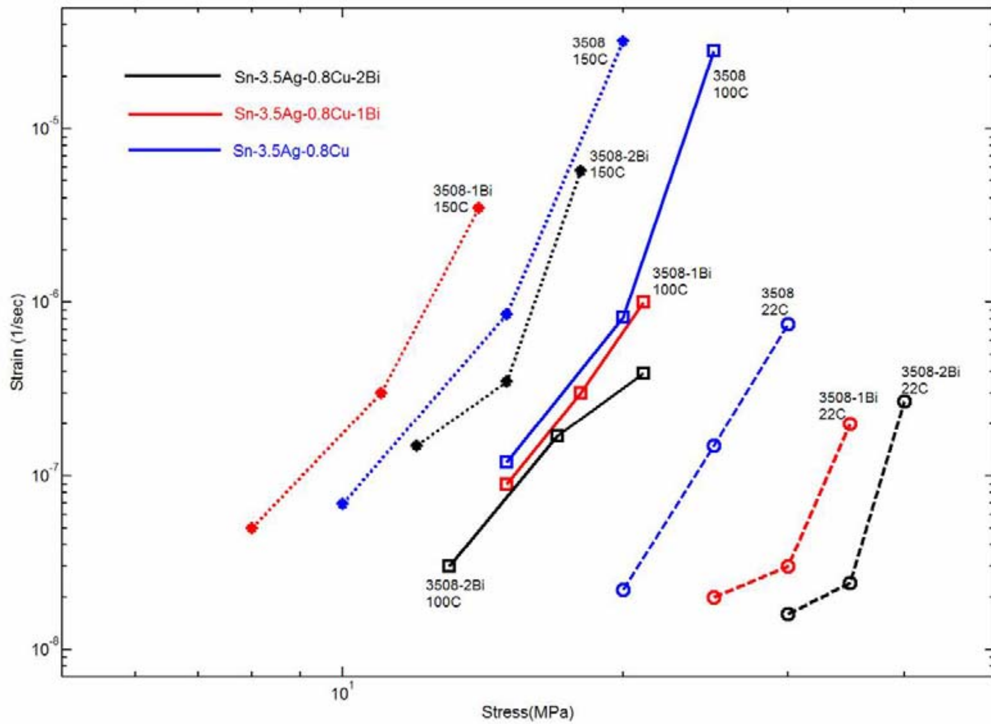

Figure 4.7 Comparison of creep data of Sn-3.5Ag-0.8Cu-2Bi, Sn-3.5Ag-0.8Cu-1Bi and Sn-3.5Ag-0.8Cu at initial as-cast condition

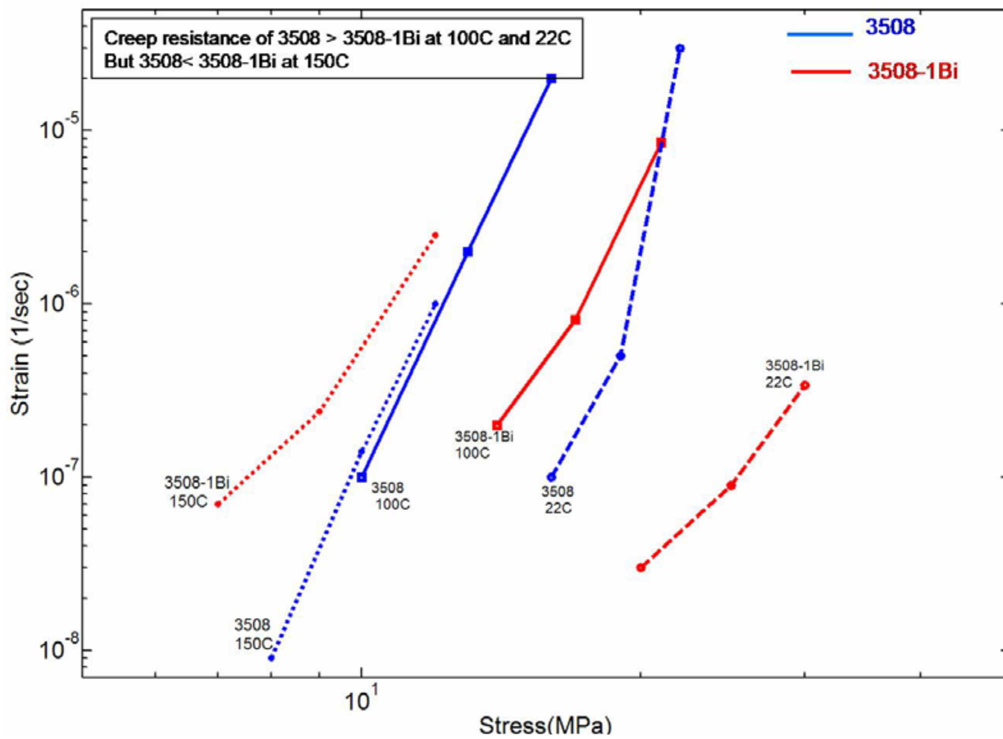

Figure 4.8 Comparison of creep data between Sn-3.5Ag-0.8Cu-1Bi and Sn-3.5Ag-0.8Cu with 100h aging at 125 ^{o}C

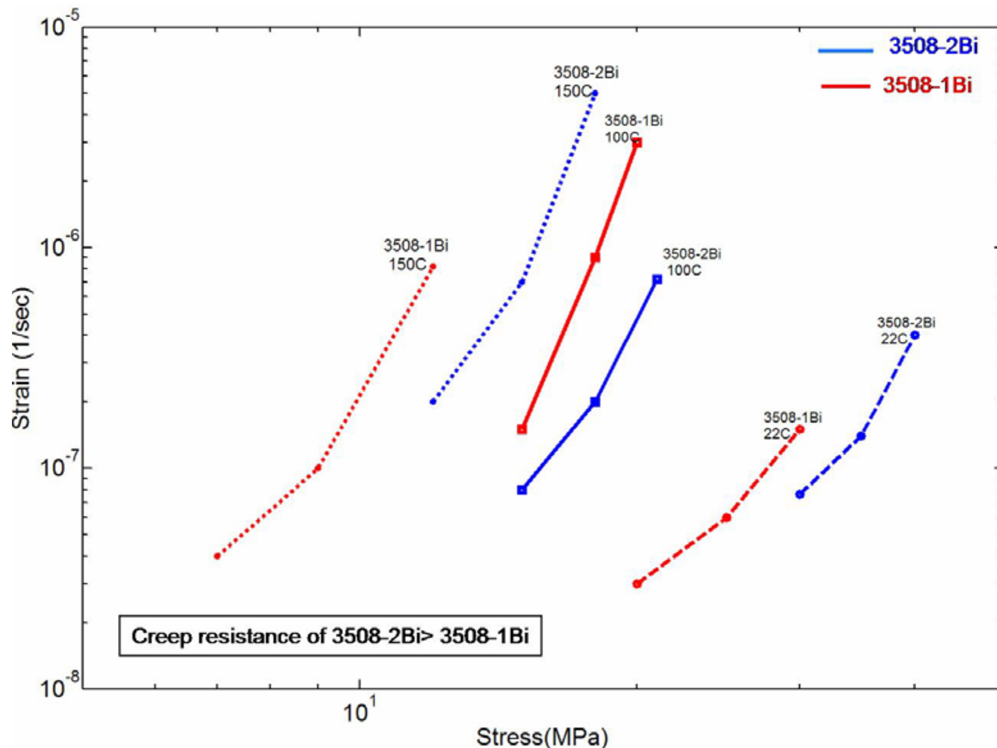

Figure 4.9 Comparison of creep data between Sn-3.5Ag-0.8Cu-1Bi and Sn-3.5Ag-0.8Cu-2Bi with 24h aging at 125°C condition

A comparison of the creep data of Sn-3.5Ag-0.8Cu-2Bi, Sn-3.5Ag-0.8Cu-1Bi and Sn-3.5Ag-0.8Cu at initial as-cast aging condition (Figures 4.7) shows that the creep resistance of Sn-3.5Ag-0.8Cu-1Bi and Sn-3.5Ag-0.8Cu-2Bi are higher than Sn-3.5Ag-0.8Cu at temperatures of 22°C and 100°C, but the creep data of Sn-3.5Ag-0.8Cu-2Bi and Sn-3.5Ag-0.8Cu are close at 150 °C and the creep resistance of Sn-3.5Ag-0.8Cu-1Bi is lower than Sn-3.5Ag-0.8Cu. Figure 4.8 compares the creep data between Sn-3.5Ag-0.8Cu-1Bi and Sn-3.5Ag-0.8Cu after 100h aging and shows the creep resistance of Sn-3.5Ag-0.8Cu-1Bi is higher than Sn-3.5Ag-0.8Cu at 22 °C, but lower at 100 °C and 150 °C. This experiment result needs further investigation. A comparison of the creep data between Sn-3.5Ag-0.8Cu-1Bi and Sn-3.5Ag-0.8Cu-2Bi (Figures 4.9) shows a slightly higher creep resistance for Sn-3.5Ag-0.8Cu-2Bi than for Sn-3.5Ag-0.8Cu-1Bi.

4.4 Microstructure Analysis for Sn-3.5Ag-0.8Cu-1Bi and Sn-3.5Ag-0.8Cu-2Bi

4.4.1 Microstructural Change With Aging Time

Sn-Ag-Cu-Bi quaternary alloys undergo strong microstructural changes after aging. Figures 4.10 and 4.11 show the microstructure for initial as cast, aging for 24h at 125 °C and aging for 100h at 125 °C specimens of Sn-3.5Ag-0.8Cu-1Bi and Sn-3.5Ag-0.8Cu-2Bi, respectively. The SEM images clearly show the slow phase coarsening that develops during aging and the intermetallic needle-like or spherical particles that merge

to form the larger intermetallic particles, which appear as platelets. Figure 4.10 (d) is the 2 times magnification of Figure 4.10 (c) which shows the Bi particles that were detected by EDS. Adding Bi to the Sn-Ag-Cu alloy provides nucleation sites during solidification and therefore refines the microstructure for both the Sn-rich phase and the Ag_3Sn precipitates in the second phase [59]. As the microstructures of Sn-3.5Ag-0.8Cu-1Bi and Sn-3.5Ag-0.8Cu-2Bi were not coarsened as quickly as Sn-Ag-Cu alloy when aging times increased, the tensile properties of Sn-3.5Ag-0.8Cu-1Bi and Sn-3.5Ag-0.8Cu-2Bi were not changed as significantly as Sn-Ag-Cu alloy.

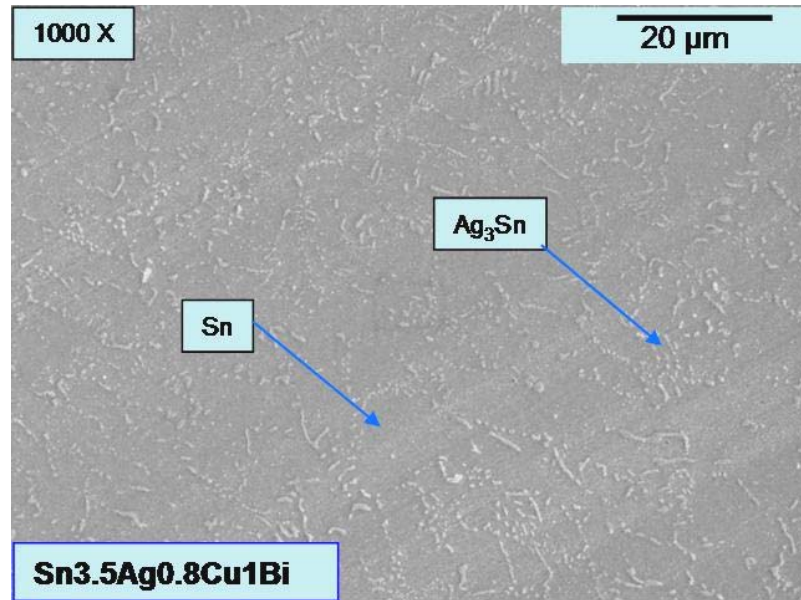

Figure 4.10 (a) SEM microstructure of Sn-3.5Ag-0.8Cu-1Bi at initial as-cast condition

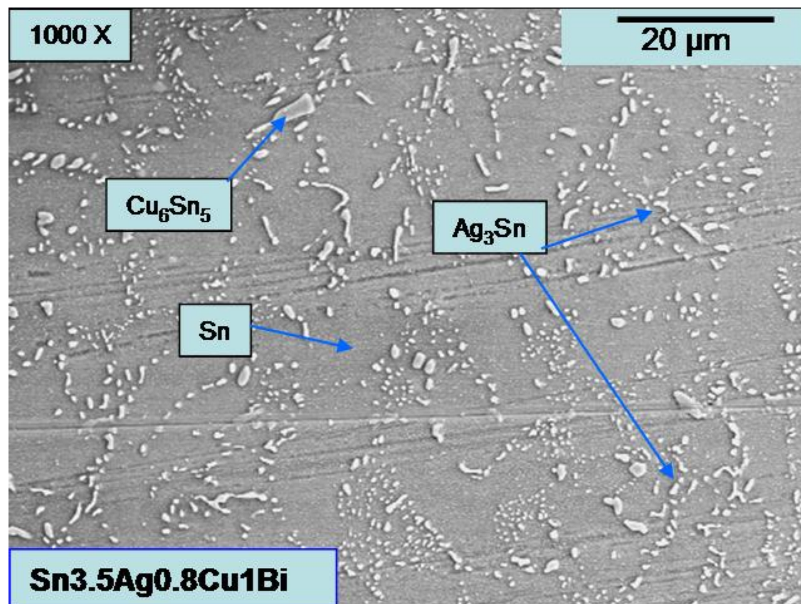

Figure 4.10 (b) SEM microstructure of Sn-3.5Ag-0.8Cu-1Bi after 24h aging at 125 ^oC

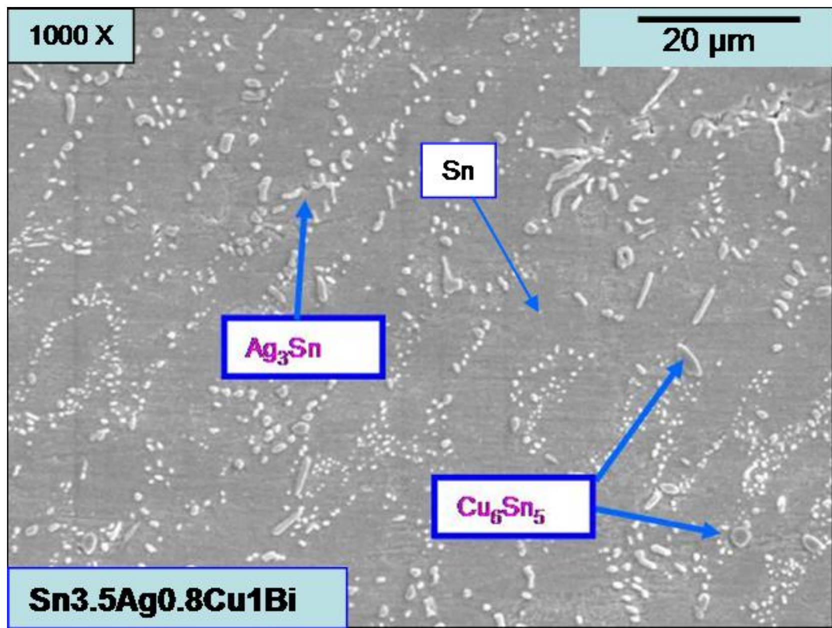

Figure 4.10 (c) SEM microstructure of Sn-3.5Ag-0.8Cu-1Bi after 100h aging at 125 ^{o}C

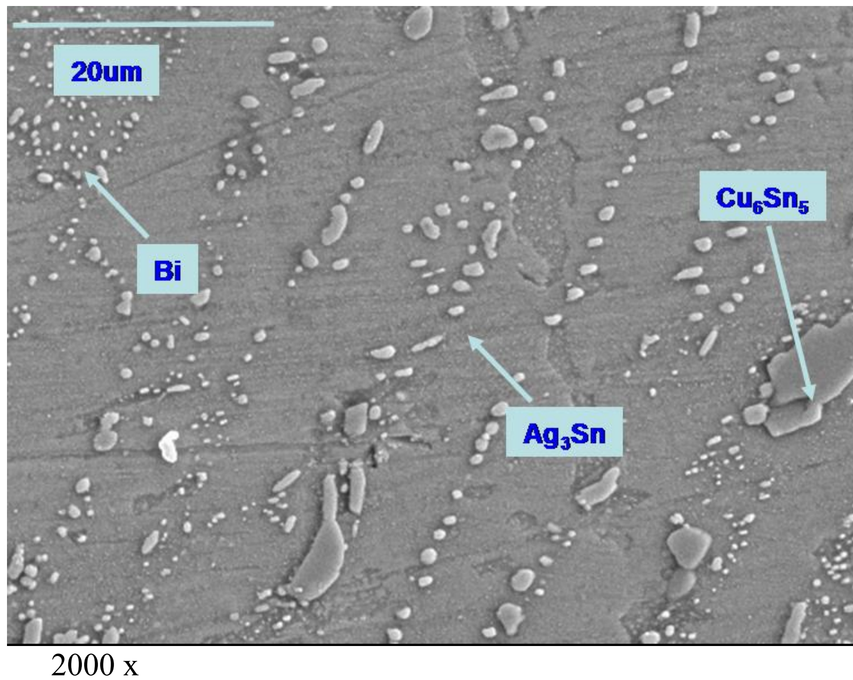

2000 x

Figure 4.10 (d) SEM microstructure of Sn-3.5Ag-0.8Cu-1Bi after 100h aging at 125 ^{o}C

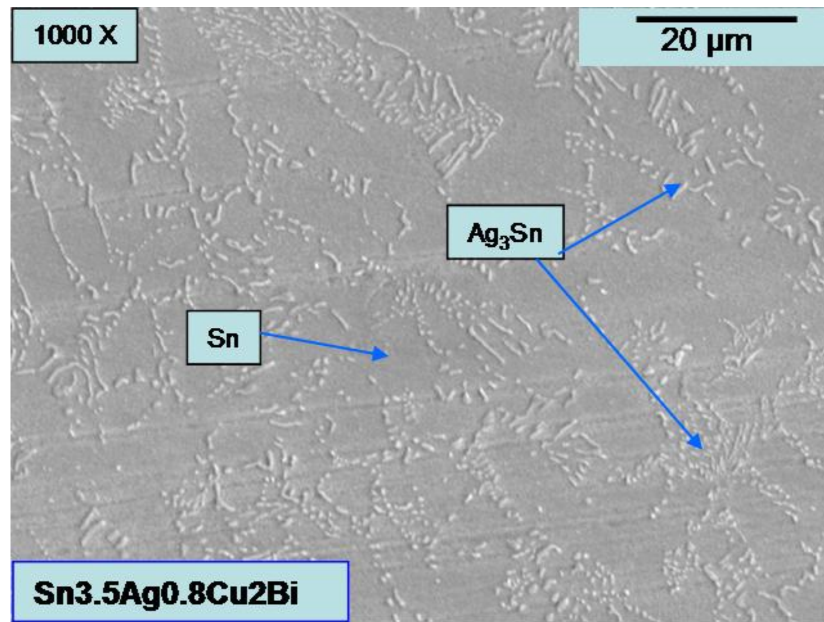

Figure 4.11 (a) SEM microstructure of Sn-3.5Ag-0.8Cu-2Bi at initial as-cast condition

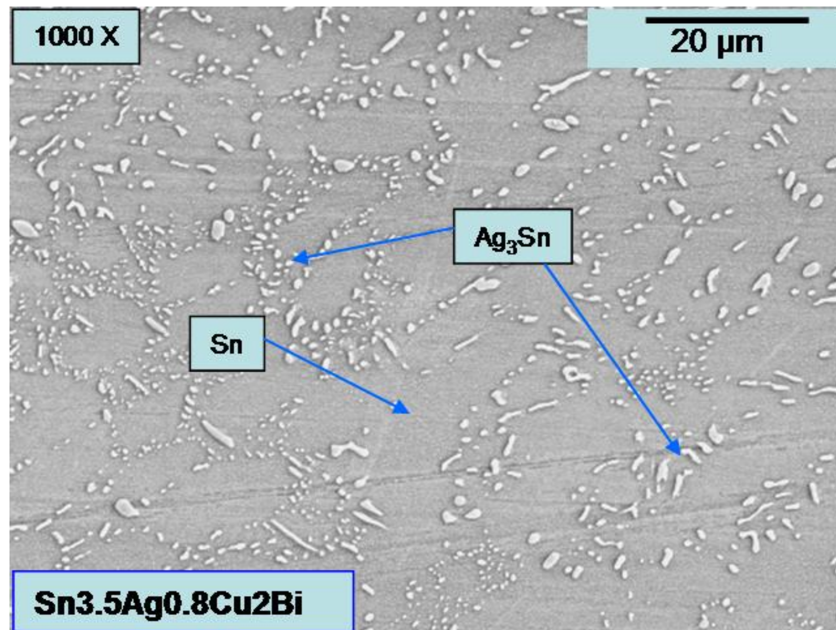

Figure 4.11 (b) SEM microstructure of Sn-3.5Ag-0.8Cu-2Bi after 24h aging at 125 ^{o}C

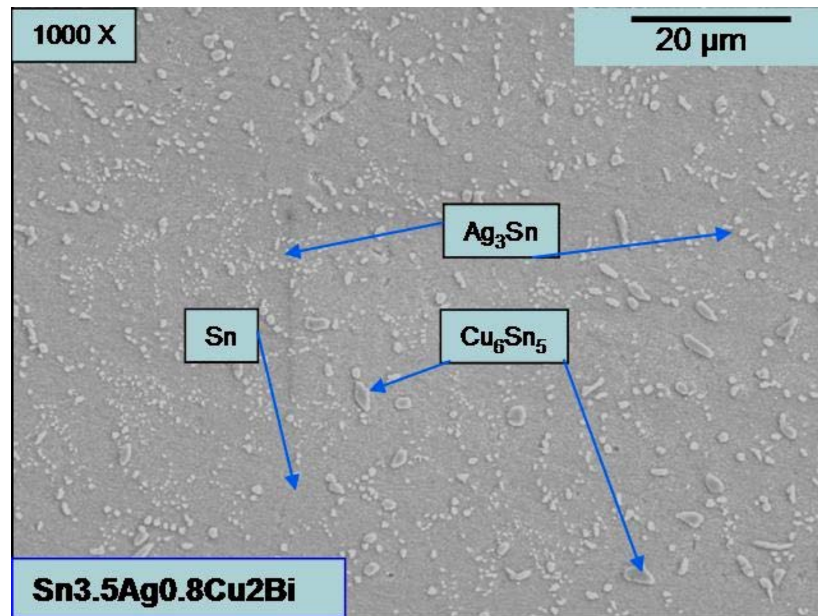

Figure 4.11 (c) SEM microstructure of Sn-3.5Ag-0.8Cu-2Bi after 100h aging at 125 °C

4.4.2 Creep Fracture Microstructure Analysis

Creep fracture surface analysis and cross-section microstructure evaluation were conducted on a few selected creep fracture specimens. Figure 4.12 shows the creep fracture surface for Sn-3.5Ag-0.8Cu-1Bi at different testing temperatures, aging times and stress levels. Both images show the rough cavity surface created at the initial break point of creep specimen, while there are also break lines in the specimen.

The addition of Bi to the Sn-Ag-Cu alloy system increased the propensity for brittle creep fracture. For Bi containing alloys, creep rupture occurred primarily via the mechanism of high temperature dislocation creep, with contributions from nucleation and the growth of creep cavities, grain boundary sliding and intergranular brittle fracture. [37]

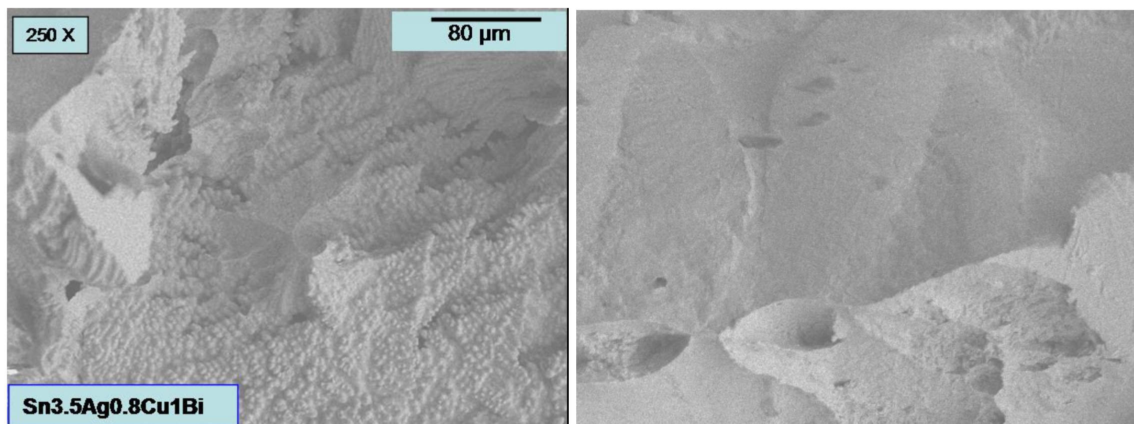

Figure 4.12 (a) Sn-3.5Ag-0.8Cu-1Bi at 150 °C with 24h aging at a creep stress of 12MPa

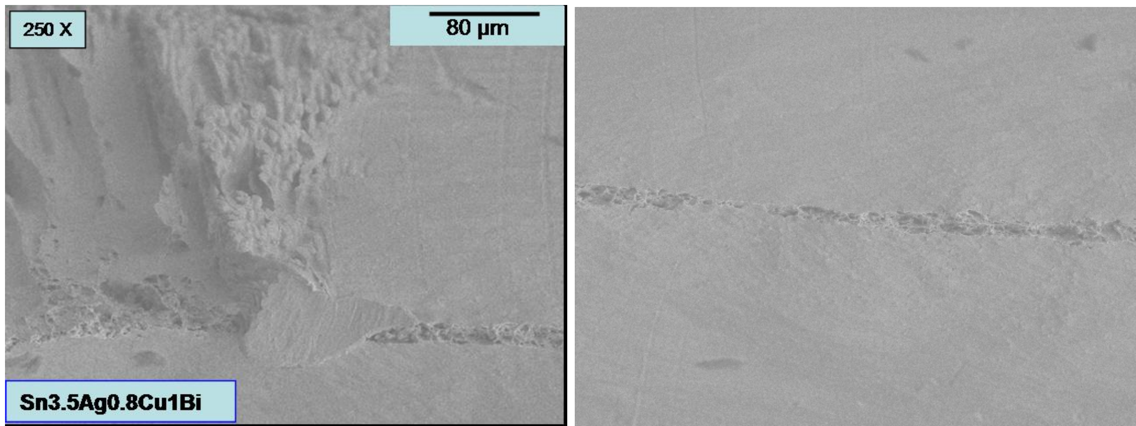

Figure 4.12 (b) Sn-3.5Ag-0.8Cu-1Bi at 100 ^{o}C with 100h aging at a creep stress of 21MPa

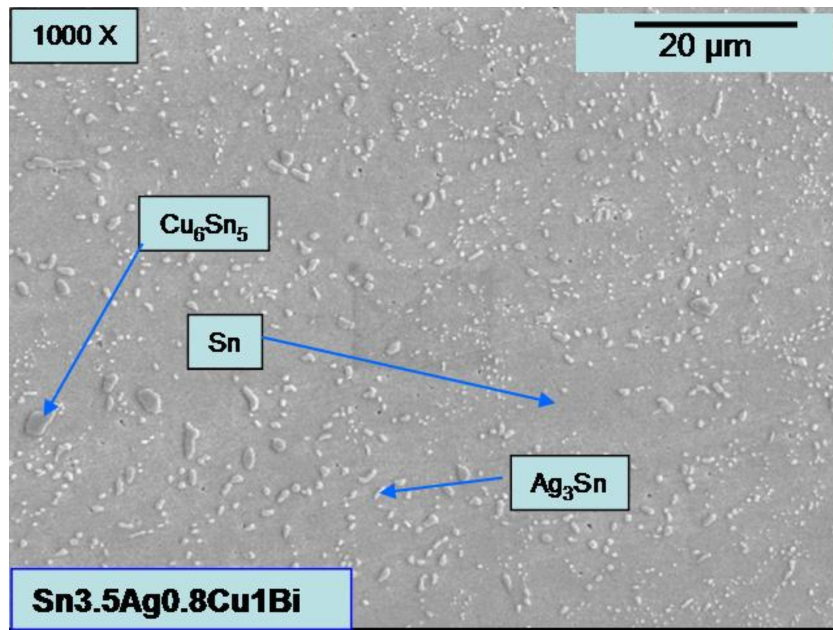

Figure 4.13 (a) Sn-3.5Ag-0.8Cu-1Bi-testing temp:100 ^{o}C; creep stress: 21MPa; aging :100h

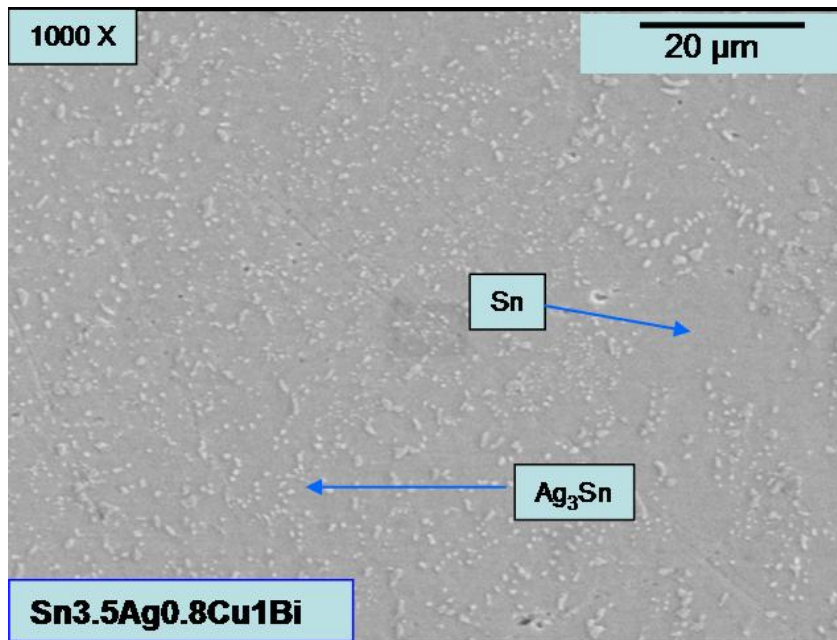

Figure 4.13 (b) Sn-3.5Ag-0.8Cu-1Bi-testing temp: 150 ^{o}C; creep stress:12MPa; aging: 24h

Figure 4.13 shows the microstructure of Sn-3.5Ag-0.8Cu-1Bi revealed by SEM at different testing temperatures, creep stress levels and aging times after creep testing (i.e. after fracture). SEM pictures and EDS analysis revealed that Sn_3Ag or small amounts of Cu_6Sn_5 and small Bi particles are randomly dispersed in Sn rich areas. The effect of aging will cause the coarsening of the microstructure, while there is no significant difference in the microstructure before and after creep test.

4.5 Summary

There is no difference for the Young's modulus at initial as-cast and 24h aging between Sn-3.5Ag-0.8Cu-1Bi and Sn-3.5Ag-0.8Cu, while the Young's modulus of Sn-3.5Ag-0.8Cu-1Bi is higher than Sn-3.5Ag-0.8Cu after 100h at 125 ^{o}C aging. The yield stress for Sn-3.5Ag-0.8Cu-1Bi are higher than those for Sn-3.5Ag-0.8Cu at as-cast, 24h aging and 100h aging, which indicted that adding Bi to the Sn-Ag-Cu alloy system improves the tensile properties of the Sn-Ag-Cu alloy. The tensile properties decreased as the aging time increased for Sn-Ag-Cu-Bi alloys. There is no significant difference for tensile properties between the alloy Sn-Ag-Cu-1Bi and Sn-Ag-Cu-2Bi, while the tensile properties with Bi-containing alloy do not decrease as much with aging as Sn-3.5Ag-0.8Cu. Adding Bi weight percent from 1% to 2% will have no significant improvement for tensile properties, while the experiment showed that the alloy Sn-3.5Ag-0.8Cu-2Bi tends to be brittle and broke earlier in the test.

The creep resistance of Sn-3.5Ag-0.8Cu-1Bi and Sn-3.5Ag-0.8Cu-2Bi were higher than Sn-3.5Ag-0.8Cu at temperatures of 22°C and 100°C, but the creep data of Sn-3.5Ag-0.8Cu-2Bi and Sn-3.5Ag-0.8Cu are close at 150 ^{o}C and the creep resistance of Sn-3.5Ag-0.8Cu-1Bi was lower than Sn-3.5Ag-0.8Cu. The comparison of the creep data

between Sn-3.5Ag-0.8Cu-1Bi and Sn-3.5Ag-0.8Cu after 100h aging shown the creep resistance of Sn-3.5Ag-0.8Cu-1Bi is higher than Sn-3.5Ag-0.8Cu at 22 ^{o}C, but lower at 100 ^{o}C and 150 ^{o}C. This experiment result needs further investigation. A comparison of the creep data between Sn-3.5Ag-0.8Cu-1Bi and Sn-3.5Ag-0.8Cu-2Bi shown a slightly higher creep resistance for Sn-3.5Ag-0.8Cu-2Bi than for Sn-3.5Ag-0.8Cu-1Bi.

After creep fracture, the Sn-Ag-Cu-Bi alloy specimens had rough cavity surfaces at the initial break point of the creep specimen and there were also break lines in the specimen. Microstructural analysis of the creep fracture cross-section of the Sn-3.5Ag-0.8Cu-1Bi alloy revealed that Sn_3Ag or small amounts of Cu_6Sn5 and tiny Bi particles were randomly dispersed in the Sn rich area. The effect of aging will cause the coarsening of the microstructure, while there is no significant difference in the microstructure before and after creep test.

CHAPTER 5

CONCLUSIONS

5.1 Measurement of Tensile Properties and Microstructural Analysis of Sn-Ag-Cu Lead Free Solders as a Function of Composition

The mechanical and microstructural properties of Sn-Ag-Cu alloys with Ag varying from 2wt% to 4wt% and Cu varying from 0.5wt% to 1.5wt% were systematically studied. A suitable specimen preparation process was developed using small rectangular cross-section glass tubes. Three sample preparation techniques (water quenched, oil quenched and water quenched followed by reflow) were studied and the oil quenched specimen microstructure was found to be comparable to that of a reflow soldered CSP solder joint. The water quenched sample had a finer grain structure, while the water quenched and reflowed sample had a coarser grain structure compared to the CSP solder joint. Both the oil quenched specimen and CSP solder joint exhibited a eutectic region of Sn with moderately dispersed Ag_3Sn intermetallic, surrounded by a dendritic Sn-rich phase.

For oil quenched specimens, Young's modulus as a function of alloy composition (Ag=2%~4%, Cu = 0.5% ~1.5%) ranged from 37-41 GPa and decreased to 30-32 GPa after aging for 100 hours and 250 hours at 125 ^{o}C. There was no significant difference in Young's Modulus as a function of alloy composition. After an initial decrease in modulus after 100 hours at 125 ^{o}C, there was an insignificant change with further aging. Young's modulus ranged from 31-40 GPa for water quenched with reflow specimens, indicating that there was significant change as a function of alloy composition.

For the oil quenched specimens, the distribution of 0.2% strain yield stress and ultimate tensile strength as a function of alloy composition was more significant. Both were significantly higher for higher levels of silver and copper composition, gradually decreasing to the lowest value for low silver and copper compositions. The absolute values of the yield stress and ultimate tensile strength both decreased during the high temperature aging process. The specimens that were water quenched with reflow exhibited the same trend, but had different values compared to the specimens that were oil quenched.

The tensile properties for selected alloy oil quenched specimens degraded significantly after aging for 24h at 125 ^{o}C. Yield strength and ultimate tensile strength decreased more markedly than Young's modulus. This was confirmed by microstructural analysis, which showed there was already a significant coarsening effect after only 24h of aging.

5.2 Aging Effect on Creep Behavior of Sn-Ag-Cu Lead Free Solder System

The tensile creep behavior was investigated at three temperatures (22 ^{o}C, 100 ^{o}C 150 ^{o}C) for five selected alloy compositions (Sn-4Ag-1.5Cu, Sn-4Sg-0.5Cu, Sn-2Ag-

1.5Cu, Sn-2Ag-0.5Cu, Sn-3.5Ag-0.8Cu) as-cast, after aging at 125 ^{o}C for 100 hours and after aging at 125 ^{o}C for 250 hours. The creep resistance decreased as the testing temperature increased for all alloy compositions. For each alloy composition, the creep resistance decreased as the aging time at 125 ^{o}C increased. Sn-4Ag-1.5Cu had the highest creep resistance and Sn-3.5Ag-0.5Cu ranked second, while the curves for Sn-2Ag-0.5Cu, Sn-4Ag-0.5Cu and Sn-2Ag-1.5Cu were similar.

A hyperbolic-sine power-law creep constitutive model was developed to provide an acceptable description for all selected alloy compositions at different aging conditions over wide applied stress ranges. Comparison of the hyperbolic-sine creep model data for the selected Sn-Ag-Cu alloys showed that the stress exponent n varied from 4.1 to 5.9, while the activation energy Q varied from 53 kJ /mol to 66 kJ/mol.

The creep fracture surface and cross-section analysis were conducted on a few selected specimens by SEM and EDS to reveal the fracture mechanism after creep fracture. The SEM images of fracture surface indicated the presence of a tough shear surface at the initial cavity break area and the break line in the specimen along the failure direction. SEM pictures of the cross section for creep fracture specimens indicated similar microstructures, composed of a dendritic tin rich area surrounded by a eutectic area with dispersed Sn_3Ag at initial as-cast aging condition, which was related to higher creep resistance in creep data measurements. The microstructure tended to coarsen after aging, which was related to the decreased creep resistance as aging time increased.

5.3 Effect of Quaternary Element Bi on the Mechanical Properties of Sn-Ag-Cu Lead Free Solder

There was no difference for the Young's modulus at initial as-cast and 24h aging between Sn-3.5Ag-0.8Cu-1Bi and Sn-3.5Ag-0.8Cu, while the Young's modulus of Sn-3.5Ag-0.8Cu-1Bi was higher than Sn-3.5Ag-0.8Cu after 100h at 125 ^{o}C aging. The yield stress for Sn-3.5Ag-0.8Cu-1Bi was higher than for Sn-3.5Ag-0.8Cu at as-cast, 24h aging and 100h aging indicating that adding Bi to the Sn-Ag-Cu alloy system improved the tensile properties of the Sn-Ag-Cu alloy. The tensile properties decreased as the aging time increased for Sn-Ag-Cu-Bi alloys. There was no significant difference for tensile properties between the alloy Sn-Ag-Cu-1Bi and Sn-Ag-Cu-2Bi, while the tensile properties with Bi-containing alloy did not decrease as much with aging as Sn-3.5Ag-0.8Cu. Adding Bi weight percent from 1% to 2% had no significant improvement for tensile properties, while in the experiment it was found that the alloy Sn-3.5Ag-0.8Cu-2Bi tended to be brittle and broke earlier in the test.

The creep resistance of Sn-3.5Ag-0.8Cu-1Bi and Sn-3.5Ag-0.8Cu-2Bi were higher than Sn-3.5Ag-0.8Cu at temperatures of 22°C and 100°C, but the creep data of Sn-3.5Ag-0.8Cu-2Bi and Sn-3.5Ag-0.8Cu were close at 150 ^{o}C and the creep resistance of Sn-3.5Ag-0.8Cu-1Bi was lower than Sn-3.5Ag-0.8Cu. The comparison of the creep data between Sn-3.5Ag-0.8Cu-1Bi and Sn-3.5Ag-0.8Cu after 100h aging showed the creep resistance of Sn-3.5Ag-0.8Cu-1Bi was higher than Sn-3.5Ag-0.8Cu at 22 ^{o}C, but lower at 100 ^{o}C and 150 ^{o}C. This experiment result needs further investigation. A comparison of the creep data between Sn-3.5Ag-0.8Cu-1Bi and Sn-3.5Ag-0.8Cu-2Bi showed a slightly higher creep resistance for Sn-3.5Ag-0.8Cu-2Bi than for Sn-3.5Ag-0.8Cu-1Bi.

After creep fracture, the Sn-Ag-Cu-Bi alloy specimens had rough cavity surfaces at the initial break point of the creep specimen and there were also break lines in the specimen. Microstructural analysis of the creep fracture cross-section of the Sn-3.5Ag-0.8Cu-1Bi alloy revealed that Sn_3Ag or small amounts of Cu_6Sn5 and tiny Bi particles were randomly dispersed in the Sn rich area. Aging caused coarsening of the microstructure while there was no significant difference in the microstructure before and after creep test.

BIBLIOGRAPHY

[1] Qian, Z.; Abhijit, D.; Peter, H.; "Creep and High-temperature Isothermal Fatigue of Pb-free Solders", Proc. IPACK2003-35361, *International Electronic Packaging Technical Conference,* July 6-11, 2003 Maui Hawaii, USA.

[2] M. Tisza, "Physical Metallurgy for Engineers," 2001 ASM International and Freund Publishing House Ltd., ISBN 0-87170-725-X

[3] J. Nottay, M. Dusek, C. Hunt, " Creep Properties of SnAgCu Solder in Surface Mount Assemblies," National Physical Laboratory, *Report MATC (A) 51, ISSN1473-2734,* August, 2001, Teddington, Middlesex, UK TW11 0LW.

[4] Qiang, X.; Luu, N.; William, D.; "Aging and Creep Behavior of Sn3.9Ag0.6Cu Solder Alloy", *Electronic Components and Technology Conf*erence, 2004, pp1325-1332.

[5] Jean, P.; "Sn-Ag-Cu Properties and Creep data", National Institute of Standards and Technology, http://www.metallurgy.nist.gov/solder/clech/introduction.htm

[6] Schubert, A.; Walter, H.; Dudek, R.; Michel, B.; "Thermo-Mechanical Properties and Creep Deformation of Lead-Containing and Lead-Free Solders", *International Symposium on Advanced Packaging Materials,* 2001, pp. 129-134.

[7] John, H.; Pang, L.; Xiong, B.S.; Low, T.H.; "Creep and Fatigue Characterization of Lead Free 95.5Sn-3.8Ag-0.7Cu Solder", *Electronic Components and Technology Conference,* 2004, pp. 1333-1337.

[8] Yoshiharu, K.; Mashes, O.; William, J.P.; "The Constitutive Creep Equation for a Eutectic Son-Ag Alloy Using the Modified Theta-Projection Concept", *Journal of Electronic Materials,* Vol. 32, No.12, 2003, pp. 1398-1442.

[9] J. Lau, W. Dauksher, J. Smetana, etc, "HDPUG's Design for Lead-Free Solder Joint Reliability of High-Density Packages," *IPC SMEMA Council APEX® 2003,* S42-p1~8.

[10] L. Ning-Cheng, "Getting Ready for Lead Free Solders," *Indium Corporation of America*, Utica, NY, USA, Tel: 1-315-853-4900; Fax: 1-315-853-4320

[11] http://www.metallurgy.nist.gov/phase/solder/agcusn.html

[12] F.H. Hayes, H.L. Lukas, G. Effenberg and G.Petzow, Z. Metallkde. 77 (1986) 749-754

[13] C.-S. Oh, J.-H. Shim, B.-J. Lee and D.N. Lee, J. Alloys and Compounds 238 (1996) 155-166

[14] J.H. Shim, C.-S. Oh, B.-J. Lee and D.N. Lee, Z. Metallkde. 87 (1996) 205-212

[15] D. R. Askeland, " The Science and Engineering of Materials", Second Edition, PWS-KENT Publishing Company, 1989

[16] http://www.practicalcomponents.com/amkor/amkor-pbga.html

[17] http://www.amkor.com/products/all_products/fcCSP.cfm

[18] H. Nose, M. Sakane, Y. Tsukada, H. Nishimura, "Temperature and Strain Rate Effects on Tensile Strength and Inelastic Constitutive Relationship of Sn-Pb Solders", Journal of Electronic Packaging, Vol. 125, MARCH (2003), 59-66.

[19] J. H. L. Pang, B. S. Xiong, C. C. Neo, X. R. Zhang, T. H. Low, "Bulk Solder and Solder Joint Properties for Lead Free 95.5Sn-3.8Ag-0.7Cu Solder Alloy", Proceedings of 2003 Electronic Components and Technology Conference, 673-679.

[20] Y. Kariya, T. Hosoi, S. Terashima, M. Tanaka, M. Otsuka, "Isothermal Shear Fatigue Life of Sn-xAg-0.5Cu Flip Interconnects", Proceedings of IPACK03, International Electronic Packaging Technical Conference and Exhibition, July 6-11, 2003, Maui, Hawaii, USA, 1-6.

[21] Q. Xiao, H.J. Bailey, W. D. Armstrong, "Aging Effects on Microstructure and Tensile Property of Sn3.9Ag0.6Cu Solder Alloy", Journal of Electronic Packaging, Vol.126, June (2004).

[22] Shi X. Q., Yang Q. J., Wang Z. P., Pang H. L. J., Zhou W., "Reliability assessment of PBGA solder joints using the new creep constitutive relationship and modified energy-based life prediction model", IEEE, Electronics Packaging Technology Conference, 398-405 (2000).

[23] N. Chawla, F. Ochoa, V. V. Ganesh, X. Deng, M. Koopman, K. K. Chawla, S. Scarritt, "Measurement and Prediction of Young's Modulus of a Pb-free Solder', Journal of Materials Science: Materials in Electronics, vol. 15 (2004), 385-388.

[24] B. Yeung, J.- W. Jang, "Correlation between Mechanical Tensile Properties and Microstructure of Eutectic Sn-3.5Ag Solder", Journal of Materials Science Letters, Vol. 21(2002), 723-726.

[25] S. Wiese, E. Meusel, K.- J. Wolter, "Microstructural Dependence of Constitutive Properties of Eutectic SnAg and SnAgCu Solders", Proceedings of Electronic Components and Technology Conference (2003), 197-206.

[26] U. Marquez and D. Barbini, "The Importance of Cooling Rate in the Developing the Totally Controlled Reflow Process for Lead Free and Eutectic Tin Lead Processing", *IPC SMEMA Council APEX 2003*, S11-3-1—S11-3-13.

[27] T. K. Korhonen, P. Turpeinen, L. P. Lehman, B. Bowman, G. H. Thiel, R. C. Parkes, M. A. Korhonen, D. W. Henderson, K. J. Puttlitz, " Mechanical Properties of Near Eutectic Sn-Ag-Cu Alloy over a Wide Range of Temperatures and Strain Rates", Journal of Electronic Materials, Vol.33, No.12,2004, pp 1581~1588

[28] Q. Wang, W. F. Gale, R.W. Johnson, D. Lindahl, H. Ma, " Properties of Lead Free Alloys as Function of Composition Variation", Expo, APEX 2005, Anaheim , CA, Feb. 22~25, P02-6

[29] T. Y. Lee, W. J. Choi, K. N. Tu, J. W. Jang, S. M. Kuo, J. K. Lin, D. R. Frear, K. Zeng, J. K. Kivilahti, " Morphology, Kinetics, and Thermo-dynamics of Solid-state Aging of Eutectic PbSn and Pb-free Solders (Sn-3.5Ag, Sn-3.8Ag-0.7Cu and Sn-0.7Cu) on Cu." J. Mater. Res., 2002, 17(2), pp. 291-301

[30] P. T. Vianco, and J. A. Rejent, " A methodology to Establish Baseline Metrics for Assessing the isothermally aging of Sn-Pb Solder Interconnects," Soldering and Surface Mount Technology, 2002, 14(2), pp. 26-34

[31] A. Grusd, Lead Free Solders in Electronics, SMI, 1997, pp. 648-661

[32] M.L. Huang, C.M.L. Wu, J.K.L. Lai and Y.C. Chan, "Microstructural Evolution of a Lead-Free Solder Alloy Sn-Bi-Ag-Cu Prepared by Mechanical Alloying during Thermal Shock and Aging," *J. Electronic Materials*, 29, 2000, pp. 1021-1361.

[33] Dutta, "Constitutive Model for Creep of Lead-Free Solders Undergoing Strain-Enhanced Microstructural Coarsening: A First Report," *J. Electronic Materials, 2002,*

[34] H. Conrad, Z. Guo, Y. Fahmy and D. Yang, "Influence of Microstructure Size on the Plastic Deformation Kinetics, Fatigue Crack Growth Rate and Low-Cycle Fatigue of Solder Joints," *J. Electronic Materials,* 28, 1999, p.1062.

[35] U. Marquez, D. Barbini, "The Importance of Cooling Rate in the Developing the Totally Controlled Reflow Process for Lead Free and Eutectic Tin Lead Processing," *Presented at IPC SMEMA Council APEX® 2003*

[36] C.M.L. Wu and M.L. Huang, "Creep Behavior of Eutectic Sn-Cu Lead-Free Solder Alloy," *Journal of Electronic Materials* Vol.31, No.5 2002

[37] S.W Shine and Jin Yu, "Creep Deformation of Microstructurally Stable Sn-3.5Ag-xBi solders" , *2001 Int'l Symposium on Electronic Materials and Packaging*, 229-234

[38] X. Deng, **"**Influence of Initial Morphology and Thickness of Cu_6Sn_5 and Cu_3Sn Intermetallics on Growth and Evolution During Thermal Aging of Sn-Ag Solder/Cu Joints," *Journal of Electronic Materials*, 2003

[39] Kelly Stinson-Bagby, "Microstructural Evolution in Thermally Cycled Large-Area Lead and Lead-Free Solder Joints," *Masters Thesis, Virginia Polytechnic Institute and State University*, June 07, 2002

[40] F.Ochoa, J.J. Williams, and N. Chawla, "Effects of Cooling Rate on the Microstructure and Tensile Behavior of a Sn-3.5 wt.% Ag Solder," *Journal of Electronic Materials,* Vol.33, No.12, 1596-1607 (2004).

[41] P. T.Vianco, J. A. Rejent and A. C. Kilgo, "Creep Behavior of the Ternary 95.5Sn-3.9Ag-0.6Cu Solder – Part1: As-Cast Condition," Journal of Electronic Materials, Vol. 33, No. 11, 1389-1399, 2004.

[42] P. T.Vianco, J. A. Rejent and A. C. Kilgo, "Creep Behavior of the Ternary 95.5Sn-3.9Ag-0.6Cu Solder – Part11: Aged Condition," Journal of Electronic Materials, Vol. 33, No. 12, 1473-1484, 2004.

[43] Q. Xiao and W. D. Armstrong, "Tensile Creep and Microstructural Characterization of Bulk Sn3.9Ag0.6Cu Lead-Free Solder," Journal of Electronic Materials, Vol. 34, No. 2, 196-211, 2005.

[44] Q. Zhang, A. Dasgupta and P. Haswell, "Creep and High-Temperature Isothermal Fatigue of Pb-Free Solders," Proceedings of IPACK03 International Electronic Packaging Technical Conference and Exhibition, Maui, Hawaii, pp. 1-6 July 6-11, 2003.

[45] K. Y. Lee, M. Li, D. R. Olsen, W. T. Chen, Ben T. C. and S. Mhaisalkar, "Microstructure, Joint Strength and Failure Mechanism of Sn-Ag, Sn-Ag-Cu, versus Sn-Pb-Ag Solder in BGA Packages," 2001 Electronic Components and Technology Conference.

[46] S. Wiese, A. Schubert, H. Walter, R. Dudek, F. eustel, E. Meusel and B. Michel, "Constitutive Behaviour of Lead-free Solders vs. Lead-containing Solders-

Experiments on Bulk Specimens and Flip-Chip Joints," 2001 Electronic Components and Technology Conference.

[47] S. L. Allen, M. R. Notis, R.R. Chromik, R.P.Vinci, " Coarsening in tin-silver-copper lead-free solder alloys", *Center for Optical Technologies*, Lehigh University

[48] L. Ye, Z. H. Lai, J. Liu and A. Tholen, "Microstructure investigation of Sn-0.5Cu-3.5Ag and Sn-3.5Ag-0.5Cu-0.5B Lead-free solders," *Soldering & Surface Mount Technology,* 13/3, 16-20 (2001).

[49] K. Wu, N. Wade, J. Cui and K. Miyahara, "Microstructural Effect on the Creep Strength of a Sn-3.5%Ag Solder Alloy," *Journal of Electronic Materials,* Vol. 32, No. 1, 5-8, 2003.

[50] A. R. Fix, G. A. Lopez, I. Brauer, W. Nuchter and E. J. Mittemeijer, "Mircrostructural Development of Sn-Ag-Cu Joints," *Journal of Electronic Materials,* Vol. 34, No.2, 137-142, 2005.

[51] D. Lewis, S. Allen, M. Notis and A. Scotch, " Determination of the Eutectic Structure in the Ag-Cu- Sn System," *Journal of Electronic Materials,* Vol. 31, No.2, 161-167, 2002.

[52] Q. Zeng, Z. Wang, A. Xian and J. K. Shang, "Cyclic Softening of the Sn-3.8Ag-0.7Cu Lead – Free Solder Alloy with Equiaxed Grain Structure." *Journal of Electronic Materials,* Vol. 34, No.1, 62-67, 2005.

[53] Kariya Y.; Morihata T.; Hazawa E.; Otsuka M. "Assessment of Low-Cycle Fatigue Life of Sn-3.5mass%Ag-X (X = Bi or Cu) Alloy by Strain Range Partitioning Approach," *Journal of Electronics Materials*, September 2001, vol. 30, no. 9, pp. 1184-1189(6)

[54] S. W. Jeong, J. H. Kim and H. M. Lee, "Effect of Cooling Rate on Growth of the Intermetallic Compound and Fracture Mode of Near-Eutectic Sn-Ag-Cu/Cu Pad: Before and After Aging," Journal of Electronic Materials, Vol. 33, No.12, 1530-1543, 2004.

[55] D. K. Joo, J. Yu and S. W. Shin, "Creep Rupture of Lead – Free Sn-3.5Ag-Cu Solders," Journal of Electronic Materials, Vol. 32, No.6, 541-547, 2003.

[56] L. Qi, J. Zhao, X. Wang and L. Wang, "The effect of Bi on the IMC growth in Sn-3Ag-0.5Cu solder interface during aging process," 2004 International Conference on the Bussiness of Electronic Product Reliability and Liability, 42-46.

[57] S. W. Shin and J. Yu, "Creep Deformation of Sn-3.5Ag-xCu and Sn-3.5Ag-xBi Solder joints," Journal of Electronic Materials, Vol. 34, No.2, 188-195, 2005.

[58] R.W. Neu, et al, "Thermomechanical Behavior of 96Sn-4Ag and Castin Alloy", *Journal of Electronic Package,* Vol. 123 (2001), pp. 238-246.

[59] T. EL-Ashram and R. M. Shalaby, "Effect of Rapid Solidification and Small Additions of Zn and Bi on the structure and properties of Sn-Cu Eutectic Alloy," Journal of Electronic Materials, Vol. 34, No.2, 212-215, 2005.

[60] E. Bradley, III, and J. Hranisavljevic, "Characterization of the Melting and Wetting of Sn–Ag–X Solders," *IEEE TRANSACTIONS ON ELECTRONICS PACKAGING MANUFACTURING*, VOL. 24, NO. 4, OCT. 2001, pp. 255-259

[61] Jennie S. Hwang, Ph.D**.** **"**Modern Solder Technology for Competitive Electronics**,**" ISBN: 0-07-031749-6, Chapter Three, Solder Materials, pp.83

[62] M.C. Flemings, "Solidification Processing," *New York: McGraw-Hill*, 1974, p. 58.

[63] R.C. Dey, Chennai, http://www.hindu.com/thehindu/seta/2001/12/27/stories/2001122700230400.htm

[64] W. F. Gale, "An Introduction of Metallic Materials," http://www.eng.auburn.edu/users/galewil/teaching1.htm